

Review

# Electrolytes, Additives and Binders for NMC Cathodes in Li-Ion Batteries—A Review

Dhrubajyoti Das , Sanchita Manna  and Sreeraj Puravankara \*

School of Energy Science & Engineering, Indian Institute of Technology Kharagpur, Kharagpur 721302, West Bengal, India

\* Correspondence: sreeraj@iitkgp.ac.in; Tel.: +91-3222-260801

**Abstract:** Among the current battery technologies, lithium-ion batteries (LIBs) are essential in shaping future energy landscapes in stationary storage and e-mobility. Among all components, choosing active cathode material (CAM) limits a cell's available energy density ( $\text{Wh kg}^{-1}$ ), and the CAM selection becomes critical. Layered Lithium transition metal oxides, primarily,  $\text{LiNi}_x\text{Mn}_y\text{Co}_z\text{O}_2$  (NMC) ( $x + y + z = 1$ ), represent a prominent class of cathode materials for LIBs due to their high energy density and capacity. The battery performance metrics of NMC cathodes vary according to the different ratios of transition metals in the CAM. The non-electrode factors and their effect on the cathode performance of a lithium-ion battery are as significant in a commercial sense. These factors can affect the capacity, cycle lifetime, thermal safety, and rate performance of the NMC battery. Additionally, polycrystalline NMC comprises secondary clusters of primary crystalline particles prone to pulverization along the grain boundaries, which leads to microcrack formation and unwanted side reactions with the electrolyte. Single-crystal NMC (SC-NMC) morphology tackles the cycling stability issue for improved performance but falls short in enhancing capacity and rate capability. The compatibility of different combinations of electrolytes and additives for SC-NMC is discussed, considering the commercial aspects of NMC in electric vehicles. The review has targeted the recent development of non-aqueous electrolyte systems with various additives and aqueous and non-aqueous binders for NMC-based LIBs to stress their importance in the battery chemistry of NMC.



**Citation:** Das, D.; Manna, S.; Puravankara, S. Electrolytes, Additives and Binders for NMC Cathodes in Li-Ion Batteries—A Review. *Batteries* **2023**, *9*, 193. <https://doi.org/10.3390/batteries9040193>

Academic Editor: Yong-Joon Park

Received: 17 February 2023

Revised: 15 March 2023

Accepted: 21 March 2023

Published: 24 March 2023



**Copyright:** © 2023 by the authors. Licensee MDPI, Basel, Switzerland. This article is an open access article distributed under the terms and conditions of the Creative Commons Attribution (CC BY) license (<https://creativecommons.org/licenses/by/4.0/>).

## 1. Introduction

Fossil fuels are continuously being replaced by greener, sustainable forms of energy with energy storage devices to account for intermittency and efficiency. Rechargeable secondary batteries are suitable for this purpose, and lithium-ion batteries are popular among all reported batteries due to their unique advantages: high energy density, specific capacity, life span, and safety [1,2]. The performance metrics of these batteries are gradually improving to meet the increasing energy demand worldwide. Choosing cathode-active materials (CAMs) is crucial to improving energy density. LIBs use various cathode chemistries with merits and demerits concerning energy density, life span, safety, cost, and other parameters. The most widely researched CAMs broadly belong to three categories: (a) layered oxides; (b) spinel oxides; (c) polyanionic compounds [3]. Polyanionic cathodes such as  $\text{LiFePO}_4$  (LFP) show good thermal stability due to the strong covalent bond between oxygen and phosphorus. The intrinsic poor electronic conductivity of phosphates is improved by carbon coating [4,5]. Spinel oxides, such as  $\text{LiMn}_2\text{O}_4$  (LMO) and  $\text{LiNi}_{0.5}\text{Mn}_{1.5}\text{O}_4$  (LNMO), are less expensive due to the absence of costly Co elements and are high-voltage cathodes operating at ~4.7 V vs.  $\text{Li}/\text{Li}^+$ . The lack of high-voltage electrolytes, capacity fading, and low specific capacity of spinels have limited their use as commercial cathodes compared

to layered oxides [6,7]. Among the ternary layered oxides,  $\text{LiNi}_x\text{Mn}_y\text{Co}_z\text{O}_2$  (NMC) and  $\text{LiNi}_x\text{Co}_y\text{Al}_z\text{O}_2$  (NCA) are the most common high-energy-density commercial cathode materials for LIBs, especially for e-transportation. NMC is superior to NCA for cost and mechanical and thermal stability. NMC offers a better cycle life compared to polyanionic and spinel cathodes.

Extensive reports on novel synthesis methods of NMC to control morphological and compositional modifications are available in the literature [8–10]. The commercialization of NMC as a cathode is at a mature stage, led by Panasonic, Toshiba, and LG Chem. The theoretical capacity of stoichiometric NMC materials is around 275  $\text{mAh g}^{-1}$ , but its accessible capacity depends on the material's transition-metal ions ratio. In the layered transition metal oxide class  $\text{LiNi}_{1/3}\text{Co}_{1/3}\text{Mn}_{1/3}\text{O}_2$ , the Ni-rich cathodes (NMC 811) show higher capacity and operational voltage as Ni is the main active redox species ( $\text{Ni}^{2+} \rightleftharpoons \text{Ni}^{4+}$ ). The Ni-rich compounds show poor thermal stability. The role of Mn is to maintain the battery's excellent cycle life and safety. Co is responsible for the increased electronic conductivity, leading to better rate capability. In a commercial sense, (NMC111 or NMC333) are at a more mature stage as they inculcate all the advantages of the transition metals in the material. For Ni-rich NMC materials, the accessible capacity is much higher than NMC111 but suffers from various degradation processes [11], such as cation mixing [12], surface reconstruction to rock salt [13], phase transformation [14], particle cracking [15,16], transition metal dissolution [17], and parasitic reaction with electrolyte [18].

Another critical factor for excellent battery performance at high voltages is the choice of electrolyte. At higher potentials, i.e., >4.4 V, the electrolyte tends to oxidize, leading to the loss of oxygen from the cathode, increased surface reactivity in the de-lithiated phase, and the dissolution of transition metal from structural instabilities. Among the various strategies, one way to tackle this problem is using electrolyte additives to improve the capacity retention of NMC cathodes. Additives are sacrificial/non-sacrificial species that increase the cathode–electrolyte interface's stability, reduce interfacial resistance, and control the transition metal dissolution under high operating voltages through protective layer formation at the cathode. Binders are electrochemically inert materials that bind the components of the electrode materials to the current collectors in a coated electrode. The choice of which will impact the performance, cost, and environmental benignness of LIBs. NMC cathode material processing predominantly uses a polyvinylidene difluoride (PVDF) binder with a carcinogenic organic solvent, N-methyl-2-pyrrolidone (NMP). Many efforts have endeavored to replace the expensive, toxic polyvinylidene difluoride (PVDF)–N-methyl-2-pyrrolidone (NMP) binder–solvent combination with more nature-friendly water-based binders (linear polymers, co-polymers, and ion-conducting polymers) to simultaneously improve the electrochemical performances and reduce the manufacturing costs of the aqueous processing of LIBs. The review article focuses on the impact of non-electrode components on NMC cathode to develop and optimize novel functional electrolyte additive systems and polymer binders for commercialization.

## 2. Electrolytes

Electrolytes are vital in transferring  $\text{Li}^+$  ions from one electrode to another within a battery. In general, the electrolyte must follow specific characteristic properties, such as:

- (1) The viscosity of electrolytes, which influences ionic mobility, should be low (<2 cP);
- (2) The high dielectric constant (>20) of solvents helps to dissociate salt;
- (3) Ionic conductivity should be high enough with a value greater than  $1 \text{ mS cm}^{-1}$ ;
- (4) A wide electrochemical stability window (0.01–5 V vs.  $\text{Li}/\text{Li}^+$ ) of operation;
- (5) Chemical and thermal stability in a wide range of voltage and temperatures;
- (6) Inert behavior towards other battery components such as separator, current collector, and packaging materials [19,20];
- (7) Environment friendliness, cost-effectiveness, and safety in operating conditions.

Liquid electrolytes are (i) carbonate-based, (ii) ether-based, (iii) ionic liquids and common solid-state electrolytes, (i) inorganic solid-state, (ii) gel polymer, and (iii) solid polymer.

## 2.1. Non-Aqueous Solvents

### 2.1.1. Carbonate Solvents

Commercial batteries mainly use carbonate-based solvents as electrolytes. The physical properties of different carbonate solvents are given in Table 1. Carbonate esters can be divided structurally into cyclic carbonates (Propylene Carbonate (PC), Ethylene Carbonate (EC)) and linear carbonate (Dimethyl Carbonate (DMC), Ethyl methyl Carbonate (EMC)). A mixture of electrolytes optimizing the viscosity, salt-dissociation, solvation/de-solvation energies, and salt conductivity is the current norm in LIBs. EC: DMC mixture synergistically combines the high anodic stability of EC, a high dielectric constant of EC, and low viscosity of DMC. DMC can be substituted by other linear carbonates solvents such as Diethyl Carbonate (DEC) and Ethyl Methyl Carbonate (EMC). EMC can undergo a transesterification reaction and lead to the formation of DEC and DMC, whereas EC gives oligo-carbonates [21–23]. Fluorinated carbonates such as Fluoroethylene Carbonate (FEC) and 4,5-Difluoro-1,3-dioxolan-2-one (DFEC) [24,25] are effective SEI-forming additives or co-solvents. These fluorinated compounds face various types of challenges, such as high melting points and viscosity.

**Table 1.** Physical properties of carbonate solvents [26–29].

Solvent	Dielectric Constant	Viscosity (cP) (25 °C)	Ionic Conductivity (mS cm <sup>-1</sup> ) (1 M LiPF <sub>6</sub> )	Melting Point (°C)	Oxidation Potential (V vs. Li/Li <sup>+</sup> )
EC	89.78@40 °C	1.93@40 °C	8.3	36.4	5.5
PC	64.95	2.51	5.6	−54.5	5.2
DMC	3.107	0.59	6.0	4.6	5.5
DEC	2.820@20 °C	0.748	4.2	−43	5.2
EMC	2.958	0.65	3.5	−53	6.1 <sup>#</sup>
FEC	110	4.1	5.0	18	6.6

# glassy carbon is used as a working electrode instead of platinum.

### 2.1.2. Ether Solvents

In the 1980s, ethers were chosen as possible alternative solvents because of their low viscosity, high ionic conductivity, and stability during cycling. Some of the well-known ethers are tetrahydrofuran (THF), 2-Methyltetrahydrofuran (2-Me-THF), 1,2-dimethoxyethane (DME), Polymethoxy ethers, dimethoxy propane, and diethyl ether [19,30]. Ether-based solvents have oxidation stability < 4 V but provide excellent stability with Li metal electrodes. It oxidizes when the CAMs are high-voltage cathode materials (Li<sub>x</sub>MO<sub>2</sub>, M = Mn, Ni, or Co). Despite such demerits of ether solvent, a high-concentration ether-based electrolyte (LiFSI/DME) performs well in an NMC/Li-metal full cell with a capacity retention of 92% after 500 cycles at 4.3 V [31]. Ren et al. reported a localized high-concentration electrolyte (LHCE), creating an effective protective interface layer upon Ni-rich cathode material [32,33]. Again, adding some carbonate-based additive (EC or FEC) helps improve battery performance [34]. A new class of fluorinated ethers with high ionic conductivity and oxidative stability contributes electrochemical stability to Ni-rich NMC for around 100 cycles [35].

### 2.1.3. Other Solvents

Phosphorous-based organic solvents are used as non-flammable co-solvents to prevent fire hazards, mainly due to the radical propagation mechanism. Recently, they have been used to enhance the anodic stability of high-voltage cathodes by reducing flammability. The high viscosity of solvents makes them unfavorable to use because they lead to low ionic conductivity and wettability toward separators and electrodes. The phosphorus-based solvents, in combination with carbonates or ethers, can cope with high-viscosity problems [36–40].

Alkyl sulfones are another suitable option as a solvent because of their low flammability and excellent anodic stability. High melting points and high viscosity can be an

issue that hinders them in commercial applications. They are suitable for high-voltage and high-energy-density Li-ion batteries [41–44].

## 2.2. Lithium Salts

$\text{LiPF}_6$  is indispensable as Li salt because of its well-balanced properties in all the commercialized LIB electrolyte systems [45]. The improvement of the salt is taken into account at the expense of anodic stability as it gets easily oxidized on the charged surface of cathode materials below 4.0 V vs.  $\text{Li}/\text{Li}^+$ . Most salts can fulfill the solubility requirement by using a complex anion formed by stabilizing the anion core with a Lewis acid agent. In  $\text{LiPF}_6$ ,  $\text{F}^-$  ion is stabilized by Lewis acid  $\text{PF}_5$ . The anionic charge is well distributed by an electron-withdrawing Lewis acid ligand, and the salts have a low melting point and are readily soluble in low dielectric media. Milder Lewis acid-based salts such as  $\text{LiClO}_4$  and  $\text{LiMX}_n$  ( $M = \text{B}$  or  $\text{As}$ ,  $\text{P}$ , and  $\text{Sb}$  and  $X = \text{F}$  or  $\text{O}$  and  $n = 4$  or  $6$ ) are frequently used at lab-scale levels. The physical properties of lithium salts are tabulated in Table 2.

**Table 2.** Physical properties of different Lithium salts.

Salt	Mol. Wt.	Melting Point ( $T_m$ ) (°C)	$T_{\text{decomposition}}$ (°C) in Solution	Al Collector Corrosion
$\text{LiPF}_6$	151.9	200	~80 (EC/DMC)	N
$\text{LiBF}_4$	93.9	293	>100	N
$\text{LiAsF}_6$	195.9	340	>100	N
$\text{LiClO}_4$	106.4	236	>100	N
$\text{LiTFSI}$	286.9	234	>100	Y

$\text{LiPF}_6$  is very sensitive to both moistures, even at low ppm levels, and decomposes at ~70 °C, which restricts its applications and causes safety issues. The proposed reaction scheme [46,47] of  $\text{LiPF}_6$ , with residual moisture is



The interaction of  $\text{PF}_5$  with organic carbonate solvents can accelerate the formation of HF. HF can easily react with the delicate NMC surface, leading to the loss of active  $\text{Li}^+$  and even accelerating the dissolution of transition metal ions (TMs). To an extent, insulator coatings, such as  $\text{SiO}_2$ , can limit HF from reacting with the electrode material. The schematic (Figure 1) shows HF formation and  $\text{SiO}_2$  protection with  $\text{LiPF}_6$  salt. To substitute  $\text{LiPF}_6$ , other chemically stable salts, such as  $\text{LiBOB}$  [48], lithium bis(fluorosulfonyl)imide ( $\text{LiFSI}$ ) [49], lithium 4,5-dicyano-2-(trifluoromethyl) imidazolidine ( $\text{LiTDI}$ ) [50], and lithium difluoro(oxalato)borate ( $\text{LiDFOB}$ ) [51,52], have been reported.

## 2.3. Dual-Salt-Based Electrolytes

Dual-salt electrolytes were extensively researched to replace  $\text{LiPF}_6$ -containing electrolytes for high-voltage cathodes. The conventional  $\text{LiPF}_6$  carbonate-based electrolyte results in a poor SEI layer formation, consisting of many resistive decomposition products of  $\text{LiF}$  and  $\text{Li}_2\text{CO}_3$  and other inorganic and organic by-products. Dual-salt electrolytes can replace  $\text{LiPF}_6$ -containing electrolytes with no highly resistive  $\text{LiF}$  in the SEI layer. A dual-salt electrolyte of lithium bis(trifluoromethanesulfonyl)imide ( $\text{LiTFSI}$ ) and lithium bis(oxalato)borate ( $\text{LiBOB}$ ) in a carbonate solvent mixture (Figure 2b) [53,54] or using  $\text{LiPF}_6$  as an additive [55] in electrolytes results in the improved performance of full cells with NMC as the cathode and Li metal as the anode. High-voltage cathodes with Li metal as the anode in these electrolytes showed an areal capacity of 1.75  $\text{mAh cm}^{-2}$  after 450–500 cycles at a current density of 1.75  $\text{mA cm}^{-2}$  [54,55]. There are other dual salts reported in the literature, such as  $\text{LiTFSI-LiDFOB(lithium difluoro(xalate)borate)}$ ,  $\text{LiFSI}$

(lithium bis(fluorosulfonyl)imide)-LiDFOB, and LiFSI-LiDFOB. The cycling stability of the Li metal batteries with these electrolytes grades in the following order: LiTFSI-LiBOB > LiTFSI-LiDFOB > LiFSI-LiDFOB > LiPF<sub>6</sub> > LiFSI-LiBOB, which is in good accordance with the density functional theory (DFT) calculation results (Figure 2a) [54].

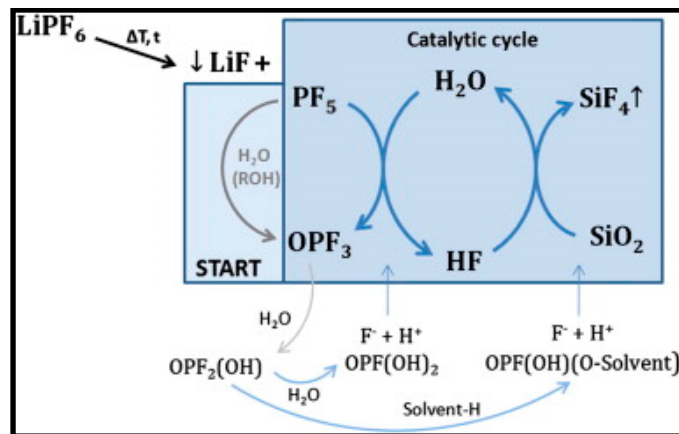


**Figure 1.** Proposed mechanism of formation of HF from LiPF<sub>6</sub> and its reaction with SiO<sub>2</sub>. Reprinted with permission from reference [47]. Copyright 2012, Elsevier.

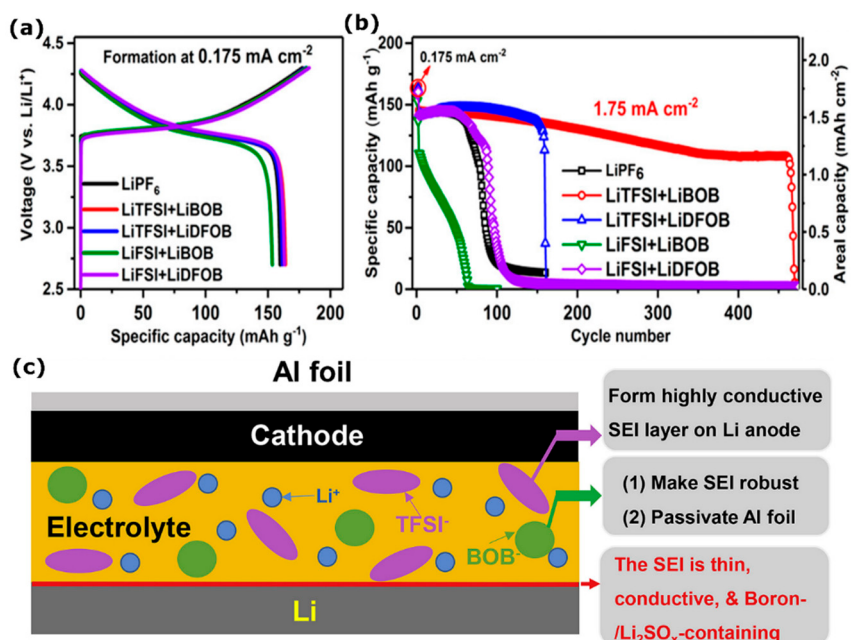


**Figure 2.** (a) Formation cycles at 0.175 mA cm<sup>-2</sup>; (b) Cycling performance with different electrolytes at 1.75 mA cm<sup>-2</sup>. Reprinted with permission from ref. [54]. Copyright 2018 American Chemical Society. (c) Schematic illustration of the role of LiTFSI–LiBOB as a dual–salt electrolyte. Reprinted with permission from reference [53]. Copyright 2016, Elsevier.

Recently, Zheng et al. confirmed 300 cycles of stable cycling of Li/NMC with an areal capacity of 0.9–4.1 mAh cm<sup>-2</sup> with the limitation of discharge current 2 mA cm<sup>-2</sup> and a charge current density of around 1 mA cm<sup>-2</sup> in a LiPF<sub>6</sub>-assisted LiTFSI-LiBOB dual-salt EC-based electrolyte [56]. Dual-salt is also reported in ether electrolyte solvent through ether oxidizing easily by highly catalytic cathode surface at lower potentials (<4 V). The concentrated ether-based electrolyte containing 2 M LiTFSI and 2 M LiDFOB in DME increases the oxidation stability of ether molecules. This dual salt also passivates the NMC cathode surface at high voltage and forms a better SEI layer on the Li metal anode,

resulting in a long Li/NMC full cell lifetime. It shows more than 90% capacity retention after 300 cycles and ~80% after 500 cycles with an upper cut-off voltage of 4.3 V [57].

#### 2.4. Additives

Additives without an effect on the skeletal composition of the electrolyte result in specifically targeted properties in a very efficient and economical way. The electrolyte's bulk properties persist as the additive forms only <5 wt% of the electrolyte. Additives are sacrificial and form a protective layer during the initial activation cycles. Usually, a solid electrolyte interface (SEI) layer-forming additive is crucial for Li metal or graphite anodes. Vinylene carbonate (VC) or 1,3-Dioxol-2-one is one of them, with a strained cyclic alky carbonate with a polymerizable double bond improving the cycle life and thermal stability of different Li-ion systems [58]. Recently, it has also shown beneficial effects on the positive electrode. Burns et al. studied the role of VC in varieties of Li-ion cells by changing the content of the additives [59]. 1–2% of VC can improve battery life and reduce cell impedance. Another group studied the effect of VC in the cycling stability of  $\text{LiNi}_{0.5}\text{Mn}_{0.3}\text{Co}_{0.2}\text{O}_2$  (NMC532)/graphite cell at a high temperature. The addition of 1% VC suppresses the formation of undesirable decomposed products [60].

LIBs have used Fluoroethylene carbonate (FEC) as an additive to improve the battery metrics. An FEC-induced SEI layer is more stable and conductive. It regulates the uniform Li stripping and plating and enhances the cycle performance of Li/NMC cells. FEC leads to the formation of LiF-containing components on Li metal anodes. This LiF-rich SEI is efficient and effective in subduing dendrite formation on Li metal. Zhang et al. presented a stable cycling of Li/NMC532 cells with an areal capacity of  $1.9 \text{ mAh cm}^{-2}$  at a current density of  $2.16 \text{ mA cm}^{-2}$  for about 100 cycles with 5% FEC in EC-based electrolyte solution [61]. Aurbach group demonstrated the performance of Li/NMC622 in different current densities of  $0.5\text{--}2 \text{ mA cm}^{-2}$  with  $33 \mu\text{L cm}^{-2}$  FEC-based electrolyte, and at  $1.5 \text{ mA cm}^{-2}$ , the cell shows an areal capacity of about  $2 \text{ mAh cm}^{-2}$  after more than 600 galvanostatic cycles [62]. Im et al. demonstrated a fluorinated electrolyte (1 M  $\text{LiPF}_6$  fluoroethylene carbonate (FEC) and methyl (2,2,2-trifluoroethyl) carbonate (FEMC) ( $\text{FEC/FEMC} = 1/9, v/v$ )) for  $\text{LiNi}_{0.5}\text{Mn}_{0.3}\text{Co}_{0.2}\text{O}_2$ /graphite system at 4.5 V [63]. FEC can be used with other co-additives  $\text{LiPO}_2\text{F}_2$  to suppress electrolyte decomposition and transition metal dissolution during cycling [46]. Both produce a stable cathode–electrolyte interface (CEI) layer on the cathode. (Figure 3).

Tris (trimethylsilyl) phosphite (TMSPi), which tends to decompose and form the CEI layer at the cathode–electrolyte interface, is another exciting additive used in NMC chemistry. This layer prevents excessive electrolyte decomposition, transition metal dissolution, and other parasitic side reactions. Mai et al. demonstrated that TMSPi was responsible for improving the cycling performance and rate capability of an NMC electrode by forming a stable and less resistive surface film due to oxidation on the cathode surface [64]. The combination of TMSPi and VC improves the long-term cycling performance of NMC111/graphite cells [65,66]. Adding 1% TMSPi and 1% VC in a standard electrolyte consisting of 1 M  $\text{LiPF}_6$  in EC: DMC (1:1 vol.) increases the capacity retention of NMC811/graphite full cell to 91% after 200 cycles at C/3 [67]. Peebles et al. compared the capability of TMSPi with structurally analogous electrolyte Triethyl Phosphite (TEPi) in NMC532/graphite full cell and proposed a mechanism for oxide film formation on the surface (Figure 4) [68].

Sulfur-containing additives are also very popular for enhancing the battery lifetime, regulating impedance growth, and suppressing gas production, especially when combined with other additives. Better coulombic efficiency with lower impedance and reduced voltage drop can be obtained using 1,3,2-dioxathiolane-2,2-dioxide (DTD) and tetramethylsulfone (TMS) additives [69]. During the formation cycles, DTD and TMS generate gases but suppress gas generation in combination with VC. Prop-1-ene-1,3-Sultone (PES) also improves the performance of NMC111/graphite in the presence of VC with less gas production and an increase in cell impedance [70,71]. A ternary mixture of PES, 1, 5, 2, 4-dioxadithiane-2, 2, 4, 4-tetraoxide (MMDS), and TMSPi or VC, MMDS, and TMSPi can yield improved battery life and excellent safety [65,72,73].

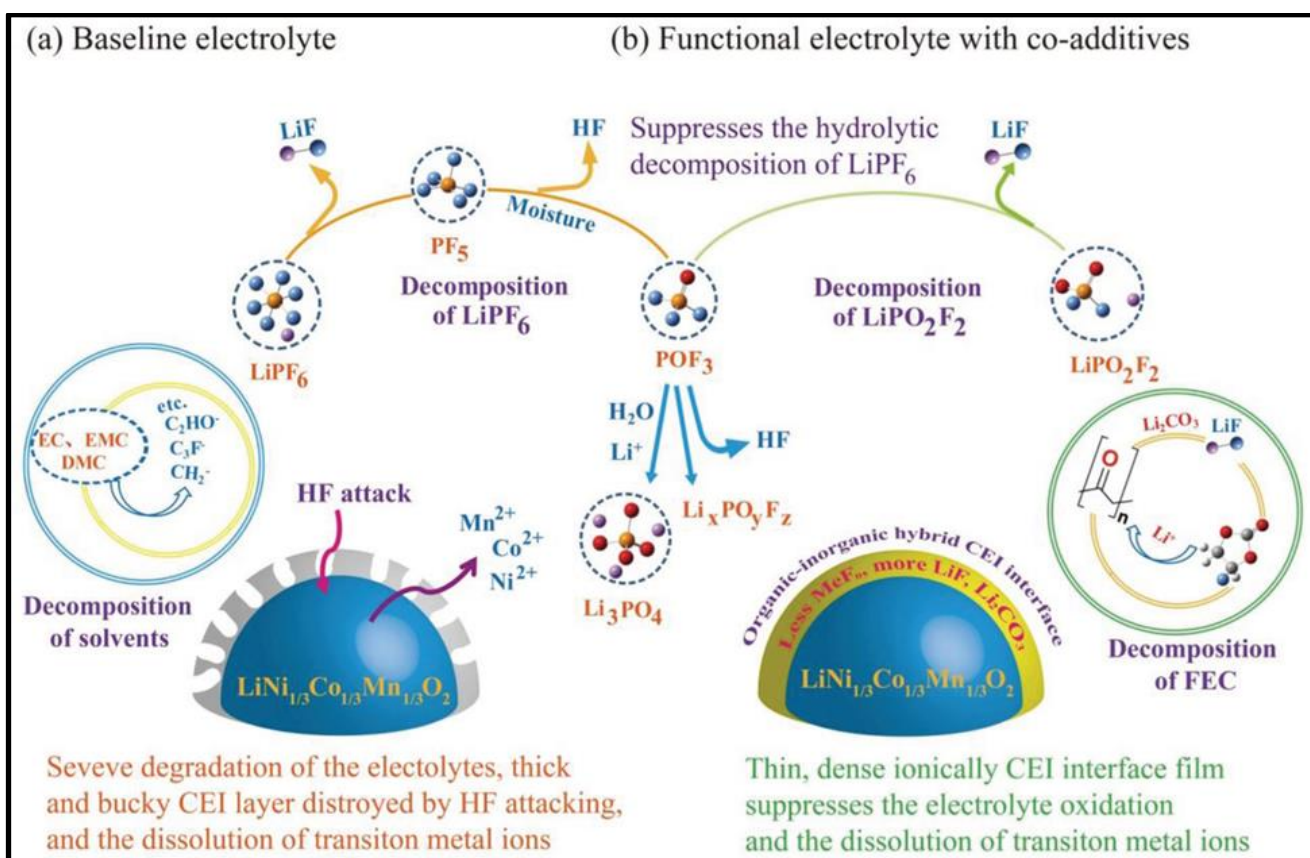


**Figure 3.** Schematic representation of the role of FEC and  $\text{LiPO}_2\text{F}_2$ . Reprinted with permission from reference [46]. Copyright 2020, John Wiley and Sons.

The main boron-containing additives reported for NMC cathode is lithium bis(oxalate)borate (LiBOB) [48,74]. LiBOB leads to the formation of a stable SEI on graphite, resists the unfavorable reactions of the electrolyte with high-voltage positive electrodes and also improves capacity retention. The cell impedance increase issue faced by LiBOB can be limited by adding triphenylamine ( $\text{Ph}_3\text{N}$ ) or 1,4-benzodioxane-6,7-diol (BDOD). The low oxidation potential of LiBOB and BDOD can protect the cathode surface by producing stable conducting polymer through the radial polymerization process [75]. Lithium difluoro(oxalato) borate (LiDFOB) is also used with LiBOB to improve cell performance by passivating the electrode surface against electrolyte decomposition and transition metal dissolution [76]. LiDFOB in a carbonate-based electrolyte (with fluorinated ether as diluent) showed capacity retention of 84% of  $\text{LiNi}_{1/3}\text{Mn}_{1/3}\text{Co}_{1/3}\text{O}_2$ /Li cell after 100 cycles [77].

Lithium Difluorophosphate (LiDFP) became a good additive for high-voltage NMC cathodes [78]. It is one of the decomposition products of  $\text{LiPF}_6$ . Wang et al. demonstrated using 1 wt% of this additive in conventional carbonate-based electrolytes for a high-voltage  $\text{LiNi}_{1/3}\text{Mn}_{1/3}\text{Co}_{1/3}\text{O}_2$ /graphite pouch cell at 4.5 V [79]. The capacity retention of the cell increased notably to 92.6% after 100 cycles and 78.2% after 200 cycles. A full cell—a  $\text{LiNi}_{0.5}\text{Co}_{0.2}\text{Mn}_{0.3}\text{O}_2$ /graphite pouch cell—at 4.5 V showed capacity retention of 93.8% after 100 cycles, and its discharge capacity obtained around  $118.9 \text{ mAh g}^{-1}$  at 5 C [80]. The Yang group also conducted a low-temperature evaluation of LiDFP on NMC532/graphite [81]. The additive improves initial capacity by 71.9% at  $-20^\circ\text{C}$  and 57.93% at  $-30^\circ\text{C}$ , improving capacity retention by 16.8% at 0.5 C after 100 cycles at 0 °C. Recently, another electrolyte additive, Tripropargyl Phosphate (TPP), was reported in the literature, which produces a protective interface layer upon both positive and negative electrodes [82].

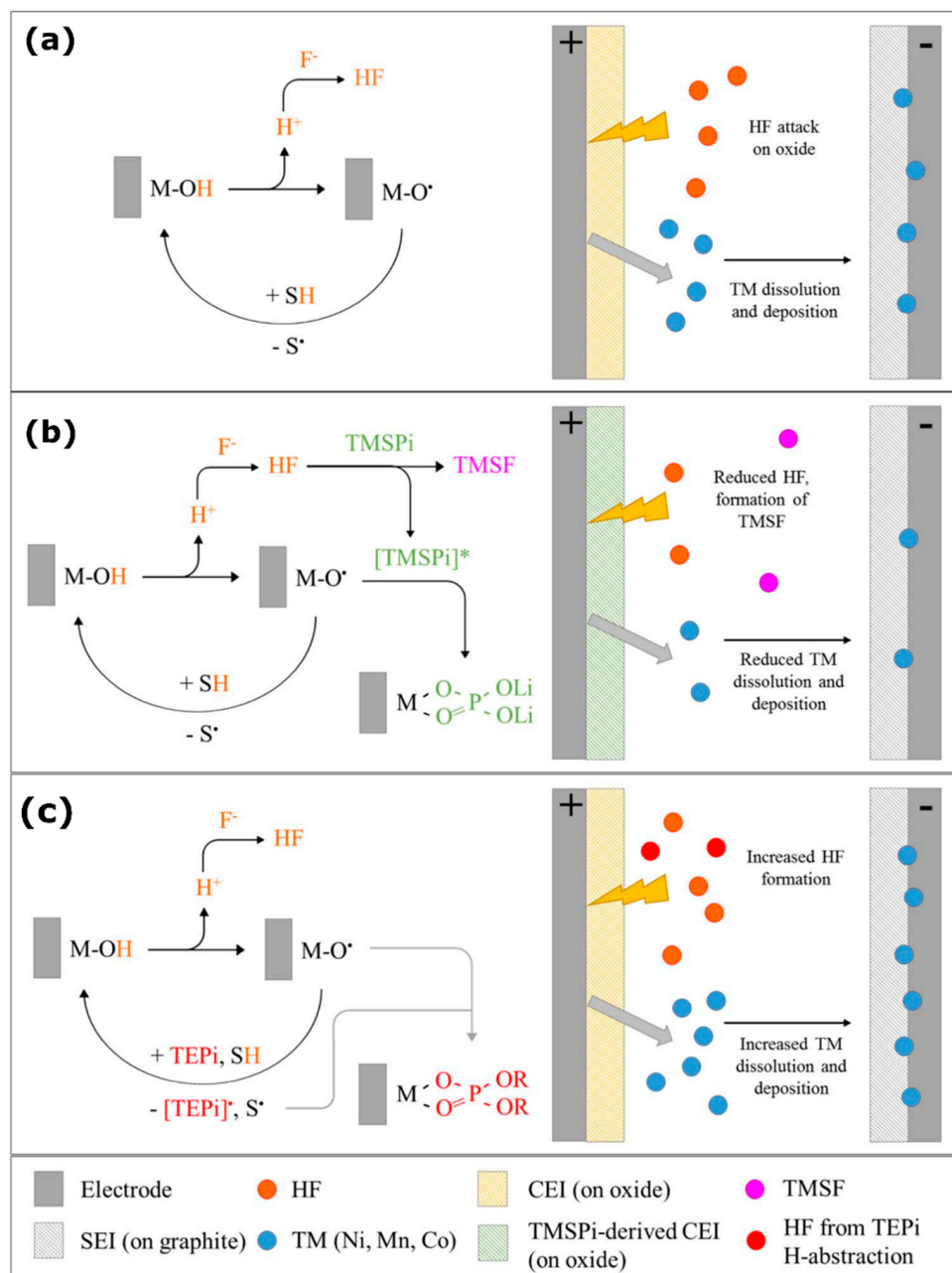


**Figure 4.** Proposed mechanism of (a) degradation of baseline cell and oxide surface film formation of (b) TMSPi and (c) TEPI. Reproduced under Creative Commons (CC BY License) [68], Electrochemical Society.

## 2.5. Ionic Liquid Electrolytes

Ionic liquid electrolytes were chosen as an alternative to conventional carbonate electrolytes for their superior properties, such as wide electrochemical windows, low volatility, and non-flammability [83,84]. They are low-temperature molten salts comprised of cations and anions without any molecular species. Two types of ionic liquid (IL) based electrolytes are often identified as (i) purely ionic electrolytes (mixture of an IL and a lithium salt) and (ii) IL-organic solvent(s) blends (mixtures of an IL, a lithium salt, and co-solvent(s)). The cyclic or linear carbonate co-solvent improves the solution's transport properties (viscosity and ionic conductivity). Chaudoy et al. demonstrated the use of room-temperature ionic liquid (RTIL)-based electrolytes in improving Li/NMC full cell compared to conventional electrolytes. RTILs mentioned in their literature are N-butyl-N-methylpyrrolidinium bis(fluorosulfonyl)amide(P14FSI) and N-propyl-

*N*-methylpyrrolidinium bis(fluorosulfonyl)amide(P13FSI), and LiTFSI was the salt. A reversible capacity of about  $145 \text{ mAh g}^{-1}$  at C/10 and  $110 \text{ mAh g}^{-1}$  at C with approximately 100% coulombic efficiency for these electrolytes in Li/NMC full cell [85]. Matsui et al. reported the ionic liquid-based electrolyte (mixture of EMIMFSI and LiTFSI), which gave a reversible capacity of  $163 \text{ mAh g}^{-1}$  in a full cell with an NMC cathode [86]. Passerini et al. showed the improvement of cycling behavior for Li/NMC half-cells at different temperatures (Figure 5a).

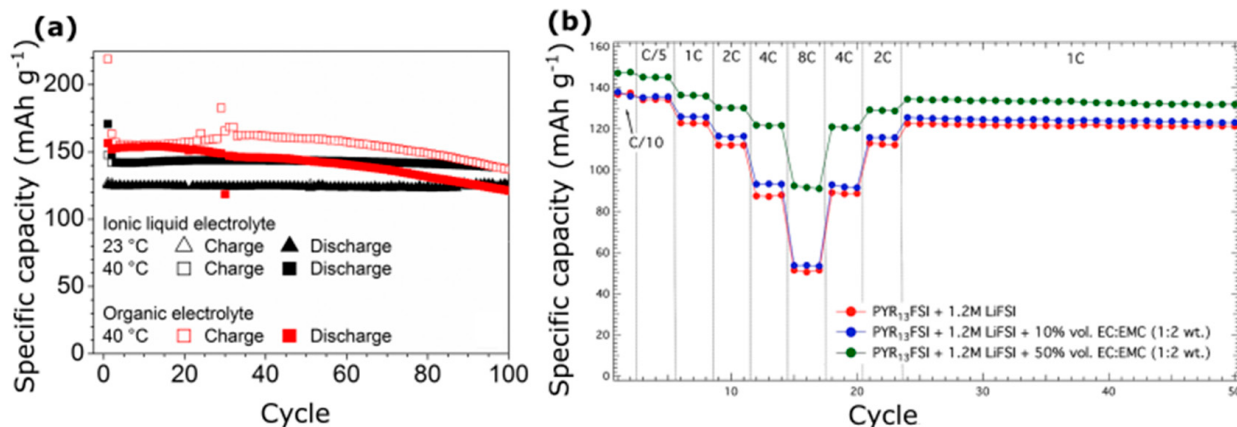


**Figure 5.** (a) Capacity retention of a Li/NMC half-cell in both ionic liquid and organic electrolyte at  $23\text{ }^{\circ}\text{C}$  and  $40\text{ }^{\circ}\text{C}$ . Reprinted with permission from reference [87]. Copyright 2016, Elsevier. (b) Effect on rate performance due to the addition of an organic solvent. Reprinted with permission from reference [88]. Copyright 2014, Elsevier.

The effect of organic solvents on the aluminum dissolution and rate performance of an NMC cathode to improve the electrochemistry were analyzed. The electrolytes used are based on a blend of P13FSI and  $1.2 \text{ mol}\cdot\text{L}^{-1}$  LiFSI or P13FSI, 10 vol% (or 50 vol%) EC: EMC (1:2 wt.) and  $1.2 \text{ mol}\cdot\text{L}^{-1}$  LiFSI (Figure 5b) [88]. Reiter et al. also reported using PP13TFSI and LiFSI or LiTFSI as electrolytes for graphite anode and NMC cathode. They also showed that graphite could produce a discharge capacity of  $340\text{--}345 \text{ mAh}\cdot\text{g}^{-1}$  at a C/10 rate with a coulombic efficiency of 97–98%, and NMC cathode material can produce a discharge capacity of  $160 \text{ mAh}\cdot\text{g}^{-1}$  with coulombic efficiency above 99% [49].

## 2.6. Solid-State Electrolytes

Conventional liquid electrolyte-based battery brings safety issues due to perennial problems such as dendrite formation on the lithium anode, electrolyte leakage, fire, and explosions [89]. Solid-state electrolytes are critical in limiting the usage of volatile organic electrolytes.

### 2.6.1. Inorganic Solid-State Electrolytes

Kato et al. reported the oxide-based solid electrolyte (Ox-SSB) Li/LLZ/NMC-LATP composite film shows good capacity retention of about 99.97% after 90 cycles at a C/10 rate at  $100\text{ }^{\circ}\text{C}$  [90,91]. There is an aerosol deposition technique to synthesize the composite films and a thick composite of crystalline NMC and amorphous solid electrolyte Li-Nb-O at room temperature. Another method to infuse solid electrolytes on electrodes is an atomic layer deposition coating of  $\text{Li}_3\text{PO}_4$ , a solid electrolyte, on Ni-rich NMC to reduce the capacity and voltage fading mechanisms [92]. Alexander et al. reported surface-modified garnet structured solid electrolyte  $\text{Li}_{6.28}\text{Al}_{0.24}\text{La}_3\text{Zr}_2\text{O}_{12}$  (LLZA), which leads to an initial capacity of  $162 \text{ mAh g}^{-1}$  at  $50 \mu\text{A cm}^{-2}$  [93]. Philip et al. introduce lithium phosphorus oxynitride (LiPON) electrolyte, which reduces the degradation of the NMC622/LiPON interface and helps in stable cycle performance [94]. Figure 6a,b show a better specific capacity for LiPON than the conventional electrolyte.

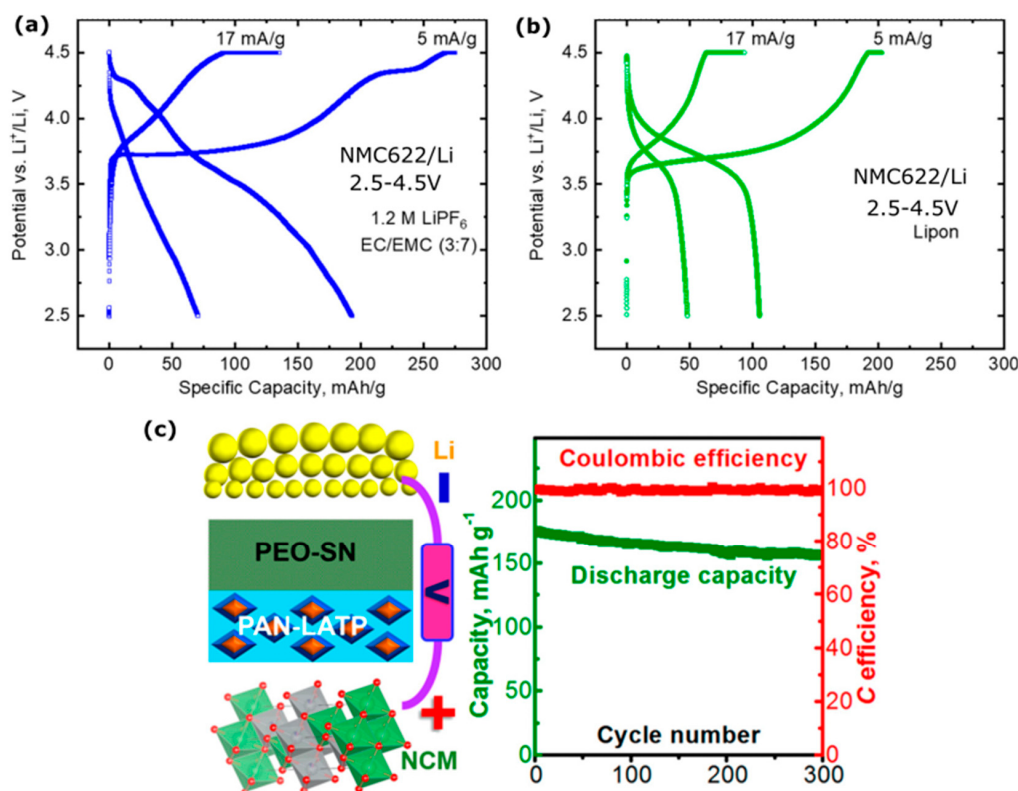


**Figure 6.** Charge–discharge curves for NMC622/Li with (a) liquid electrolyte and (b) solid electrolyte (LiPON) at two different current densities: 5  $\text{mA g}^{-1}$  and 17  $\text{mA g}^{-1}$ . Reprinted with permission from reference [94]. Copyright 2020 American Chemical Society. (c) Electrochemical performance of Li/PEO–SN–LiTFSI/PAN–LATP–LiTFSI/NCM (811) cell at a C/5 rate. Reprinted with permission from reference [95]. Copyright 2020 American Chemical Society.

### 2.6.2. Gel Polymer Electrolyte

Gupta et al. reported a polymer electrolyte that contains polyethylene oxide (PEO), LiTFSI, and IL (ionic liquid). The cell containing this electrolyte and NMC622 as a cathode gives a specific discharge capacity of 137  $\text{mAh g}^{-1}$  [96]. Goodenough and his members investigate the reason behind the degradation of PEO-based electrolytes with the help of an in situ scanning electron microscope [97]. Kobayashi et al. explained the decomposition of polymer electrolytes and the utilization of a CMC binder to suppress such degradation, leading to better performance [98].

### 2.6.3. Solid Polymer Electrolyte

The inorganic solid electrolyte has high Li<sup>+</sup> ion conductivity and a wide electrochemical stability window but with a poor and unstable interface of a Li anode or different electrodes, whereas a polymer electrolyte offers a stable interface. Goodenough et al. reported NASICON/polymer electrolyte, which gives good cycle stability (100 cycles) of Li/NMC811 at 40 °C [99]. Manthiram et al. designed a dual polymer/polymer–ceramic composite electrolyte (LDPPCCE) with an ionic conductivity of  $1.31 \times 10^{-4} \text{ S cm}^{-1}$  at room temperature (Figure 6c) [95].

## 3. Binder

The choice of binder in LIBs is critical because of its ability to control the density, porosity, and thickness of the coated cathode slurry, and it should (1) have a wide electrochemical window (0–5 V), (2) be nonreactive with other cell components, and (3) be easily soluble in appropriate aqueous and non-aqueous solvents. Polyvinylidene fluoride (PVDF) is one of the most widely used binders that dissolves in an organic solvent such as

N-methyl-2-pyrrolidone (NMP) [100,101]. NMP solvent is expensive, toxic, and not eco-friendly. Carboxy Methyl Cellulose (CMC) is a well-known binder in an aqueous solvent that is less expensive and eco-friendly [102]. In recent binder progress, another cheap and natural binder is reported, which is known as alginate, extracted from brown algae [103]. J. Xu et al. thoroughly investigated the effect of all three different binders in the case of NMC111. Figure 7 illustrates that CMC mixed with NMC shows higher cyclic performance than PVDF and alginate [104]. Aqueous binder CMC in an NMC/graphite full cell offers a coulombic efficiency of 99.96% and capacity retention of 70% after 2000 cycles [105]. CMC binder was also used with an NMC442 cathode, producing better stability than PVDF [106]. Another water-soluble binder, polyacrylic latex (LA132), exhibited higher capacity, improved cycle stability, and better rate performance than CMC and PVDF [107]. One issue with using a water-based binder for NMC is that it increases the pH value to 11 and leads to corrosion to the Aluminum (Al) substrate. Adding components ( $\gamma$ -Al<sub>2</sub>O<sub>3</sub> or SiO<sub>2</sub>) or acids (phosphoric acid or formic acid) that increase the pH of the suspension can rectify the problem to a more considerable extent [108–110]. M. Wood et al. explored nickel-rich NMC in aqueous slurry preparation for electrodes and showed structural stability with comparable capacity retention (70% after 1000 cycles) [111]. Without adding any additive to the aqueous slurry, Poly(acrylic acid) (PAA) can act as a successful binder for NMC811 without any corrosion of the Al current collector and can produce an initial capacity of 189.2 mAh g<sup>-1</sup> at a 0.2 C rate [112]. Brillonni et al. introduced a new biodegradable polymer known as pullulan, which helps in the easy recovery of cathode material after its use [113]. Apart from conventional PVDF and a water-soluble binder such as CMC, a new family of ionic conductive polymers, such as poly (ionic liquids) (PIL), was introduced in the world of binders. One of the popular PIL binders is poly(diallyldimethylammonium) (PDADMA) with various types of anionic species of ionic liquid attached to it. Vauthier et al. studied PIL on high-voltage NMC532 and produced improved capacity with fluorinated PDADMA [114]. The physical properties of popular NMC binders are tabulated in Table 3.

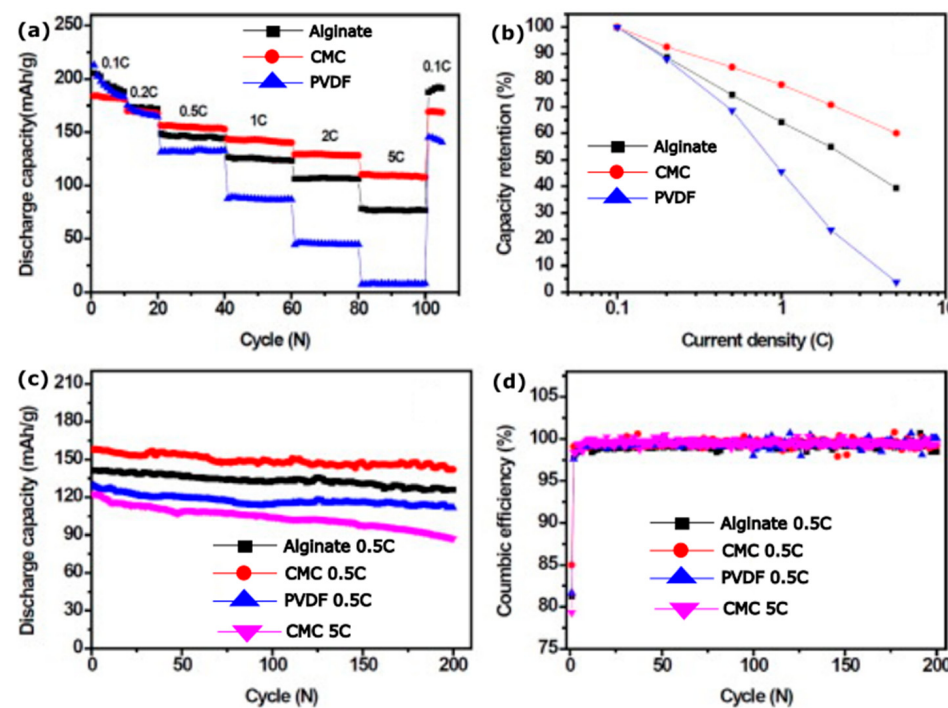


**Figure 7.** (a) Discharge capacity at different rates; (b) capacity retention; (c) cyclic performance (d) coulombic efficiency for different binders at 2.5–4.6 V. Reprinted with permission from ref. [104]. Copyright 2013, Elsevier.

**Table 3.** Physical properties of popular NMC binders [104,106,107,112–114].

Binders	Structure	Solvent	Properties
PVDF		NMP	Linear crystalline thermoplastic fluoropolymer
CMC		Water	Linear polymer; environmentally friendly; high viscous; and low ionic impedance
Na-alginate		Water	Self-healing effect; uniform distribution of carboxyl group; low ionic impedance
LA132		Water	Co-polymer of acrylamide, lithium methacrylate, and acrylonitrile; high adhesion property  (R1-Acrylamide, R2-Carboxylic acid lithium, R3 Cyano-)
PAA		Water	Linear polymer with uniform distribution of functional group; tuneable mechanical properties
PDADMA		Water	Ionic conductive polymers; wide electrochemical stability window

## 4. Anodes for NMC-Based Battery

A compatible anode is also a vital factor for NMC cathode-based LIBs. Commercially, graphite is the most desirable anode due to its considerable specific capacity ( $372 \text{ mAh g}^{-1}$ ), low cost, low operational potential (0.1 V vs. Li/Li<sup>+</sup>), high electronic conductivity, uniform SEI formation, and long cycle life [115]. Another negative electrode that shows a high theoretical capacity of  $3860 \text{ mAh g}^{-1}$  is the lithium metal anode. The perennial dendrite formation on a lithium metal anode and its safety issues restrict its use in commercial LIBs [116]. The SEI layer formation on the anode was avoided with a higher lithium intercalation potential anode such as  $\text{Li}_4\text{Ti}_5\text{O}_{12}$  (LTO) [117]. It shows a low theoretical capacity ( $175 \text{ mAh g}^{-1}$ ) compared to graphite and lithium metal and a lower energy density due to the lower operating voltage in a full cell. Björklund et al. reported the impact of the different anodes on the electrochemical performance of NMC111 [118]. Li metal-based full-cell capacity fading is more significant than graphite and LTO-based anode cells. Fang et al. also studied the effect of the anode on the cathode interface layer [119]. The studies indicate that NMC/graphite and NMC/LTO give us better cycle stability than NMC/Li. The higher operational potential of LTO (1.55 vs. Li/Li<sup>+</sup>) compromises the energy density of the full cell compared to graphite. Figure 8 shows the energy density of NMC full cells in combination with the different anodes.

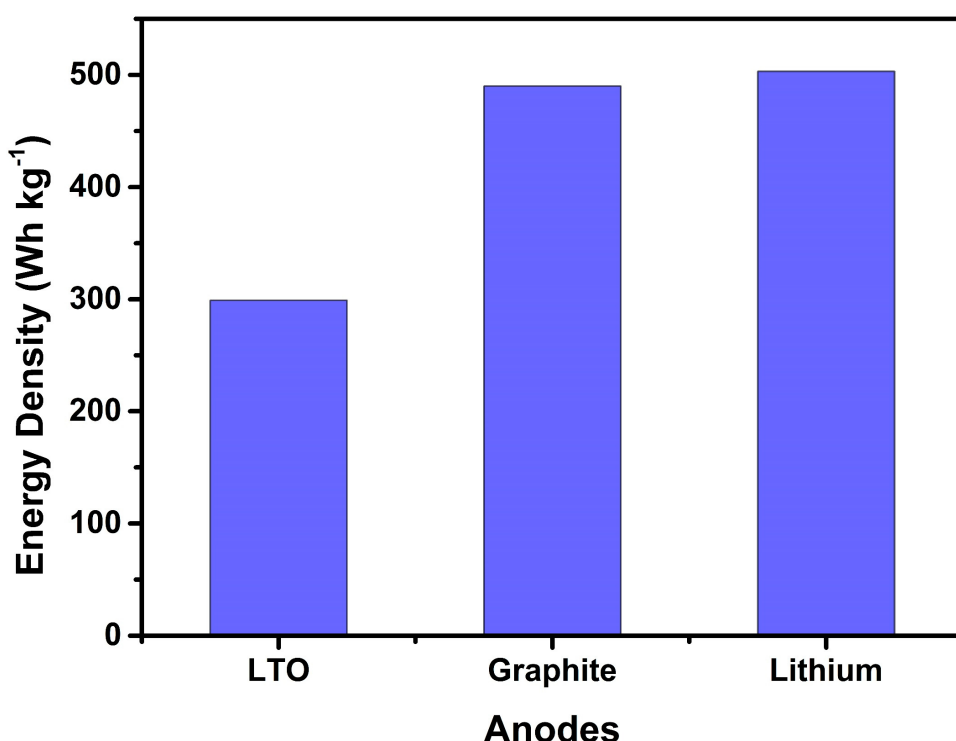


**Figure 8.** Full cell energy density of different anodes with NMC. Adapted from reference [118].

### 5. NMC Compositions

$\text{LiNi}_x\text{Mn}_y\text{Co}_z\text{O}_2$  ( $x + y + z = 1$ ) (NMC) are very popular as transition metal oxide cathodes. The percentage of elements present in the composition can vary in physical and chemical properties. The content of Ni governs the specific capacity of the material, i.e., the higher the percentage of Ni, the higher the capacity will be. Figure 9a presents the ternary diagram of different compositions of NMC with specific advantages of each element. Figure 9b represents the gravimetric and volumetric energy densities of different NMCs. Ni can show redox reactions of  $\text{Ni}^{2+} \leftrightarrow \text{Ni}^{3+} \leftrightarrow \text{Ni}^{4+}$  during the charge/discharge process; the capacity and safety are a tradeoff while designing the electrode composition. The content of Mn can improve the safety factor, while Co enhances the kinetics of the material.

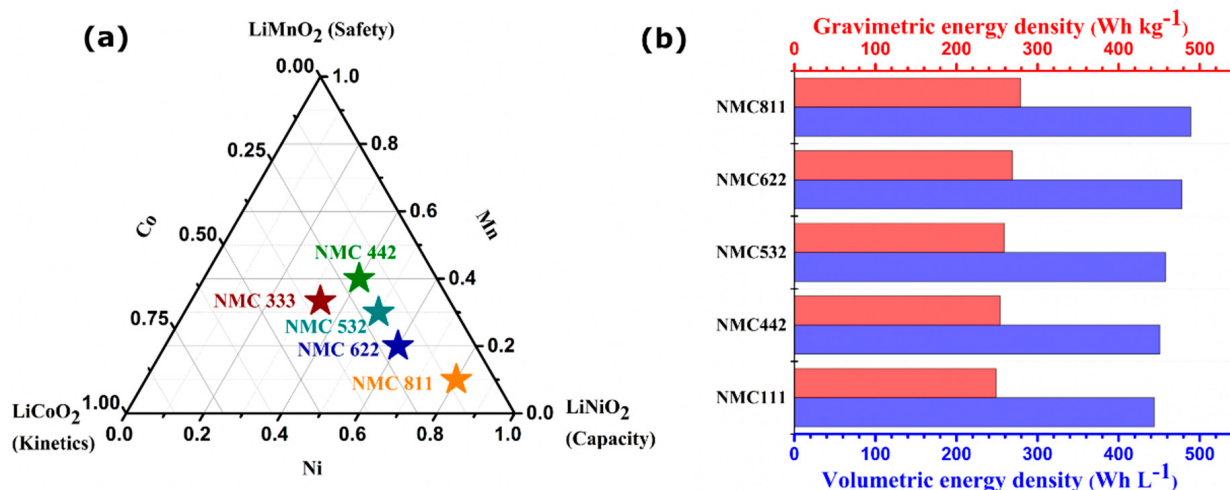


**Figure 9.** (a) Ternary phase diagram of Ni, Mn, and Co content in NMC. (b) Gravimetric and volumetric energy densities of  $\text{LiNi}_x\text{Mn}_y\text{Co}_z\text{O}_2$  ( $x + y + z = 1$ ).

### 5.1. $LiNi_{1/3}Mn_{1/3}Co_{1/3}O_2$ (NMC111)

NMC111 is considered the most commonly used commercial cathode with a theoretical capacity of 278 mAh g<sup>-1</sup> with an operating voltage of 4.3 V. Table 4 summarizes all the electrolyte and additive combinations for NMC111. Ohzuku et al. first reported the solid-state synthesis of this material and obtained 150 mAh gm<sup>-1</sup> of capacity with 1 M LiPF<sub>6</sub> in EC: DMC (3:7, v/v) within a voltage range of 2.5–4.2 V [120]. Moreover, 0.5 wt% of Tris(trimethylsilyl) phosphite (TMSPi) as an additive can push the upper cut-off voltage to 4.5 V [64]. Other linear carbonate electrolytes, such as DEC and EMC, are also used along with EC to reduce viscosity. For example, 1 M LiPF<sub>6</sub> in EC: EMC (3:7, w/w) (commonly known as LP57) is most commonly used by prominent research groups. Gasteiger et al. used LP57 to study the effect of upper cut-off voltage (UCV) on NMC111/graphite [14]. The highest specific capacity of 183.4 mAh g<sup>-1</sup> was achieved at 4.6 V but with poor capacity retention, whereas, at 4.4 V, the capacity was well maintained for 295 cycles at 1 C. Adding different electrolyte additives such as VC, PES, MMDS, DTD, TTSPi, and TTSP with a control electrolyte improves the cycling performance of an NMC/graphite pouch cell at various temperature ranges [65,72,121]. Ternary electrolyte solvent systems along with additives such as 3,3'-(ethylenedioxy)dipropiononitrile (EDPN), 3,3'-(sulfonyl)dipropiononitrile (SDPN) and di(methylsulfonyl) methane (DMSM) at UCV of 4.6 V show higher cathode voltage performances [122–124]. Boron-based additive trimethyl boroxine (TMB) with 1 M LiPF<sub>6</sub> in EC, DEC, and DMC enhances the cycle stability from 40% to 99% after 300 cycles at a 1 C rate [125]. Apart from carbonate electrolytes, thermally stable cyano-ester solvents with 1 M LiTFSI salt and 3 wt% FEC perform well in the full cell [126].

**Table 4.** Battery metrics for NMC111 full cells with various anodes, electrolytes, and additives.

Electrodes	Electrolytes	Additives	Voltage Range	Sp. Capacity (mAh g <sup>-1</sup> ) (C-Rate)	Capacity Retention, % (Cycles, C-Rate)
NMC111/graphite [14]	1 M LiPF <sub>6</sub> in EC: EMC (3:7, <i>w/w</i> )		3–4.2 V	140.2 (1 C)	93% (295, 1 C)
			3–4.4 V	162.8(1 C)	94% (295, 1 C)
			3–4.6 V	183.4(1 C)	42% (295, 1 C)
NMC111/graphite [79]	1 M LiPF <sub>6</sub> in EC: DEC (1:3, <i>w/w</i> )	1 wt% LiDFP	3–4.5 V		92.6% (100, 1 C)
NMC111/graphite [127]	1 M LiPF <sub>6</sub> in EC: EMC (3:7, <i>w/w</i> )	0.1 wt% MUI	2.8–4.6 V	197.3 (0.1 C)	63% (200, 0.3 C)
NMC111/graphite [65]	1 M LiPF <sub>6</sub> in EC: EMC (3:7, <i>w/w</i> )	2 wt% VC			84% (500, 0.4 C)
		2 wt% VC + 1 wt% MMDS			87% (500, 0.4 C)
		2 wt% VC + 1 wt% DTD			86% (500, 0.4 C)
		2 wt% VC + 1 wt% MMDS + 1 wt% TTSPi			88% (500, 0.4 C)
		2 wt% VC + 1 wt% DTD + 1 wt% TTSPi			90% (500, 0.4 C)
		3 wt% PES	2.8–4.2 V		87% (500, 0.4 C)
		2 wt% PES + 1 wt% MMDS			80% (500, 0.4 C)
		2 wt% PES + 1 wt% DTD			89% (500, 0.4 C)
		2 wt% PES + 1 wt% TTSPi			84% (500, 0.4 C)
		2 wt% PES + 1 wt% MMDS + 1 wt% TTSPi			89% (500, 0.4 C)
		2 wt% PES + 1 wt% DTD + 1 wt% TTSPi			91% (500, 0.4 C)
NMC111/graphite [72]	1 M LiPF <sub>6</sub> in EC: EMC (3:7, <i>w/w</i> )	2 wt% PES + 1 wt% MMDS + 1 wt% TTSPi	2.8–4.2 V (55 °C)		>80% (900, 0.4 C)
NMC111/graphite [121]	1 M LiPF <sub>6</sub> in EC: EMC (3:7, <i>w/w</i> )	2 wt% VC + 1 wt% DTD + 0.5 wt% TTSP + 0.5 wt% TTSPi	2.8–4.2 V (40 °C)		97% (500, C/2.2)
NMC111/graphite [126]	1 M LiTFSI in MCP	3 wt% FEC	2.8–4.2 V		94.4% (195, 1 C)
	1 M LiPF <sub>6</sub> in MCP				87.6% (195, 1 C)
	1 M LiPF <sub>6</sub> in PC				92.3% (195, 1 C)
NMC111/graphite [122]	1 M LiPF <sub>6</sub> in EC: DEC (1:3, <i>w/w</i> )	0.5 wt% EDPN	3–4.5 V 3–4.2 V	156.2 (1 C)	83.9% (100, 1 C) 91% (100, 1 C)
NMC111/graphite [123]	1 M LiPF <sub>6</sub> in EC: DMC: EMC (1:1:1, <i>w/w</i> )	0.2 wt% SDPN	3–4.6 V		77.3% (100, 0.2 C)
NMC111/graphite [124]	1 M LiPF <sub>6</sub> in EC: DMC: EMC (1:1:1, <i>w/w</i> )	0.1 wt% DMSM	3–4.6 V	175.1 (0.2 C)	80.1% (100, 0.2 C)
NMC111/graphite [128]	1 M LiPF <sub>6</sub> in EC: DMC: EMC (1:1:1, <i>w/w</i> )	0.2 wt% TFPM	3–4.6 V		75.4% (100, 0.2 C)
		0.5 wt% TFPE			76.1% (100, 0.2 C)
NMC111/Li [12]	1 M LiPF <sub>6</sub> in EC: DEC (1:1, <i>v/v</i> )		3–4.3 V (55 °C)	163 (0.1 C)	92.4% (100, 0.5 C)

**Table 4.** *Cont.*

Electrodes	Electrolytes	Additives	Voltage Range	Sp. Capacity (mAh g <sup>-1</sup> ) (C-Rate)	Capacity Retention, % (Cycles, C-Rate)
NMC111/Li [120]	1 M LiPF <sub>6</sub> in EC: DMC (3:7, v/v)		3.5–4.2 V	150 (0.17 mA/cm <sup>2</sup> )	
NMC111/Li [129]	1.2 M LiPF <sub>6</sub> in EC: PC: DMC (1:1:3, w/w)		2.9–4.6 V	200 (0.1 mA/cm <sup>2</sup> )	
NMC111/Li [130]	1 M LiPF <sub>6</sub> in EC: EMC (3:7, w/w)	2 vol% VC 2 vol% FEC 2 vol% ES	2.5–4.2 V	121 (0.1 C) 121 (0.1 C) 108 (0.1 C)	65% (150, 1 C) 95% (150, 1 C) 56% (150, 1 C)
NMC111/Li [64]	1 M LiPF <sub>6</sub> in EC: DMC (1:2, v/v)	0.5 wt% TMSPI	3–4.5 V		91.2% (100, 0.5 C)
NMC111/Li [46]	1 M LiPF <sub>6</sub> in EC: DMC: EMC (1:1:1 w/w)	1 wt% LiDFP 1 wt% LiDFP + 10 wt% FEC	2.8–4.3 V		67% (400, 1 C) 86.2% (400, 1 C)
NMC111/Li [131]	1 M LiPF <sub>6</sub> in EC: DEC (1:1 v/v)	2 wt% LiTDI	3–4.2 V (55 °C)		80% (830, 1 C)
NMC111/Li [132]	1 M LiPF <sub>6</sub> in EC: EMC: DEC (1:1:1, v/v/v)	0.5 wt% LiBOB 0.2 wt% LiDFOB	3–4.6 V	191 (0.6 C) 187.2 (0.6 C)	91.8% (60, 0.6 C) 88.2% (60, 0.6 C)
NMC111/Li [125]	1 M LiPF <sub>6</sub> in EC: DEC: DMC (3:5:2, w/w)	3 wt% TMB	3–4.5 V	154 (0.5 C)	99% (300, 1 C)
NMC111/Li [133]	1 M LiPF <sub>6</sub> in EC: EMC (3:7, w/w)	1 vol% VC	3–4.2 V	137 (0.1 C)	55% (200, 1 C)
NMC111/MCMB [133]	1 M LiPF <sub>6</sub> in EC: EMC (3:7, w/w)	1 vol% VC	3–4.2 V	132.5 (0.1 C)	97% (200, 1 C)

The respective C-rates and specific capacities are in parentheses.

### 5.2. $LiNi_{0.4}Mn_{0.4}Co_{0.2}O_2$ (NMC442)

Ni-rich NMC cathodes (NMC442) are cheaper by reducing the compound's cobalt amount, allowing for a charge potential of 4.7 V without any structural changes. The conventional electrolyte starts to degrade over the positive electrode above 4.3 V. All the electrolyte–additive combinations for NMC442 are tabulated in Table 5. Aiken et al. performed NMC442/graphite pouch cells at higher voltage (>4.2 V) in different temperature conditions and observed less gaseous product formation with 2 wt% PES additive in baseline electrolytes [134,135]. Nelson et al. studied the impedance growth of full cells after long-term cycling and reduced them with appropriate electrolyte additives [136]. The ternary mixture of additives such as PES211 is beneficial in mitigating impedance growth and retains its capacity up to 85% after 500 cycles at 4.4 V under 45 °C [72,137]. Petibon et al. tried to develop a new electrolyte combination free of EC that works better in all required electrochemical aspects [138]. Fluorinated electrolytes and 1 wt% PES showed better cycle stability of about 80% than binary and ternary additives-based EC: EMC (3:7, v/v) electrolytes [139]. As a high-voltage electrolyte, EC co-solvent can be replaced by sulfolane (SL), which has high anodic stability [140]. Rong and his co-workers have studied ternary electrolyte combinations and Tris (trimethylsilyl) phosphate (TMSP) as an additive for an NMC422 full cell, and it exhibited better rate performance [141].

**Table 5.** Battery metrics for NMC442 full cells with various anodes, electrolytes, and additives.

Electrodes	Electrolytes	Additives	Voltage Range	Sp. Capacity (mAh g <sup>-1</sup> ) (C-Rate)	Capacity Retention, % (Cycles, C-Rate)
NMC442/graphite [72,137]	1 M LiPF <sub>6</sub> in EC: EMC (3:7, <i>w/w</i> )	2 wt%PES + 1 wt%MMDS + 1 wt%TTSPi	3–4.4 V (45 °C)		85% (500, C/2.5)
NMC442/graphite [138]	1 M LiPF <sub>6</sub> in EMC:VC (98:2, <i>w/w</i> )	1% TAP or 1% PPF	2.8–4.4 (55 °C)		80% (350, C/2.5)
NMC442/graphite [139]	1 M LiPF <sub>6</sub> in FEC: TFEC (1:1, <i>w/w</i> )	1 wt% PES	2.8–4.5 (40 °C)		~80% (800, C/2.4)
NMC442/graphite [140]	1 M LiPF <sub>6</sub> in SL: EMC (3:7, <i>w/w</i> )	2 wt% VC + 2 wt% TAP	2.8–4.4 (40 °C)		80% (500, C/2.4)
NMC442/graphite [141]	1 M LiPF <sub>6</sub> in EC: DMC: EMC (1:1:1, <i>v/v</i> )	1 wt% TMSP	2.75–4.35 V	164.6(1 C)	90.8%(70, 1 C)

The respective C-rates and specific capacities are in parentheses.

### 5.3. $LiNi_{0.5}Mn_{0.3}Co_{0.2}O_2$ (NMC532)

Liu et al. applied one of the most popular additive VC in an NMC532/graphite full cell and tested it at an elevated temperature. VC-containing electrolyte cells produce fewer decomposition products than free ones [60]. A fluorinated additive such as FEC was studied in a Li metal battery and performed excellently [61]. Table 6 summarizes all the electrolyte additive combinations with NMC532. Phosphorus-containing electrolyte additive tris(trimethylsilyl)phosphite (TMSPi) and triethyl phosphite (TEPi) produce a protective surface film on the cathode side [68]. Salt-type additives such as lithium difluoro phosphate (LiDFP) are quite popular in Ni-rich cathode-based full cells with graphite as an anode at various temperatures [80,142]. Zuo et al. exhibited lower impedance due to interfacial modification by adding only 1 wt% of LiBF<sub>4</sub> in the baseline electrolyte [143]. A novel electrolyte additive, N, O-bis(trimethylsilyl)-trifluoroacetamide (NOB), is a nitrogen and silicon-containing compound that acts as an HF scavenger sacrificial additive [144]. Dimethyl sulfite (DMS) is a sulfur-containing electrolyte additive that performs under low temperatures of  $-10\text{ }^{\circ}\text{C}$  and outperforms commercially available additives [145]. Zuo et al. retained about 92.3% of initial capacity by adding 0.5 wt% of tris(trimethylsilyl)borate (TMSB) due to forming a thinner film on the surface [146]. Adding 1,10-sulfonyldiimidazole (SDM) can improve the electrochemical performance at high voltages [147]. The modified version of DTD, namely [4,4'-bi(1,3,2-dioxathiolane)] 2,2'-dioxide (BDTD), is also developed as a cathode additive, which improved the cycle retention up to 91.6% [148]. Shi and his co-workers used the synergistic effect of lithium sulfide ( $Li_2S$ ) salt and acetonitrile (AN) solvent additive and developed a stable cathode–electrolyte interface (CEI) layer, which reduced the electrolyte decomposition [149].

**Table 6.** Battery metrics for NMC532 full cells with various anodes, electrolytes, and additives.

Electrodes	Electrolytes	Additives	Voltage Range	Sp. Capacity (mAh g <sup>-1</sup> ) (C-Rate)	Capacity Retention, % (Cycles, C-Rate)
NMC532/graphite [60]	1 M LiPF <sub>6</sub> in EC: DEC (1:1 v/v)	1 wt% VC	2.5–4.2 V (60 °C)	159 (75 mA gm <sup>-1</sup> )	79% (100, 75 mA gm <sup>-1</sup> )
NMC532/graphite [68]	1.2 M LiPF <sub>6</sub> in EC: EMC (3:7 w/w)	1 wt% TMSPi 1 wt% TEPI	3–4.4 V	190 (0.1 C) 194.5 (0.1 C)	88.8% (119, 0.3 C) 81.7% (119, 0.3 C)
NMC532/graphite [80]	1 M LiPF <sub>6</sub> in EC: DEC (1:3 w/w)	1 wt% LiDFP	3–4.5 V	152.8 (0.1 C)	93.8% (100, 1 C)
NMC532/graphite [142]	1 M LiPF <sub>6</sub> in EC: EMC (1:2 w/w)	2 wt% LiDFP	2.75–4.4 V (25 °C) 2.75–4.4 V (45 °C) 2.75–4.2 V (-10 °C)		93% (150, 1 C) 86% (150, 1 C) 92.7% (100, 0.3 C)
NMC532/graphite [143]	1 M LiPF <sub>6</sub> in EC: EMC (1:2 w/w)	1 wt% LiBF <sub>4</sub>	3–4.5 V	178.1 (1 C)	90.1% (100, 1 C)
NMC532/graphite [144]	1 M LiPF <sub>6</sub> in EC: EMC: DEC (3:5:2 w/w)	1 wt% NOB	2.75–4.5 V (25 °C)		73% (100, 1 C)
NMC532/graphite [145]	1 M LiPF <sub>6</sub> in EC: EMC (1:2 w/w)	0.5 wt% DMS	2.75–4.2 V (-10 °C)		98.84% (50, 0.2 C)
			2.75–4.2 V (25 °C)		89.04% (350, 1 C)
		0.5 wt% DTD	2.75–4.2 V (45 °C) 2.75–4.2 V (-10 °C)		95.3% (100, 1 C) 81.14% (50, 0.2 C)
NMC532/graphite [146]	1 M LiPF <sub>6</sub> in EC: EMC (1:2 w/w)	0.5 wt% TMSB	2.5–4.4 V 3–4.4 V	181 (0.2 C) 167.9 (1 C)	92.3% (150, 1 C)
NMC532/graphite [147]	1 M LiPF <sub>6</sub> in EC: DEC: EMC (3:2:5, w/w)	0.25 wt% SDM	2.75–4.5 V		96.9% (50, 0.2 C)
NMC532/Li [150]	1 M LiPF <sub>6</sub> in EC: DMC (1:1 v/v)		3–4.3 V	150 (0.4 C)	95% (50, 0.4 C)
NMC532/Li [151]	1 M LiPF <sub>6</sub> in EC: DEC (1:1 v/v)		3–4.4 V	179.6 (0.2 C)	94.8% (80, 0.2 C)
NMC532/Li [61]	1 M LiPF <sub>6</sub> in EC: DEC (1:1 v/v)	5 vol% FEC	3–4.3 V	154 (1 C)	65% (100, 1 C)
NMC532/Li [152]	1 M LiPF <sub>6</sub> in EC: EMC (3:7 v/v)	2 wt% DTD	2.75–4.5 V		84% (100, 0.5 C)
NMC532/Li [148]	1 M LiPF <sub>6</sub> in EC: EMC (3:7 v/v)	2 wt% BDTD	3–4.6 V	189 (0.5 C)	91.6% (100, 0.5 C)
NMC532/Li [153]	1 M LiPF <sub>6</sub> in EC: DMC: DEC (1:1:1 v/v) 1 M LiBF <sub>4</sub> in FEC:SN (1:4 w/w)		3–4.5 V		56.3% (100, 0.5 C)
			3–4.7 V		35.5% (100, 0.5 C)
			3–4.5 V		81.6% (100, 0.5 C)
			3–4.7 V		73.6% (100, 0.5 C)
NMC532/Li [149] NMC532/graphite	1 M LiPF <sub>6</sub> in EC: DMC (3:7 v/v)	0.01 mg ml <sup>-1</sup> Li <sub>2</sub> S + 0.5 vol% AN	3–4.5 V 2.8–4.5 V		80.74% (200, 1 C) 81% (180, 0.5 C)

The respective C-rates and specific capacities are in parentheses.

#### 5.4. $LiNi_{0.6}Mn_{0.2}Co_{0.2}O_2$ (NMC622)

NMC622 is a more recent material than other matured NMC cathodes, and commercialization needs further modification. The advantage of increased energy density with Ni content attracts commercialization and reduces battery pack costs. Electrolyte additives or solvents that are stable at the upper cut-off voltage need to be developed to utilize the full potential of NMC622. The electrolyte optimization in a combination of solvents and additives for NMC622 is detailed in Table 7. Gasteiger et al. performed testing of NMC622/graphite full cells with different upper cut-off potential and temperature conditions to observe oxygen release due to electrolyte decomposition [154]. Small amounts of 1,4-phenylene diisocyanate (PPDI) acted as HF and  $H_2O$  scavengers and film-forming additives over the NMC622 cathode surface in pouch cells and exhibited long-term cyclability at a 1 C rate [155]. Liao et al. introduced a new kind of additive, namely 1-(2-cyanoethyl) pyrrole (CEP), which suppresses HF formation from cycling at high voltages [156]. Hexamethylene diisocyanate (HDI) [157] and 4-propyl-[1–3]dioxathiolane-2,2-dioxide (PDTD) [158] in 1 M LiPF<sub>6</sub> in EC: EMC (1:2, *w/w*) can reduce the interfacial impedance and increase cycling performance. Functional additives such as (3-(N, N-dimethylamino) diethoxypropyl) pentamethyldisiloxane (DSON) [159], p-toluenesulfonyl fluoride (pTSF) [160], triisopropyl borate (TIB) [161], diphenyldimethoxysilane (DPDMS) [162], 2,4,6,8-tetramethyl-2,4,6,8-tetravinylcyclotetrasiloxane (ViD4) [163], 3-hexylthiophene (3HT) [164], and tris(hexafluoroisopropyl)phosphate (THFP) [165] are assigned with different roles, such as film-forming ability, HF scavenger, gas-suppressing agent, and thermal safety.

**Table 7.** Battery metrics for NMC622 full cells with various anodes, electrolytes, and additives.

Electrodes	Electrolytes	Additives	Voltage Range	Sp. Capacity (mAh g <sup>-1</sup> ) (C-Rate)	Capacity Retention, % (Cycles, C-Rate)
NMC622/graphite [154]	1 M LiPF <sub>6</sub> in EC: EMC (3:7 w/w)		3–4.4 V (25 °C)	174 (1 C)	84% (308, 1 C)
			3–4.4 V (40 °C)	184 (1 C)	85% (308, 1 C)
			3–4.4 V (50 °C)	190 (1 C)	73% (308, 1 C)
NMC622/graphite [166]	2.3 mol kg <sup>-1</sup> LiTFSI in EC: DME (1:2 v/v)		2.75–4.2 V	169.3 (0.5 C)	98.7% (50, 0.5 C)
NMC622/graphite [155]	1 M LiPF <sub>6</sub> in EC: EMC (1:2, w/w)	0.5 wt% PPDI	3–4.2 V (rt) 3–4.2 V (45 °C)		84.9% (600, 1 C) 81.3% (300, 1 C)
NMC622/graphite [156]	1 M LiPF <sub>6</sub> in EC: EMC (1:2, w/w)	1 wt% CEP	3–4.5 V		81.5% (50, 1 C)
NMC622/graphite [157]	1 M LiPF <sub>6</sub> in EC: EMC (1:2, w/w)	0.1 wt% HDI	3–4.2 V		82.9% (600, 1 C)
NMC622/graphite [158]	1 M LiPF <sub>6</sub> in EC: EMC (1:2, w/w)	1 wt% PDTD	3–4.2 V		83.7% (500, 1 C)
NMC622/Li [159] NMC622/graphite	1 M LiPF <sub>6</sub> in EC: EMC: DMC (1:1:1, v/v)	0.25 wt% DSON	3–4.3 V 3–4.2 V (55 °C)		84.7% (100, 1 C) 66.8% (50, 0.5 C)
NMC622/graphite [160] NMC622/Li	1 M LiPF <sub>6</sub> in EC: DEC: EMC (3:2:5, w/w)	1 wt% pTSF	3–4.35 V (25 °C)		88% (600, 1 C)
			3–4.35 V (55 °C)		75% (300, 1 C) 89% (100, 1 C)
NMC622/Li [167]	1.2 M LiPF <sub>6</sub> in DFEC: EMC (3:7 v/v)		3–4.4 V	189.9 (0.1 C)	83% (400, C/3)
NMC622/Li [168]	1.15 M LiPF <sub>6</sub> in EC: EMC (3:7, v/v)	2 wt% VC	3–4.3 V (60 °C)	180.9 (C/5)	91.2% (60, 1 C)
NMC622/Li [169]	1 M LiPF <sub>6</sub> in EC: EMC: DEC (1:1:1, v/v/v)	10 wt% FEC	2.8–4.6 V	196.3 (1 C)	87.3% (100, 1 C)
NMC622/Li [161]	1 M LiPF <sub>6</sub> in EC: EMC: DEC (1:1:1, w/w/w)	1 wt% TIB	3–4.5 V	183.4 (1 C)	82.7% (300, 1 C)
NMC622/Li [162]	1 M LiPF <sub>6</sub> in EC: EMC: DMC (1:1:1, v/v/v)	1 wt% DPDMS	2.8–4.3 V	168.2 (1 C, 25 °C)	93.3% (200, 2 C, 55 °C)
NMC622/Li [163]	1 M LiPF <sub>6</sub> in EC: EMC: DMC (1:1:1, v/v/v)	0.5 wt% ViD4	3–4.5 V	187.2 (0.2 C)	83.6% (150, 1 C)
		0.5 wt% D4		187.7 (0.2 C)	81.3% (150, 1 C)
		0.5 wt% OMCTS		187 (0.2 C)	81.9% (150, 1 C)
NMC622/Li [164]	1 M LiPF <sub>6</sub> in EC: EMC (3:7, w/w)	0.5 wt% LiDFOB 0.25 wt% 3HT	2.8–4.5 V		91.6% (50, 0.1 C) 93.5% (50, 0.1 C)
NMC622/Li [165]	1 M LiPF <sub>6</sub> in PC: EMC: TEP (42.5:42.5:15, v/v)	2 wt% THFP	2.8–4.3 V	160 (100 mA g <sup>-1</sup> )	82% (200, 100 mA g <sup>-1</sup> )

The respective C-rates and specific capacities are in parentheses.

### 5.5. $LiNi_{0.8}Mn_{0.1}Co_{0.1}O_2$ (NMC811)

Another Ni-rich NMC, NMC811, is also quite popular in battery research labs due to its high specific capacity of 200 mAh  $gm^{-1}$  at 4.3 V and low cost (less cobalt). However, its low cycling stability at high voltages and inferior safety issue makes it a poor choice for a commercial approach. An optimized combination of electrolytes with its additives enhances the performance of NMC811 with both graphite and lithium metal anodes. The battery metrics of NMC811 with various electrolyte–additive combinations are tabulated in Table 8. Gasteiger et al. studied oxygen release and cycle stability in NMC811/graphite full cells at different end-of-charge potentials [14]. A combination of VC and TMSPi additives in 1 M LiPF<sub>6</sub> in EC: DMC (1:1, v/v) enhances the capacity retention and achieves 91% after 200 cycles [67]. The addition of triphenylphosphine oxide (TPPO) to the baseline electrolyte improves the cell’s first coulombic efficiency and specific capacity [170]. Lan et al. proposed a new additive, phenyl trans-styryl sulfone (PTSS), which builds a stable interfacial film on the surface during the charge–discharge process [171]. The multifunctional film-forming additive, 4-fluorobenzene sulfonate (PFBS), constructs a stable interface layer on both positive and negative electrodes and protects the electrolyte solvent from decomposition and structural degradation [172]. Adiponitrile (ADN) is a nitrile group that contains additives favorable for high-voltage performance and low flammability [173].

3,3-diethylene di-sulfite (DES) forms a stable protection layer on the cathode surface and assists in the Li<sup>+</sup> ion extraction/insertion process [174]. Cheng et al. proposed binary additives, which are comprised of lithium difluoro(oxalato)borate (LiDFOB) and tris(trimethylsilyl)phosphate (TMSP), and checked their capability in both half-cell and full-cell and even in the commercial pouch cell at different conditions. The synergistic effect of both additives produces B-, Si-, and F-rich interface layers, which protect electrolyte decomposition, gas formation, and the cathode from structural degradation [175]. Film-forming additives such as tris(trimethylsilyl)borate (TMSB) [176], triphenyl phosphate (TPPa) [177], phenyl vinyl sulfone (PVS) [178], and 2,4,6-triphenyl boroxine (TPBX) [179] are also reported in NMC811-cathode-based Li-metal batteries. Multifunctional organic electrolyte additives such as ethoxy(pentafluoro) cyclotriphosphazene (PFN) [180] and trimethylsilyl trifluoroacetate (TMSTFA) [181] act as both the HF/H<sub>2</sub>O scavenger and the stable CEI layer-forming agent. Hu et al. reported a functional electrolyte additive, cyclopropane sulphonic amide (CPSA), combined with ether electrolyte to improve electrochemical properties [182].

**Table 8.** Battery metrics for NMC811 full cells with various anodes, electrolytes, and additives.

Electrodes	Electrolytes	Additives	Voltage Range	Sp. Capacity (mAh g <sup>-1</sup> ) (C-Rate)	Capacity Retention, % (Cycles, C-Rate)
NMC811/graphite [14]	1 M LiPF <sub>6</sub> in EC: EMC (3:7 w/w)		3–4.0 V 3–4.1 V 3–4.2 V	131.9 (1 C) 149.3 (1 C) 172.5 (1 C)	90% (296, 1 C) 77% (296, 1 C) 66% (296, 1 C)
NMC811/graphite [67]	1 M LiPF <sub>6</sub> in EC: DMC (1:1, v/v)	1 vol% VC + 1 vol% TMSPi	2.75–4.2 V		91% (200, C/3)
NMC811/graphite [170]	1 M LiPF <sub>6</sub> in EC: EMC (3:7, w/w)	0.5 wt% TPPO	2.8–4.3 V	198 (0.1 C)	92% (97, 0.5 C)
NMC811/graphite [171]	1 M LiPF <sub>6</sub> in EC: DMC (3:7, w/w)	1 wt% PTSS	3–4.35 V	117 (0.2 C)	62.7% (100, 1 C)
NMC811/graphite [172]	1 M LiPF <sub>6</sub> in EMC:EC: DMC (5:3:2, w/w)	1 w% PFBS	3–4.2 V (25 °C) 3–4.2 V (45 °C)		89.9% (400, 1 C) 89.01% (400, 1 C)
NMC811/graphite [173]	1 M LiPF <sub>6</sub> in EC: EMC (3:7, v/v)	0.5 wt% ADN	2.7–4.3 V		85.60% (200, 0.3 C)
NMC811/graphite [174]	1 M LiPF <sub>6</sub> in EC: EMC (1:2, w/w)	0.25 wt% DES 1 wt% DES	2.75–4.3 V 2.75–4.5 V		77.25% (300, 1 C) 82.53% (150, 1 C)
NMC811/Li [175]			2.7–4.5 V 2.7–4.7 V		74.5% (800, 1 C) 76.3% (500, 1 C)
	1.1 M LiPF <sub>6</sub> in EC: DEC (1:1, v/v)	0.1 M LiDFOB + 2 wt% TMSP	2.7–4.3 V (45 °C) 2.7–4.5 V (45 °C)		85% (500, 1 C) 90% (400, 1 C)
NMC811/graphite			2.7–4.5 V		82.8% (500, 1 C)
NMC811/Li Pouch			2.7–4.5 V		94% (200, 1 C)
NMC811/Li [176]	1 M LiPF <sub>6</sub> in EC: DEC (1:1, v/v)	0.5 wt% TMSB	2.7–4.3 V	165.8 (0.2 C)	
NMC811/Li [177]	1 M LiPF <sub>6</sub> in EC: EMC (1:2, v/v)	2 wt% TPPa	3–4.3 V (55 °C)	210.5 (0.1 C)	63.5% (100, 1 C)
NMC811/Li [178]	1 M LiPF <sub>6</sub> and 0.1 M LiDFOB in EC: FEC: EMC: DEC (2:1:5:2 w/w)	1 wt% PVS	3–4.3 V		80.8% (400, 0.5 C) 80.0% (400, 1 C)
NMC811/Li [179]	1 M LiPF <sub>6</sub> in EC: EMC: DEC (5:3:2, w/w/w)	5 wt% TPBX	3–4.35 V	192.1 (1 C)	78% (100, 1 C)
NMC811/Li [180]	1 M LiPF <sub>6</sub> in FEC: DMC (1:1, v/v)	3 wt% PFN 3 wt% PFN + 2 wt% LiDFOB	2.7–4.4 V		92.5% (50, 0.5 C) 84.2% (100, 0.5 C)
NMC811/Li [181]	1 M LiPF <sub>6</sub> in EC: DMC: EMC (1:1:1, v/v/v)	0.2 wt% TMSTFA	3–4.3 V	149 (1 C)	80% (200, 1 C)
NMC811/Li [182]	1 M LiFSI in DOL: DME (1:1, w/w)	1 wt% CPSA	3–4.3 V	157.08 (0.5 C)	82.39% (180, 0.5 C)

The respective C-rates and specific capacities are in parenthesis.

## 6. Single-Crystal NMC

Commercially available NMC cathodes are poly-crystalline. Polycrystals are secondary particles with many nano-sized primary particles. Significant challenges experienced by polycrystal cathodes are cathode–electrolyte interface (CEI) layer formation, cation disordering, micro-cracks formation, and evolution of gaseous product during continuous cycling [183,184]. Single-crystal NMC (SC-NMC) synthesis can be a cutting-edge approach to mitigate all of these problems. The advantages of single-crystal NMCs compared to polycrystals (PCs) are a longer cycle life, high-voltage stability, higher volumetric energy density, less stress crack formation, less unwanted interfacial reaction, controllable crystal facet orientation, a low amount of gas formation, and higher mechanical and thermal stability [185,186]. The absence of intergranular stress micro-cracks originating from the phase change helps improve cyclic performance. The packing density is higher for SC-NMC due to the excellent distribution of primary particles, facilitating higher volumetric energy density. However, there are similarities in synthesis methods for polycrystals and single crystals due to the matching crystal growth process with SC-NMC requiring more synthetic control for particle morphology, size, and dispersion. The sintering process involves conventional solid-state and molten salt methods. For SC-NMC, the solid-state method is more widely accepted commercially for SCs and requires higher sintering temperatures and excess lithium sources than PCs with a secondary sintering process in the case of the agglomeration of the particles. The molten salt method generates uniform crystal growth at relatively low temperatures in a molten salt medium. The method has the following challenges for large-scale production: (i) volatilization of molten salt, (ii) cost of the salt, (iii) post-washing, and (iv) post-heat treatment. The need for an excess lithium salt source and tedious heat treatment is another common problem for both SCs synthesis methods and affects the production cost for industrial applications.

Dahn's group has extensively studied single-crystal NMC532 by optimizing it with different electrolytes and other testing conditions to obtain stable cycles (5000) for pouch cells [187,188]. Dahn et al. reported cathodes with nickel-rich content ( $\text{Ni} \geq 0.6$ ) to increase energy output [189–191]. NMC6.5:2.5:1 is an optimized composition due to higher capacity retention above 4.2 V, favorable specific capacity, and less reactivity with electrolytes at temperatures  $\sim 40^\circ\text{C}$  [192]. The demerits associated with SC-NMC are kinetic limitation of lithium diffusion, cation disordering during high-temperature sintering, intragranular micro-cracks formation, and unwanted parasitic reactions at the cathode–electrolyte interface at a high voltage or temperature [189,193–197]. Different modification strategies such as surface coating, elemental doping, morphology regulation, and electrolyte system optimization with additives are applied to mitigate all problems that directly or indirectly affect their electrochemical performances.

PVDF binder with NMP solvent is the most commonly reported binder for single-crystal cathode materials. Electrolytes with different functional additives help build protective layers on cathode surfaces. Table 9 summarizes all the data of SC-NMC with varying types of electrolyte systems and additives. Apart from the liquid electrolytes, some researchers have also studied the capability of SC-NMC in solid-state lithium-ion batteries [198–203]. Wang et al. obtained an almost  $30 \text{ mAh g}^{-1}$  higher capacity at a C/10 rate for SC-NMC532 compared to the polycrystalline one, and the capacity gain increases with higher current densities. A higher lithium diffusion coefficient is also responsible for better rate performance [204]. Crystal morphology and facet modifications can improve the solid-state battery performance by providing better contact and a smooth 3D lithium-ion diffusion pathway. The octahedral crystal morphology of NMC622 with exposed (012) facets shows superior rate capability compared to other morphological counterparts [205]. A polymer-composite-based electrolyte is also used with  $\text{LiNi}_{0.6}\text{Mn}_{0.1}\text{Co}_{0.3}\text{O}_2$  (NMC613) to alleviate intergranular crack formation during cycling [206]. Further modification of the Ni-rich cathode with a surface coating of  $\text{Li}_{1.4}\text{Al}_{0.4}\text{Ti}_{1.6}(\text{PO}_4)_3$  (LATP) decelerates structural degradation and stabilizes cycling performances [207].

**Table 9.** Electrochemical performance of single-crystal NMC in half cells and full cells with various electrolyte–additive compositions.

Electrodes	Electrolytes	Additives	Voltage Range (V)	Temperature (°C)	Sp. Capacity (mAh g <sup>-1</sup> ) (C-Rate)	Capacity Retention, % (Cycles, C-Rate)
NMC111/Li [208]	1 M LiPF <sub>6</sub> in EC: EMC (3:7 w/w)		2.8–4.3 V		163.9 (0.1 C)	~85% (300, 0.5 C)
NMC111/Li [209]	1 M LiPF <sub>6</sub> in EC: DMC (3:7 v/v)		2.8–4.4 V	25	160 (0.1 C)	
NMC111/Li [210]	1 M LiPF <sub>6</sub> in EC: DMC (1:1 v/v)		2.5–4.4 V	25 55	171 (0.1 C)	97.2% (100, 0.1 C) 96.2% (80, 0.1 C)
NMC111/Li [211]	1 M LiPF <sub>6</sub> in EC: DEC: EMC (1:1:1 v/v)		2.8–4.4 V		173.1 (0.1 C)	88.7% (50, 0.1 C)
LiNi <sub>0.5</sub> Co <sub>0.25</sub> Mn <sub>0.25</sub> O <sub>2</sub> /Li [212]	1 M LiClO <sub>4</sub> in EC: EMC (3:7 w/w)	1 wt% LiPO <sub>2</sub> F <sub>2</sub>	3–4.3 V	25 55	154 (1 C) 156 (1 C)	95.3% (200, 1 C) 91.6% (100, 1 C)
NMC532/Li [213]			2.75–4.4 V	25	177.5 (1 C)	90.6% (100, 1 C)
	1 M LiPF <sub>6</sub> in EC: DEC (1:1 v/v)		2.75–4.6 V	25	187.4 (1 C)	81% (100, 1 C)
NMC532/graphite			2.75–4.4 V	55	175.9 (1 C)	92.6% (100, 1 C)
			2.75–4.4 V	45	172.6 (1 C)	98.7% (500, 1 C)
NMC532/Li [214]	1 M LiPF <sub>6</sub> in EC: EMC: DMC (3:2:5 v/v)		3–4.5 V		167.3 (1 C)	90.3% (100, 1 C)
NMC532/graphite [215]	1 M LiPF <sub>6</sub> in EMC: DEC: DMC (1:1:1 v/v)		3–4.2 V	25	141.2 (1 C)	99% (1000, 1 C)
NMC532/graphite [216]	1 M LiPF <sub>6</sub> in EC: EMC (3:7 w/w) 1 M LiPF <sub>6</sub> in EMC	2 wt% PES + 1 wt% TTSPi + 1 wt% DTD 5 wt% FEC	3–4.4 V	40		~97% (800, C/2) ~96% (800, C/2)
NMC532/graphite [217]	1 M LiPF <sub>6</sub> in EC: EMC (3:7 w/w)	1 wt% DTD 2 wt% FEC 2 wt% VC 2 wt% FEC + 1 wt% DTD 2 wt% VC + 1 wt% DTD	3–4.2 V	40		96.8% (400, C/3) 96.4% (400, C/3) 95.8% (400, C/3) 97.6% (400, C/3) 97.3% (400, C/3)
NMC622/Li [218]	1 M LiPF <sub>6</sub> in EC: DEC: DMC (1:1:1 v/v)		2.8–4.3 V		183.7 (0.2 C)	89.93% (100, 0.2 C)
NMC622/Li [219]	1 M LiPF <sub>6</sub> in EC: DEC: DMC (1:1:1 v/v)		2.8–4.3 V	25	171.3 (0.1 C)	83.3% (200, 1 C)
NMC622/graphite			2.8–4.35 V	25	179.3 (0.1 C)	85.24% (800, 1 C)
NMC622/Li [220]	1 M LiPF <sub>6</sub> in EC: DMC: EMC (1:1:1 v/v)		2.8–4.5 V		190.4 (0.1 C)	96.5% (50, 1 C)
NMC622/Li [221]	1 M LiPF <sub>6</sub> in EC: DMC (1:1 v/v)		2.8–4.3 V		175.5 (0.1 C)	84.4% (100, 1 C)
NMC622/Li [222]	1 M LiPF <sub>6</sub> in EC: DMC (1:1 v/v)		2.8–4.5 V		190.1 (1 C)	96% (50, 1 C)
NMC622/Li [208]	1 M LiPF <sub>6</sub> in EC: EMC (3:7 w/w)		2.8–4.3 V		176 (0.1 C)	87.1% (200, 0.5 C)

**Table 9.** Cont.

Electrodes	Electrolytes	Additives	Voltage Range (V)	Temperature (°C)	Sp. Capacity (mAh g <sup>-1</sup> ) (C-Rate)	Capacity Retention, % (Cycles, C-Rate)
NMC622/Li [223]	1 M LiPF <sub>6</sub> in EC: EMC (3:7 w/w)	2 wt% VC	2.8–4.3 V	30 55 30	183 (0.1 C)	~94% (300, 1 C) ~85% (300, 1 C) 80% (800, 1 C)
NMC622/graphite						
NMC622/Li [189]	1 M LiPF <sub>6</sub> in EC: DEC (1:2 v/v)	2 wt% FEC + 1 wt% DTD	3–4.4 V	30		~96% (50, C/5)
NMC811/Li [224]	1 M LiPF <sub>6</sub> in EC: DMC (1:1 v/v)		2.7–4.3 V	25	206.3 (0.1 C)	93% (100, 0.1 C)
NMC811/Li [225]	1 M LiPF <sub>6</sub> in EC: DMC (1:1 v/v)		3–4.3 V		203.4 (0.1 C)	95.5% (300, 1 C)
NMC811/Li [226]	1 M LiPF <sub>6</sub> in EC: DMC (1:1 v/v)		2.8–4.3 V		226.9 (0.1 C)	95.1% (100, 1 C)
NMC811/Li [227]	1 M LiPF <sub>6</sub> in EC: EMC (3:7 w/w)		2.8–4.5 V		199 (C/2)	
NMC811/Li [228]	1 M LiPF <sub>6</sub> in EC: DEC: FEC (3:6:1 v/v)		2.5–4.3 V	30	162 (C/20)	90% (90, C/5)
NMC811/Li [229]	1 M LiPF <sub>6</sub> in EC: DMC: EMC (1:1:1 v/v)		2.8–4.5 V		221.2 (0.1 C)	91.6% (50, 1 C)
NMC811/Li [230]	1 M LiPF <sub>6</sub> in EC: DMC: DEC (1:1:1 v/v)		3–4.3 V		206 (0.1 C)	92% (200, 0.5 C)
NMC811/Li [231]	1 M LiPF <sub>6</sub> in EC: DMC: EMC (1:1:1 v/v)		2.8–4.3 V		196.7 (0.2 C)	95.2% (100, 1 C)
NMC811/Li [232]	1 M LiPF <sub>6</sub> in EC: DMC: EMC (1:1:1 v/v)		3–4.4 V	25 55 25	216 (0.1 C) 209 (1 C)	81.8% (200, 1 C) 85.3% (100, 1 C) 85% (100, 4 C)
NMC811/Li [233]	1 M LiPF <sub>6</sub> in EC: DMC: EMC (1:1:1 w/w)		2.8–4.3 V		198.9 (0.1 C)	96.2% (150, 1 C)
NMC811/Li [234]	1.15 M LiPF <sub>6</sub> in EC: DMC: EMC (3:3:4 v/v)		3–4.45 V		176 (0.1 C)	
NMC811/Li [190]	1.5 M LiPF <sub>6</sub> in EC: EMC: DMC (25:5:70 v/v)	2 wt% FEC + 1 wt% LFO	3–4.2 V	55		~85% (1000, C/3)
LiNi <sub>0.83</sub> Mn <sub>0.07</sub> Co <sub>0.10</sub> O <sub>2</sub> /Li [235]	1 M LiPF <sub>6</sub> in EC: DEC (3:7 w/w)		3–4.5 V 3–4.9 V 3–4.35 V			94.5% (30, 0.5 C) 93.3% (15, 0.1 C) 84.8% (400, 0.5 C)
LiNi <sub>0.83</sub> Mn <sub>0.07</sub> Co <sub>0.10</sub> O <sub>2</sub> /graphite						
LiNi <sub>0.83</sub> Mn <sub>0.05</sub> Co <sub>0.12</sub> O <sub>2</sub> /Li [236]	1 M LiPF <sub>6</sub> in EC: DEC (1:1 v/v)		2.75–4.3 V	25	209.7 (0.1 C)	99.56% (100, 0.2 C)
LiNi <sub>0.83</sub> Mn <sub>0.05</sub> Co <sub>0.12</sub> O <sub>2</sub> /Li [237]	1.2 M LiPF <sub>6</sub> in EC: EMC (3:7 v/v)	2 wt% VC	2.8–4.3 V		209 (0.1 C)	96.6% (100, 1 C) 93.1% (200, 1 C)
LiNi <sub>0.9</sub> Co <sub>0.055</sub> Mn <sub>0.045</sub> O <sub>2</sub> /Li [238]	1 M LiPF <sub>6</sub> in EC: DMC: EMC (1:1:1 v/v)		2.8–4.3 V	27	220.6 (0.1 C)	93% (50, 1 C)
LiNi <sub>0.91</sub> Mn <sub>0.03</sub> Co <sub>0.06</sub> O <sub>2</sub> /Li [239]	1 M LiPF <sub>6</sub> in EC: DMC: EMC (1:1:1 v/v)		3–4.3 V		203.8 (0.1)	80.8% (70, 0.5 C)

The respective C-rates and specific capacities are in parenthesis.

## 7. Commercial Aspects of NMC

Over the past few decades, electric vehicles have boomed with lithium-ion batteries that have high energy contents of  $260 \text{ Wh kg}^{-1}$  or  $700 \text{ Wh L}^{-1}$  at the cell level and higher efficiencies (>99%) [240]. The cathode seems critical in achieving these energy densities with high reversible specific capacities and discharge potentials vs. Li/Li<sup>+</sup>. Table 10 represents cell chemistry present in different electric vehicles with their specifications. The battery cost is another vital controlling factor before commercialization, looking for a pack cost of USD 100–125 kWh<sup>-1</sup> to compete with conventional combustion energy-driven vehicles.

Wentker et al. introduced a bottom-up approach model to calculate the cost and performance of commercial cathode materials [241]. An estimate of the cost-to-performance ratio (R) to evaluate their economic prospects is provided, as Tyagi et al. suggested [242].

$$R = \frac{\text{Cost } (\frac{\$}{\text{kWh}})}{\text{Energy density } (\frac{\text{Wh}}{\text{kg}})}$$

Figure 10a,b show the cost and energy density of different compositions of NMC with calculated R-values for commercialization. The R-value decreases with the reduction in Co content. Figure 10c,d show commercial electric vehicles' energy density and R-values with organic liquid electrolytes.

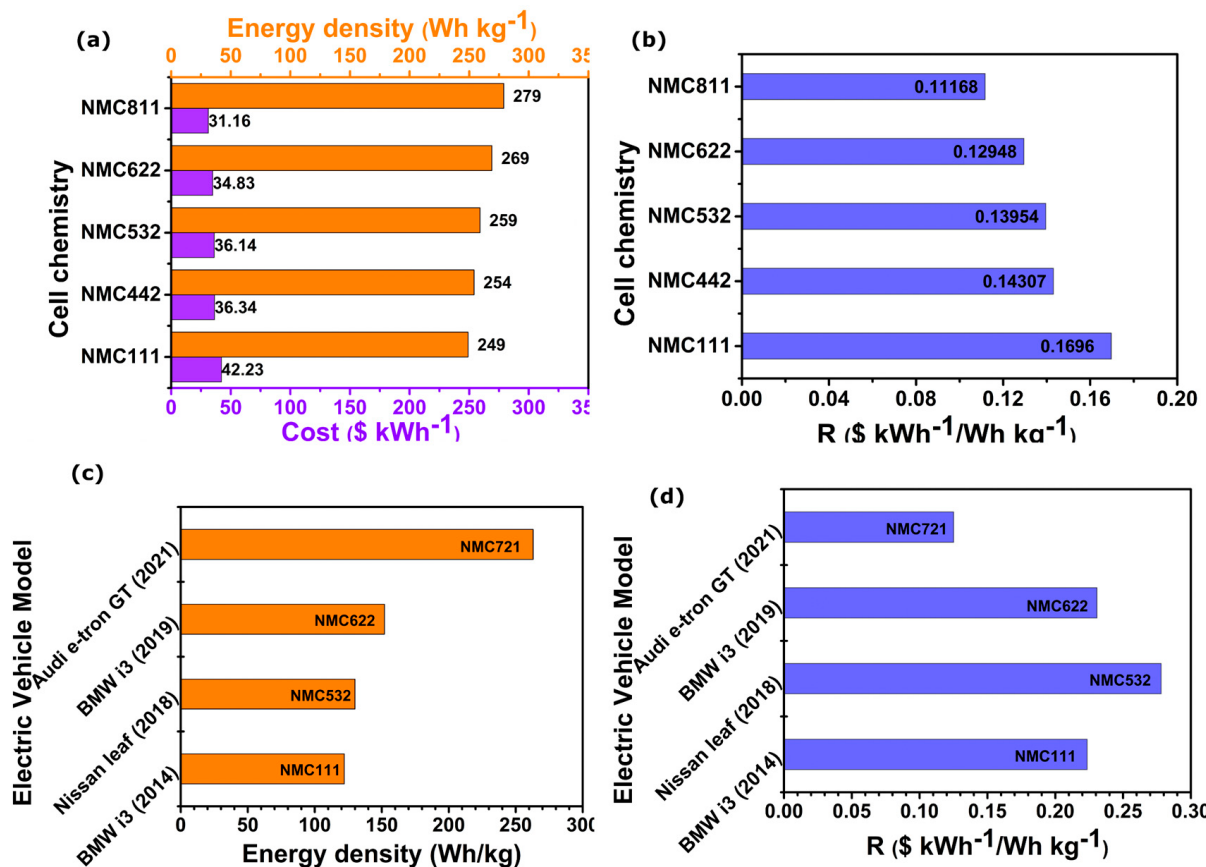


**Figure 10.** (a) Cathode active material cost and energy density; (b) R-value, i.e., cost to performance ratio of different NMC compositions (adapted from reference [241]); (c) energy density; (d) R-value of NMC in other commercial electric vehicles.

**Table 10.** Energy output and driving range of commercialized NMC cathode from automobile manufacturers (2013–2021) [243–245].

Cell Chemistry (Cathode/ Anode)	Cell Specification						Battery Packs		Electric Vehicle Model
	Producer	Type	Capacity (Ah)	Voltage(V)	Specific Energy (Wh kg <sup>-1</sup> )	Energy Density (Wh L <sup>-1</sup> )	Energy (kWh)	Range (km)	
NMC/LTO	Toshiba	Prismatic	20	2.30	89	200	20	130	Honda Fit EV (2013)
NMC111/C	Li-Tec	Pouch	52	3.65	152	316	17	145	Smart Fortwo EV (2013)
NMC111/C	Samsung SDI	Prismatic	60	3.7	122	228	22	130	BMW i3 (2014)
NMC622/C	SK Innovation	Pouch	38	3.70			27	145	Kia Soul EV (2014)
NMC/C	Panasonic	Prismatic	25	3.70	130	215	24	190	VW e-Golf (2015)
NMC/C	LG Chem	Pouch	56	3.65	186	393	60	383	Chevrolet Bolt (2016)
NMC111/C	Samsung SDI	Prismatic	94	3.7	189	357	33	183	BMW i3 (2017)
NMC721/C	LG Chem	Pouch	59	3.70	241	466	41	400	Renault Zoe (2017)
NMC532/C	AESC	Pouch	56.3	3.65	130	205	39	240	Nissan Leaf (2018)
NMC622/C	Samsung SDI	Prismatic	120	3.7			42	246	BMW i3 (2019)
NMC721/C	LG Chem	Pouch	64.6	3.7	259	648	93.4	100	Porsche Taycan (2019)
NMC532/C	LG Chem	Pouch					78	292	Volvo XC40 (2019)
NMC721/C	LG Chem	Pouch	145	1.85	164	267	58	350–544	Volkswagen ID.3
NMC622/C	LG Chem	Pouch	55	3.75	151	228	65	417	Chevrolet Bolt (2020)
NMC622/C (Li-ion Polymer)	SK Innovation	Pouch	180	3.56	250		64	391	Kia Soul EV (2020)
NMC622/C	LG Chem	Laminated	56.3		151		62	364	Nissan Leaf E plus (2020)
NMC721/C	LG Chem	Pouch	64.6	3.65	263	648	85	392	Audi e-tron GT (2021)
NMC721/C	LG Chem	Pouch	78	3.65	156		77	305	Audi Q4 e-tron-SUV (2021)
NMC622/C	LG Chem (Umicore)	Pouch	60		142	164	64	484	Hyundai KONA Electric (2021)
NMC/C (Li-ion Polymer)	LG Chem	Pouch					77	488	Hyundai ioniq 5-LR AWD (2021)
NMC811/C (Li-ion Polymer)	SK Innovation	Pouch	180	3.56	250		64	370	Kia Niro (2021)
NMC811/C (Li-ion Polymer)	LG Chem	Pouch	11.2		163	230	78	303	Kia EV6-LR AWD (2021)

## 8. Summary and Perspectives

$\text{LiNi}_x\text{Mn}_y\text{Co}_z\text{O}_2$  (NMC) is the most successful cathode material due to its improved energy density and the smaller amount of cobalt. NMC333, NMC442, and NMC532 are state-of-the-art cathode materials in the LIB market. Ni-rich cathodes such as NMC622 and NMC811 are maturing cathodes for EVs with high specific capacities and lower costs. Ni-rich NMC cathodes face challenges such as cation mixing, detrimental side reactions, and phase transformations, leading to rapid capacity fading and poor battery performance. Strategies and modifications/optimizations on structural stability, binder, electrolyte, and electrolyte additives to extract maximum battery performance without appreciable degradation on cycling are currently aplenty in the literature. In this review, the effects of various binders and electrolytes/additives for NMC cathode-based half/full cells were collated extensively from the literature and critically analyzed.

To extract the best characteristics of the NMC cathodes, a compatible binder and electrolyte system has to be designed by optimizing the electrolyte–additives and binder to enhance the cycling capability without any deterioration in the cathode crystal structure. The synthesis of novel additives with different functional groups (nitrile, amine, fluorocarbon, ether, ester) and interfacial engineering for the electrode–electrolyte interface can improve the structural integrity and stability of the SEI layer. Figure 11a,b show the specific capacity and normalized capacity retention of NMC-based full-cell and half-cell compositions, respectively. The best combinations of electrolyte systems with additives (line marks) and without additives in the best voltage range of performance are graphically summarized [68,127,132,141,148,156,169,170,179]. In full cells with graphite, NMC 111 and NMC 811 have comparable specific capacities, but NMC 811 shows drastic improvement in reversible capacity in an optimized additive/electrolyte combination (Figure 11a).

Single-crystal (SC) NMC cathodes can provide better structural integrity, cycling stability, and thermal safety than polycrystals. SC-NMC consists of micron-sized particles with highly compacted and volumetric energy density. Novel optimized synthetic methods, hetero-atom doping, and surface coating can further improve the SC-NMC cathodes. The impact of non-electrode components on SC-NMC, which was missing until now, is presented in this review. Compared to polycrystals, SC-NMC (optimized for reversible capacity and C-rate capabilities) shows better electrochemical performance with solid-state electrolytes and can be favorable for the future commercial market. The literature is inconsistent about the battery metrics of SC-NMC; the cycling retention improves, but the capacity and rate capability of SC-NMC must be optimized for further commercialization of the cathodes. The improvement in cyclic retention with the right choice of electrolyte–additive combinations is shown in Figure 11. As evident from the figure, the half-cell performance of NMC 811 in the polycrystalline case ( $\sim 190 \text{ mAh g}^{-1}$ ) is improved upon in the single-crystalline morphology ( $\sim 225 \text{ mAh g}^{-1}$ ) of NMC 811 in an optimized binder–electrolyte–additive combination. Figure 11c shows the best combinations of electrolytes, additives, and binders for single-crystal morphology of NMC [210,213,220,226,236,238].

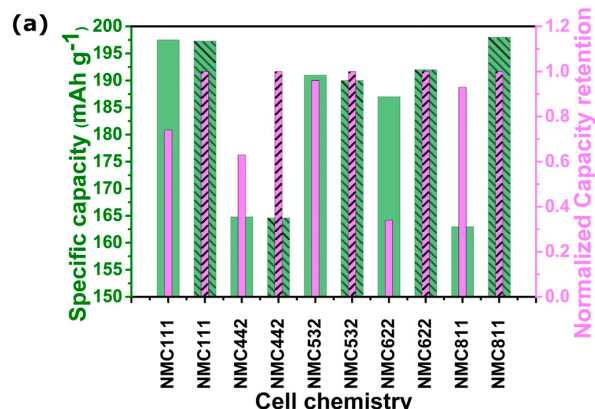
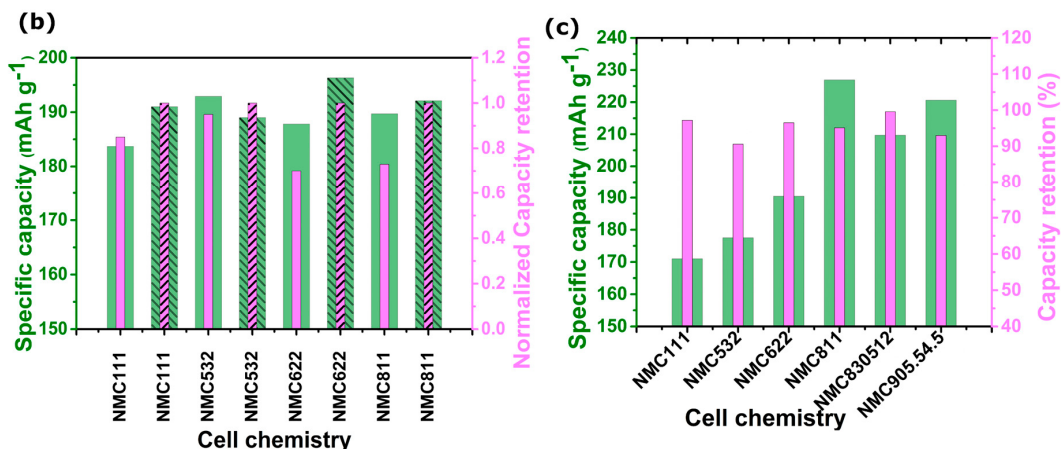


Figure 11. Cont.



**Figure 11.** The specific capacity and normalized capacity retention of different NMC compositions without additives and with additives (line marks) in (a) full cells and (b) half cells. (c) Electrochemical performance of a NMC single-crystal cathode in a half cell.

The electrolyte–additive combinations with the best battery metric for each polycrystalline NMC composition are tabulated in Table 11.

**Table 11.** The electrolyte–additive combinations with the best battery metric for each polycrystalline NMC composition [68,127,132,141,148,156,169,170,179].

Electrodes	Electrolytes	Additives	Voltage Range	Capacity Reported (mAh g <sup>-1</sup> )	Cycle Stability
NMC111/graphite	1 M LiPF <sub>6</sub> in EC: EMC (3:7, w/w)	0.1 wt% MUI without	2.8–4.6 V	197.3 (0.1 C) 197.5 (0.1 C)	63% (200, 0.3 C) 47% (200, 0.3 C)
NMC442/graphite	1 M LiPF <sub>6</sub> in EC: DMC: EMC (1:1:1, v/v)	1 wt% TMSP without	2.75–4.35 V	164.6 (1 C)	90.8% (70, 1 C)
NMC532/graphite	1.2 M LiPF <sub>6</sub> in EC: EMC (3.7 w/w)	1 wt% TMSPi without	3–4.4 V	190 (0.1 C) 191 (0.1 C)	88.8% (119, 0.3 C) 85.6% (119, 0.3 C)
NMC622/graphite	1 M LiPF <sub>6</sub> in EC: EMC (1:2, w/w)	1 wt% CEP without	3–4.5 V	192 187	81.5% (50, 1 C) 27.4% (50, 1 C)
NMC811/graphite	1 M LiPF <sub>6</sub> in EC: EMC (3:7, w/w)	0.5 wt% TPPO without	2.8–4.3 V	198 (0.1 C) 163 (0.1 C)	92% (97, 0.5 C) 86% (97, 0.5 C)
NMC111/Li	1 M LiPF <sub>6</sub> in EC: EMC: DEC (1:1:1, v/v/v)	0.5 wt% LiBOB without	3–4.6 V	191 (0.6 C) 183.7 (0.6 C)	91.8% (60, 0.6 C) 78.8% (60, 0.6 C)
NMC532/Li	1 M LiPF <sub>6</sub> in EC: EMC (3.7 v/v)	2 wt% BDTD without	3–4.6 V	189 (0.5 C) 192.9 (0.5 C)	91.6% (100, 0.5 C) 87.2% (100, 0.5 C)
NMC622/Li	1 M LiPF <sub>6</sub> in EC: EMC: DEC (1:1:1, v/v/v)	10 wt% FEC without	2.8–4.6 V	196.3 (1 C) 187.8 (1 C)	87.3% (100, 1 C) 60.8% (100, 1 C)
NMC811/Li	1 M LiPF <sub>6</sub> in EC: EMC: DEC (5:3:2, w/w/w)	5 wt% TPBX without	3–4.35 V	192.1 (1 C) 189.7 (1 C)	78% (100, 1 C) 57% (100, 1 C)

The electrolyte–additive combinations with the best battery metric for each SC-NMC (single crystalline) composition are tabulated in Table 12.

**Table 12.** The electrolyte–additive combinations with the best battery metric for each SC-NMC (single crystalline) composition [210,213,220,226,236,238].

Electrodes	Electrolytes	Voltage Range (V)	Capacity Reported (mAh g <sup>-1</sup> )	Cycle Stability
NMC111/Li	1 M LiPF <sub>6</sub> in EC: DMC (1:1 v/v)	2.5–4.4 V	171 (0.1 C)	97.2% (100, 0.1 C)
NMC532/Li	1 M LiPF <sub>6</sub> in EC: DEC (1:1 v/v)	2.75–4.4 V	177.5 (1 C)	90.6% (100, 1 C)
NMC622/Li	1 M LiPF <sub>6</sub> in EC: DMC: EMC (1:1:1 v/v)	2.8–4.5 V	190.4 (0.1 C)	96.5% (50, 1 C)
NMC811/Li	1 M LiPF <sub>6</sub> in EC: DMC (1:1 v/v)	2.8–4.3 V	226.9 (0.1 C)	95.1% (100, 1 C)
LiNi <sub>0.83</sub> Mn <sub>0.05</sub> Co <sub>0.12</sub> O <sub>2</sub> /Li	1 M LiPF <sub>6</sub> in EC: DEC (1:1 v/v)	2.75–4.3 V	209.7 (0.1 C)	99.56% (100, 0.2 C)
LiNi <sub>0.9</sub> Co <sub>0.055</sub> Mn <sub>0.045</sub> O <sub>2</sub> /Li	1 M LiPF <sub>6</sub> in EC: DMC: EMC (1:1:1 v/v)	2.8–4.3 V	220.6 (0.1 C)	93% (50, 1 C)

**Author Contributions:** D.D.: Methodology, resources, figures—permission, reproduction, and adaptation, and writing—original draft preparation, review, and editing. S.M.: Resources, figures—permission, reproduction, adaption, and editing. S.P.: Conceptualization, supervision, visualization, resources, writing—review and editing, funding acquisition, and project administration. All authors have read and agreed to the published version of the manuscript.

**Funding:** This research received no external funding.

**Data Availability Statement:** Not applicable.

**Acknowledgments:** D.D. thanks CSIR, New Delhi, India, for his fellowship (09/081(1343)/2019-EMR-I). S.M. thanks DST, INSPIRE, India, for her fellowship (IF190531).

**Conflicts of Interest:** The authors declare no conflict of interest.

## References

- Xu, Z.; Yang, J.; Li, H.; Nuli, Y.; Wang, J. Electrolytes for Advanced Lithium Ion Batteries Using Silicon-Based Anodes. *J. Mater. Chem. A* **2019**, *7*, 9432–9446. [[CrossRef](#)]
- Morigaki, K.I. In Situ Analysis of the Interfacial Reactions between MCMB Electrode and Organic Electrolyte Solutions. *J. Power Sources* **2002**, *103*, 253–264. [[CrossRef](#)]
- Manthiram, A. A Reflection on Lithium-Ion Battery Cathode Chemistry. *Nat. Commun.* **2020**, *11*, 1550. [[CrossRef](#)] [[PubMed](#)]
- Jiao, L.; Liu, Z.; Sun, Z.; Wu, T.; Gao, Y.; Li, H.; Li, F.; Niu, L. An Advanced Lithium Ion Battery Based on a High Quality Graphitic Graphene Anode and a  $\text{Li}[\text{Ni}_{0.6}\text{Co}_{0.2}\text{Mn}_{0.2}]\text{O}_2$  Cathode. *Electrochim. Acta* **2018**, *259*, 48–55. [[CrossRef](#)]
- Gören, A.; Costa, C.M.; Silva, M.M.; Lanceros-Méndez, S. State of the Art and Open Questions on Cathode Preparation Based on Carbon Coated Lithium Iron Phosphate. *Compos. Part B Eng.* **2015**, *83*, 333–345. [[CrossRef](#)]
- Amine, K.; Liu, J.; Kang, S.; Belharouak, I.; Hyung, Y.; Vissers, D.; Henriksen, G. Improved Lithium Manganese Oxide Spinel/Graphite Li-Ion Cells for High-Power Applications. *J. Power Sources* **2004**, *129*, 14–19. [[CrossRef](#)]
- Xue, L.; Ueno, K.; Lee, S.Y.; Angell, C.A. Enhanced Performance of Sulfone-Based Electrolytes at Lithium Ion Battery Electrodes, Including the  $\text{LiNi}_{0.5}\text{Mn}_{1.5}\text{O}_4$  High Voltage Cathode. *J. Power Sources* **2014**, *262*, 123–128. [[CrossRef](#)]
- Malik, M.; Chan, K.H.; Azimi, G. Review on the Synthesis of  $\text{LiNi}_x\text{Mn}_y\text{Co}_{1-x-y}\text{O}_2$  (NMC) Cathodes for Lithium-Ion Batteries. *Mater. Today Energy* **2022**, *28*, 101066. [[CrossRef](#)]
- Geldasa, F.T.; Kebede, M.A.; Shura, M.W.; Hone, F.G. Identifying Surface Degradation, Mechanical Failure, and Thermal Instability Phenomena of High Energy Density Ni-Rich NCM Cathode Materials for Lithiumion Batteries: A Review. *RSC Adv.* **2022**, *12*, 5891–5909. [[CrossRef](#)]
- Yan, W.; Yang, S.; Huang, Y.; Yang, Y.; Yuan, G. A Review on Doping/Coating of Nickel-Rich Cathode Materials for Lithium-Ion Batteries. *J. Alloys Compd.* **2020**, *819*, 153048. [[CrossRef](#)]
- Li, T.; Yuan, X.-Z.; Zhang, L.; Song, D.; Shi, K.; Bock, C. *Degradation Mechanisms and Mitigation Strategies of Nickel-Rich NMC-Based Lithium-Ion Batteries*; Springer: Singapore, 2020; Volume 3, ISBN 0123456789.
- Noh, H.J.; Youn, S.; Yoon, C.S.; Sun, Y.K. Comparison of the Structural and Electrochemical Properties of Layered  $\text{Li}[\text{Ni}_x\text{Co}_y\text{Mn}_z]\text{O}_2$  ( $x = 1/3, 0.5, 0.6, 0.7, 0.8$  and  $0.85$ ) Cathode Material for Lithium-Ion Batteries. *J. Power Sources* **2013**, *233*, 121–130. [[CrossRef](#)]
- Tornheim, A.; Sharifi-Asl, S.; Garcia, J.C.; Bareño, J.; Iddir, H.; Shahbazian-Yassar, R.; Zhang, Z. Effect of Electrolyte Composition on Rock Salt Surface Degradation in NMC Cathodes during High-Voltage Potentiostatic Holds. *Nano Energy* **2019**, *55*, 216–225. [[CrossRef](#)]
- Jung, R.; Metzger, M.; Maglia, F.; Stinner, C.; Gasteiger, H.A. Oxygen Release and Its Effect on the Cycling Stability of  $\text{LiNi}_x\text{Mn}_y\text{Co}_z\text{O}_2$  (NMC) Cathode Materials for Li-Ion Batteries. *J. Electrochem. Soc.* **2017**, *164*, A1361–A1377. [[CrossRef](#)]
- Li, W.; Liu, X.; Xie, Q.; You, Y.; Chi, M.; Manthiram, A. Long-Term Cyclability of NCM-811 at High Voltages in Lithium-Ion Batteries: An In-Depth Diagnostic Study. *Chem. Mater.* **2020**, *32*, 7796–7804. [[CrossRef](#)]
- Sun, H.H.; Manthiram, A. Impact of Microcrack Generation and Surface Degradation on a Nickel-Rich Layered  $\text{Li}[\text{Ni}_{0.9}\text{Co}_{0.05}\text{Mn}_{0.05}]\text{O}_2$  Cathode for Lithium-Ion Batteries. *Chem. Mater.* **2017**, *29*, 8486–8493. [[CrossRef](#)]
- Jung, R.; Linsenmann, F.; Thomas, R.; Wandt, J.; Solchenbach, S.; Maglia, F.; Stinner, C.; Tromp, M.; Gasteiger, H.A. Nickel, Manganese, and Cobalt Dissolution from Ni-Rich NMC and Their Effects on NMC622-Graphite Cells. *J. Electrochem. Soc.* **2019**, *166*, A378–A389. [[CrossRef](#)]
- Tataro, R.; Yu, Y.; Karayaylali, P.; Chan, A.K.; Zhang, Y.; Jung, R.; Maglia, F.; Giordano, L.; Shao-Horn, Y. Enhanced Cycling Performance of Ni-Rich Positive Electrodes (NMC) in Li-Ion Batteries by Reducing Electrolyte Free-Solvent Activity. *ACS Appl. Mater. Interfaces* **2019**, *11*, 34973–34988. [[CrossRef](#)]
- Xu, K. Nonaqueous Liquid Electrolytes for Lithium-Based Rechargeable Batteries. *Chem. Rev.* **2004**, *104*, 4303–4417. [[CrossRef](#)]
- Xu, K. Electrolytes and Interphases in Li-Ion Batteries and Beyond. *Chem. Rev.* **2014**, *114*, 11503–11618. [[CrossRef](#)] [[PubMed](#)]
- Yoshida, H.; Fukunaga, T.; Hazama, T.; Terasaki, M.; Mizutani, M.; Yamachi, M. Degradation Mechanism of Alkyl Carbonate Solvents Used in Lithium-Ion Cells during Initial Charging. *J. Power Sources* **1997**, *68*, 311–315. [[CrossRef](#)]

22. Laszczynski, N.; Solchenbach, S.; Gasteiger, H.A.; Lucht, B.L. Understanding Electrolyte Decomposition of Graphite/NCM811 Cells at Elevated Operating Voltage. *J. Electrochem. Soc.* **2019**, *166*, A1853–A1859. [[CrossRef](#)]
23. Strehle, B.; Solchenbach, S.; Metzger, M.; Schwenke, K.U.; Gasteiger, H.A. The Effect of CO<sub>2</sub> on Alkyl Carbonate Trans-Esterification during Formation of Graphite Electrodes in Li-Ion Batteries. *J. Electrochem. Soc.* **2017**, *164*, A2513–A2526. [[CrossRef](#)]
24. Xia, J.; Petibon, R.; Xiong, D.; Ma, L.; Dahn, J.R. Enabling Linear Alkyl Carbonate Electrolytes for High Voltage Li-Ion Cells. *J. Power Sources* **2016**, *328*, 124–135. [[CrossRef](#)]
25. Xiong, D.J.; Bauer, M.; Ellis, L.D.; Hynes, T.; Hyatt, S.; Hall, D.S.; Dahn, J.R. Some Physical Properties of Ethylene Carbonate-Free Electrolytes. *J. Electrochem. Soc.* **2018**, *165*, A126–A131. [[CrossRef](#)]
26. Logan, E.R.; Tonita, E.M.; Gering, K.L.; Ma, L.; Bauer, M.K.G.; Li, J.; Beaulieu, L.Y.; Dahn, J.R. A Study of the Transport Properties of Ethylene Carbonate-Free Li Electrolytes. *J. Electrochem. Soc.* **2018**, *165*, A705–A716. [[CrossRef](#)]
27. Aurbach, D. *Nonaqueous Electrochemistry*; CRC Press: Boca Raton, FL, USA, 1999; ISBN 0824773349.
28. Lee, J.; Kim, Y.J.; Jin, H.S.; Noh, H.; Kwack, H.; Chu, H.; Ye, F.; Lee, H.; Kim, H.T. Tuning Two Interfaces with Fluoroethylene Carbonate Electrolytes for High-Performance Li/LCO Batteries. *ACS Omega* **2019**, *4*, 3220–3227. [[CrossRef](#)] [[PubMed](#)]
29. Flamme, B.; Rodriguez Garcia, G.; Weil, M.; Haddad, M.; Phansavath, P.; Ratovelomanana-Vidal, V.; Chagnes, A. Guidelines to Design Organic Electrolytes for Lithium-Ion Batteries: Environmental Impact, Physicochemical and Electrochemical Properties. *Green Chem.* **2017**, *19*, 1828–1849. [[CrossRef](#)]
30. Koch, V.R.; Goldman, J.L.; Mattos, C.J.; Mulvaney, M. Specular Lithium Deposits from Lithium Hexafluoroarsenate/Diethyl Ether Electrolytes. *J. Electrochem. Soc.* **1982**, *129*, 1. [[CrossRef](#)]
31. Ren, X.; Zou, L.; Jiao, S.; Mei, D.; Engelhard, M.H.; Li, Q.; Lee, H.; Niu, C.; Adams, B.D.; Wang, C.; et al. High-Concentration Ether Electrolytes for Stable High-Voltage Lithium Metal Batteries. *ACS Energy Lett.* **2019**, *4*, 896–902. [[CrossRef](#)]
32. Ren, X.; Zou, L.; Cao, X.; Engelhard, M.H.; Liu, W.; Burton, S.D.; Lee, H.; Niu, C.; Matthews, B.E.; Zhu, Z.; et al. Enabling High-Voltage Lithium-Metal Batteries under Practical Conditions. *Joule* **2019**, *3*, 1662–1676. [[CrossRef](#)]
33. Yamada, Y.; Yaegashi, M.; Abe, T.; Yamada, A. A Superconcentrated Ether Electrolyte for Fast-Charging Li-Ion Batteries. *Chem. Commun.* **2013**, *49*, 11194–11196. [[CrossRef](#)] [[PubMed](#)]
34. Jia, H.; Xu, Y.; Burton, S.D.; Gao, P.; Zhang, X.; Matthews, B.E.; Engelhard, M.H.; Zhong, L.; Bowden, M.E.; Xiao, B.; et al. Enabling Ether-Based Electrolytes for Long Cycle Life of Lithium-Ion Batteries at High Charge Voltage. *ACS Appl. Mater. Interfaces* **2020**, *12*, 54893–54903. [[CrossRef](#)]
35. Amanchukwu, C.V.; Yu, Z.; Kong, X.; Qin, J.; Cui, Y.; Bao, Z. A New Class of Ionically Conducting Fluorinated Ether Electrolytes with High Electrochemical Stability. *J. Am. Chem. Soc.* **2020**, *142*, 7393–7403. [[CrossRef](#)] [[PubMed](#)]
36. Dalavi, S.; Xu, M.; Ravdel, B.; Zhou, L.; Lucht, B.L. Nonflammable Electrolytes for Lithium-Ion Batteries Containing Dimethyl Methylphosphonate. *J. Electrochem. Soc.* **2010**, *157*, A1113. [[CrossRef](#)]
37. Jin, Z.; Wu, L.; Song, Z.; Yan, K.; Zhan, H.; Li, Z. A New Class of Phosphates as Co-Solvents for Nonflammable Lithium Ion Batteries Electrolytes. *ECS Electrochem. Lett.* **2012**, *1*, 55–58. [[CrossRef](#)]
38. Xu, M.; Lu, D.; Garsuch, A.; Lucht, B.L. Improved Performance of LiNi<sub>0.5</sub>Mn<sub>1.5</sub>O<sub>4</sub> Cathodes with Electrolytes Containing Dimethylmethylphosphonate (DMMP). *J. Electrochem. Soc.* **2012**, *159*, A2130–A2134. [[CrossRef](#)]
39. Von Aspern, N.; Leissing, M.; Christian Wölke, D.D.; Takeshi Kobayashi, M.B.; Stubbmann-Kazakova, O.; Kozel, V.; Röschenhaler, G.-V.; Smiatek, J.; Sascha Nowak, M.W.; Cekic-Laskovic, I. Non-Flammable Fluorinated Phosphorus III-Based Electrolytes for Advanced Lithium-Ion Battery Performance. *ChemElectroChem* **2020**, *7*, 1499–1508. [[CrossRef](#)]
40. Gu, Y.; Fang, S.; Yang, L.; Hirano, S.I. Tris (2,2,2-Trifluoroethyl) Phosphate as a Cosolvent for a Nonflammable Electrolyte in Lithium-Ion Batteries. *ACS Appl. Energy Mater.* **2021**, *4*, 4919–4927. [[CrossRef](#)]
41. Wu, W.; Bai, Y.; Wang, X.; Wu, C. Sulfone-Based High-Voltage Electrolytes for High Energy Density Rechargeable Lithium Batteries: Progress and Perspective. *Chin. Chem. Lett.* **2020**, *32*, 1309–1315. [[CrossRef](#)]
42. Flamme, B.; Haddad, M.; Phansavath, P.; Ratovelomanana-Vidal, V.; Chagnes, A. Anodic Stability of New Sulfone-Based Electrolytes for Lithium-Ion Batteries. *ChemElectroChem* **2018**, *5*, 2279–2287. [[CrossRef](#)]
43. Flamme, B.; Świątowska, J.; Haddad, M.; Phansavath, P.; Ratovelomanana-Vidal, V.; Chagnes, A. Sulfone Based-Electrolytes for Lithium-Ion Batteries: Cycling Performances and Passivation Layer Quality of Graphite and LiNi<sub>1/3</sub>Mn<sub>1/3</sub>Co<sub>1/3</sub>O<sub>2</sub> Electrodes. *J. Electrochem. Soc.* **2020**, *167*, 070508. [[CrossRef](#)]
44. Su, C.C.; He, M.; Redfern, P.C.; Curtiss, L.A.; Shkrob, I.A.; Zhang, Z. Oxidatively Stable Fluorinated Sulfone Electrolytes for High Voltage High Energy Lithium-Ion Batteries. *Energy Environ. Sci.* **2017**, *10*, 900–904. [[CrossRef](#)]
45. Lux, S.F.; Chevalier, J.; Lucas, I.T.; Kostecki, R. HF Formation in LiPF<sub>6</sub>-Based Organic Carbonate Electrolytes. *ECS Electrochem. Lett.* **2013**, *2*, 2013–2016. [[CrossRef](#)]
46. Chen, Y.; Zhao, W.; Zhang, Q.; Yang, G.; Zheng, J.; Tang, W.; Xu, Q.; Lai, C.; Yang, J.; Peng, C. Armoring LiNi<sub>1/3</sub>Co<sub>1/3</sub>Mn<sub>1/3</sub>O<sub>2</sub> Cathode with Reliable Fluorinated Organic-Inorganic Hybrid Interphase Layer toward Durable High Rate Battery. *Adv. Funct. Mater.* **2020**, *30*, 2000396. [[CrossRef](#)]
47. Lux, S.F.; Lucas, I.T.; Pollak, E.; Passerini, S.; Winter, M.; Kostecki, R. The Mechanism of HF Formation in LiPF<sub>6</sub> Based Organic Carbonate Electrolytes. *Electrochim. Commun.* **2012**, *14*, 47–50. [[CrossRef](#)]
48. Dalavi, S.; Xu, M.; Knight, B.; Lucht, B.L. Effect of Added LiBOB on High Voltage (LiNi<sub>0.5</sub>Mn<sub>1.5</sub>O<sub>4</sub>) Spinel Cathodes. *Electrochim. Solid-State Lett.* **2012**, *15*, 28–31. [[CrossRef](#)]

49. Reiter, J.; Nádherná, M.; Dominko, R. Graphite and LiCo<sub>1/3</sub>Mn<sub>1/3</sub>Ni<sub>1/3</sub>O<sub>2</sub> Electrodes with Piperidinium Ionic Liquid and Lithium Bis(Fluorosulfonyl)Imide for Li-Ion Batteries. *J. Power Sources* **2012**, *205*, 402–407. [CrossRef]
50. Xu, C.; Hernández, G.; Abbrecht, S.; Kobera, L.; Konefal, R.; Brus, J.; Edström, K.; Brandell, D.; Mindemark, J. Unraveling and Mitigating the Storage Instability of Fluoroethylene Carbonate-Containing LiPF<sub>6</sub> Electrolytes to Stabilize Lithium Metal Anodes for High-Temperature Rechargeable Batteries. *ACS Appl. Energy Mater.* **2019**, *2*, 4925–4935. [CrossRef]
51. Shui Zhang, S. An Unique Lithium Salt for the Improved Electrolyte of Li-Ion Battery. *Electrochim. Commun.* **2006**, *8*, 1423–1428. [CrossRef]
52. Gu, Y.; Fang, S.; Yang, L.; Hirano, S. ichi A Safe Electrolyte for High-Performance Lithium-Ion Batteries Containing Lithium Difluoro(Oxalato)Borate, Gamma-Butyrolactone and Non-Flammable Hydrofluoroether. *Electrochim. Acta* **2021**, *394*, 139120. [CrossRef]
53. Xiang, H.; Shi, P.; Bhattacharya, P.; Chen, X.; Mei, D.; Bowden, M.E.; Zheng, J.; Zhang, J.G.; Xu, W. Enhanced Charging Capability of Lithium Metal Batteries Based on Lithium Bis(Trifluoromethanesulfonyl)Imide-Lithium Bis(Oxalato)Borate Dual-Salt Electrolytes. *J. Power Sources* **2016**, *318*, 170–177. [CrossRef]
54. Li, X.; Zheng, J.; Engelhard, M.H.; Mei, D.; Li, Q.; Jiao, S.; Liu, N.; Zhao, W.; Zhang, J.G.; Xu, W. Effects of Imide-Orthoborate Dual-Salt Mixtures in Organic Carbonate Electrolytes on the Stability of Lithium Metal Batteries. *ACS Appl. Mater. Interfaces* **2018**, *10*, 2469–2479. [CrossRef] [PubMed]
55. Zheng, J.; Engelhard, M.H.; Mei, D.; Jiao, S.; Polzin, B.J.; Zhang, J.G.; Xu, W. Electrolyte Additive Enabled Fast Charging and Stable Cycling Lithium Metal Batteries. *Nat. Energy* **2017**, *2*, 17012. [CrossRef]
56. Jiao, S.; Zheng, J.; Li, Q.; Li, X.; Engelhard, M.H.; Cao, R.; Zhang, J.G.; Xu, W. Behavior of Lithium Metal Anodes under Various Capacity Utilization and High Current Density in Lithium Metal Batteries. *Joule* **2018**, *2*, 110–124. [CrossRef]
57. Jiao, S.; Ren, X.; Cao, R.; Engelhard, M.H.; Liu, Y.; Hu, D.; Mei, D.; Zheng, J.; Zhao, W.; Li, Q.; et al. Stable Cycling of High-Voltage Lithium Metal Batteries in Ether Electrolytes. *Nat. Energy* **2018**, *3*, 739–746. [CrossRef]
58. Aurbach, D.; Gamolsky, K.; Markovsky, B.; Gofer, Y.; Schmidt, M.; Heider, U. On the Use of Vinylene Carbonate (VC) as an Additive to Electrolyte Solutions for Li-Ion Batteries. *Electrochim. Acta* **2002**, *47*, 1423–1439. [CrossRef]
59. Burns, J.C.; Electrochem, J.; Soc, A.; Burns, J.C.; Petibon, R.; Nelson, K.J.; Sinha, N.N.; Kassam, A.; Way, B.M.; Dahn, J.R. Studies of the Effect of Varying Vinylene Carbonate (VC) Content in Lithium Ion Cells on Cycling Performance and Cell Impedance. *J. Electrochem. Soc.* **2013**, *160*, A1668. [CrossRef]
60. Liu, Y.; Takeda, S.; Kaneko, I.; Yoshitake, H.; Mukai, T.; Yanagida, M.; Saito, Y.; Sakai, T. Understanding the Improved High-Temperature Cycling Stability of Comprehensive Analysis Approach Utilizing LC-MS and DART-MS. *J. Phys. Chem. C* **2018**, *122*, 5864–5870. [CrossRef]
61. Zhang, X.Q.; Cheng, X.B.; Chen, X.; Yan, C.; Zhang, Q. Fluoroethylene Carbonate Additives to Render Uniform Li Deposits in Lithium Metal Batteries. *Adv. Funct. Mater.* **2017**, *27*, 1605989. [CrossRef]
62. Salitra, G.; Markevich, E.; Afri, M.; Talyosef, Y.; Hartmann, P.; Kulisch, J.; Sun, Y.K.; Aurbach, D. High-Performance Cells Containing Lithium Metal Anodes, LiNi<sub>0.6</sub>Co<sub>0.2</sub>Mn<sub>0.2</sub>O<sub>2</sub> (NCM 622) Cathodes, and Fluoroethylene Carbonate-Based Electrolyte Solution with Practical Loading. *ACS Appl. Mater. Interfaces* **2018**, *10*, 19773–19782. [CrossRef]
63. Im, J.; Lee, J.; Ryoo, M.-H.; Lee, Y.M.; Cho, K.Y. Fluorinated Carbonate-Based Electrolyte for High-Voltage Li(Ni<sub>0.5</sub>Mn<sub>0.3</sub>Co<sub>0.2</sub>)O<sub>2</sub>/Graphite Lithium-Ion Battery. *J. Electrochem. Soc.* **2017**, *164*, A6381–A6385. [CrossRef]
64. Mai, S.; Xu, M.; Liao, X.; Hu, J.; Lin, H.; Xing, L.; Liao, Y.; Li, X.; Li, W. Tris (Trimethylsilyl) Phosphite as Electrolyte Additive for High Voltage Layered Lithium Nickel Cobalt Manganese Oxide Cathode of Lithium Ion Battery. *Electrochim. Acta* **2014**, *147*, 565–571. [CrossRef]
65. Wang, D.Y.; Xia, J.; Ma, L.; Nelson, K.J.; Harlow, J.E.; Xiong, D.; Downie, L.E.; Petibon, R.; Burns, J.C.; Xiao, A.; et al. A Systematic Study of Electrolyte Additives in Li[Ni<sub>1/3</sub>Mn<sub>1/3</sub>Co<sub>1/3</sub>]O<sub>2</sub> (NMC)/Graphite Pouch Cells. *J. Electrochem. Soc.* **2014**, *161*, A1818–A1827. [CrossRef]
66. Sinha, N.N.; Burns, J.C.; Dahn, J.R. Comparative Study of Tris (Trimethylsilyl) Phosphate and Tris (Trimethylsilyl) Phosphite as Electrolyte Additives for Li-Ion Cells. *J. Electrochem. Soc.* **2014**, *161*, A1084–A1089. [CrossRef]
67. Laveda, J.V.; Low, J.E.; Pagani, F.; Stilp, E.; Dilger, S.; Baran, V.; Heere, M.; Battaglia, C. Stabilizing Capacity Retention in NMC811/Graphite Full Cells via TMSPI Electrolyte Additives. *ACS Appl. Energy Mater.* **2019**, *2*, 7036–7044. [CrossRef]
68. Peebles, C.; Sahore, R.; Gilbert, J.A.; Garcia, J.C.; Tornheim, A.; Bareño, J.; Iddir, H.; Liao, C.; Abraham, D.P. Tris (Trimethylsilyl) Phosphite (TMSPI) and Triethyl Phosphite (TEPi) as Electrolyte Additives for Lithium Ion Batteries: Mechanistic Insights into Differences during LiNi<sub>0.5</sub>Mn<sub>0.3</sub>Co<sub>0.2</sub>O<sub>2</sub>-Graphite Full Cell Cycling. *J. Electrochem. Soc.* **2017**, *164*, A1579–A1586. [CrossRef]
69. Xia, J.; Sinha, N.N.; Chen, L.P.; Dahn, J.R. A Comparative Study of a Family of Sulfate Electrolyte Additives. *J. Electrochem. Soc.* **2014**, *161*, A264–A274. [CrossRef]
70. Xia, J.; Ma, L.; Aiken, C.P.; Nelson, K.J.; Chen, L.P.; Dahn, J.R. Comparative Study on Prop-1-Ene-1,3-Sultone and Vinylene Carbonate as Electrolyte Additives for Li(Ni<sub>1/3</sub>Mn<sub>1/3</sub>Co<sub>1/3</sub>)O<sub>2</sub>/Graphite Pouch Cells. *J. Electrochem. Soc.* **2014**, *161*, A1634–A1641. [CrossRef]
71. Madec, L.; Petibon, R.; Xia, J.; Sun, J.-P.; Hill, I.G.; Dahn, J.R. Understanding the Role of Prop-1-Ene-1,3-Sultone and Vinylene Carbonate in LiNi<sub>1/3</sub>Mn<sub>1/3</sub>Co<sub>1/3</sub>O<sub>2</sub>/Graphite Pouch Cells: Electrochemical, GC-MS and XPS Analysis. *J. Electrochem. Soc.* **2015**, *162*, A2635–A2645. [CrossRef]

72. Ma, L.; Xia, J.; Dahn, J.R. Ternary Electrolyte Additive Mixtures for Li-Ion Cells That Promote Long Lifetime and Less Reactivity with Charged Electrodes at Elevated Temperatures. *J. Electrochem. Soc.* **2015**, *162*, A1170–A1174. [[CrossRef](#)]
73. Li, B.; Wang, Y.; Lin, H.; Wang, X.; Xu, M.; Wang, Y.; Xing, L.; Li, W. Performance Improvement of Phenyl Acetate as Propylene Carbonate-Based Electrolyte Additive for Lithium Ion Battery by Fluorine-Substituting. *J. Power Sources* **2014**, *267*, 182–187. [[CrossRef](#)]
74. An, Y.; Zuo, P.; Cheng, X.; Liao, L.; Yin, G. The Effects of LiBOB Additive for Stable SEI Formation of PP13TFSI-Organic Mixed Electrolyte in Lithium Ion Batteries. *Electrochim. Acta* **2011**, *56*, 4841–4848. [[CrossRef](#)]
75. Zhu, Y.; Li, Y.; Bettge, M.; Abraham, D.P. Electrolyte Additive Combinations That Enhance Performance of High-Capacity  $\text{Li}_{1.2}\text{Ni}_{0.15}\text{Mn}_{0.55}\text{Co}_{0.1}\text{O}_2$ -Graphite Cells. *Electrochim. Acta* **2013**, *110*, 191–199. [[CrossRef](#)]
76. Zhu, Y.; Li, Y.; Bettge, M.; Abraham, D.P. Positive Electrode Passivation by LiDFOB Electrolyte Additive in High-Capacity Lithium-Ion Cells. *J. Electrochem. Soc.* **2012**, *159*, A2109–A2117. [[CrossRef](#)]
77. Jiao, S.; Liu, J.; Xu, W.; Zhang, J. A Localized High-Concentration Electrolyte with Optimized Solvents and Lithium Di Fl Uoro(Oxalate)Borate Additive for Stable Lithium Metal Batteries. *ACS Energy Lett.* **2018**, *3*, 2059–2067. [[CrossRef](#)]
78. Tan, S.; Shadike, Z.; Li, J.; Wang, X.; Yang, Y.; Lin, R.; Cresce, A.; Hu, J.; Hunt, A.; Waluyo, I.; et al. Additive Engineering for Robust Interphases to Stabilize High-Ni Layered Structures at Ultra-High Voltage of 4.8 V. *Nat. Energy* **2022**, *7*, 484–494. [[CrossRef](#)]
79. Wang, C.; Yu, L.; Fan, W.; Liu, J.; Ouyang, L.; Yang, L.; Zhu, M. Lithium Difluorophosphate As a Promising Electrolyte Lithium Additive for High-Voltage Lithium-Ion Batteries. *ACS Appl. Energy Mater.* **2018**, *1*, 2647–2656. [[CrossRef](#)]
80. Wang, C.; Yu, L.; Fan, W.; Liu, R.; Liu, J.; Ouyang, L.; Yang, L.; Zhu, M. Enhanced High-Voltage Cyclability of  $\text{LiNi}_{0.5}\text{Co}_{0.2}\text{Mn}_{0.3}\text{O}_2$ -Based Pouch Cells via Lithium Difluorophosphate Introducing as Electrolyte Additive. *J. Alloys Compd.* **2018**, *755*, 1–9. [[CrossRef](#)]
81. Yang, B.; Zhang, H.; Yu, L.; Fan, W.Z.; Huang, D. Lithium Difluorophosphate as an Additive to Improve the Low Temperature Performance of  $\text{LiNi}_{0.5}\text{Co}_{0.2}\text{Mn}_{0.3}\text{O}_2$ /Graphite Cells. *Electrochim. Acta* **2016**, *221*, 107–114. [[CrossRef](#)]
82. Qian, Y.; Kang, Y.; Hu, S.; Shi, Q.; Chen, Q.; Tang, X.; Xiao, Y.; Zhao, H.; Luo, G.; Xu, K.; et al. Mechanism Study of Unsaturated Tripropargyl Phosphate as An efficient electrolyte additive forming multifunctional interphases in lithium ion and lithium metal batteries. *ACS Appl. Mater. Interfaces* **2020**, *12*, 10443–10451. [[CrossRef](#)]
83. Skyler, J.S. Challenges of the Future. *Endocrinologist* **1993**, *3*, 233–238. [[CrossRef](#)]
84. Lewandowski, A.; Swiderska-Mocek, A. Ionic Liquids as Electrolytes for Li-Ion Batteries-An Overview of Electrochemical Studies. *J. Power Sources* **2009**, *194*, 601–609. [[CrossRef](#)]
85. Chaudoy, V.; Ghamous, F.; Jacquemin, J.; Houdbert, J.C.; Tran-Van, F. On the Performances of Ionic Liquid-Based Electrolytes for Li-NMC Batteries. *J. Solut. Chem.* **2015**, *44*, 769–789. [[CrossRef](#)]
86. Matsui, Y.; Kawaguchi, S.; Sugimoto, T.; Kikuta, M.; Higashizaki, T.; Kono, M.; Yamagata, M.; Ishikawa, M. Charge-Discharge Characteristics of a  $\text{LiNi}_{1/3}\text{Mn}_{1/3}\text{Co}_{1/3}\text{O}_2$  Cathode in FSI-Based Ionic Liquids. *Electrochemistry* **2012**, *80*, 808–811. [[CrossRef](#)]
87. Simonetti, E.; Maresca, G.; Appeticchi, G.B.; Kim, G.T.; Loeffler, N.; Passerini, S. Towards  $\text{Li}(\text{Ni}0.33\text{Mn}0.33\text{Co}0.33)\text{O}_2$ /Graphite Batteries with Ionic Liquid-Based Electrolytes. I. Electrodes' Behavior in Lithium Half-Cells. *J. Power Sources* **2016**, *331*, 426–434. [[CrossRef](#)]
88. Evans, T.; Olson, J.; Bhat, V.; Lee, S.H. Effect of Organic Solvent Addition to PYR13FSI + LiFSI Electrolytes on Aluminum Oxidation and Rate Performance of  $\text{Li}(\text{Ni}_{1/3}\text{Mn}_{1/3}\text{Co}_{1/3})\text{O}_2$  Cathodes. *J. Power Sources* **2014**, *265*, 132–139. [[CrossRef](#)]
89. Zheng, F.; Kotobuki, M.; Song, S.; Lai, M.O.; Lu, L. Review on Solid Electrolytes for All-Solid-State Lithium-Ion Batteries. *J. Power Sources* **2018**, *389*, 198–213. [[CrossRef](#)]
90. Kato, T.; Iwasaki, S.; Ishii, Y.; Motoyama, M.; West, W.C.; Yamamoto, Y.; Iriyama, Y. Preparation of Thick- Fi Lm Electrode-Solid Electrolyte Composites on  $\text{Li}_7\text{La}_3\text{Zr}_2\text{O}_{12}$  and Their Electrochemical Properties. *J. Power Sources* **2016**, *303*, 65–72. [[CrossRef](#)]
91. Iwasaki, S.; Hamanaka, T.; Yamakawa, T.; West, W.C.; Yamamoto, K.; Motoyama, M.; Hirayama, T.; Iriyama, Y. Preparation of Thick-Film  $\text{LiNi}_{1/3}\text{Co}_{1/3}\text{Mn}_{1/3}\text{O}_2$  Electrodes by Aerosol Deposition and Its Application to All-Solid-State Batteries. *J. Power Sources* **2014**, *272*, 1086–1090. [[CrossRef](#)]
92. Yan, P.; Zheng, J.; Liu, J.; Wang, B.; Cheng, X.; Zhang, Y.; Sun, X.; Wang, C.; Zhang, J.G. Tailoring Grain Boundary Structures and Chemistry of Ni-Rich Layered Cathodes for Enhanced Cycle Stability of Lithium-Ion Batteries. *Nat. Energy* **2018**, *3*, 600–605. [[CrossRef](#)]
93. Alexander, G.V.; Indu, M.S.; Kamakshy, S.; Murugan, R. *Electrochimica Acta* Development of Stable and Conductive Interface between Garnet Structured Solid Electrolyte and Lithium Metal Anode for High Performance Solid-State Battery. *Electrochim. Acta* **2020**, *332*, 135511. [[CrossRef](#)]
94. Phillip, N.D.; Westover, A.S.; Daniel, C.; Veith, G.M. Structural Degradation of High Voltage Lithium Nickel Manganese Cobalt Oxide (NMC) Cathodes in Solid-State Batteries and Implications for Next Generation Energy Storage. *ACS Appl. Energy Mater.* **2020**, *3*, 1768–1774. [[CrossRef](#)]
95. Yu, X.; Li, J.; Manthiram, A. Rational Design of a Laminated Dual-Polymer/Polymer–Ceramic Composite Electrolyte for High-Voltage All-Solid-State Lithium Batteries. *ACS Mater. Lett.* **2020**, *2*, 317–324. [[CrossRef](#)]
96. Gupta, H.; Singh, S.K.; Singh, V.K.; Tripathi, A.K.; Srivastava, N.; Tiwari, R.K.; Mishra, R.; Meghnani, D.; Singh, R.K. Development of Polymer Electrolyte and Cathode Material for Li-Batteries. *J. Electrochem. Soc.* **2019**, *166*, A5187–A5192. [[CrossRef](#)]
97. Kaboli, S.; Demers, H.; Paolella, A.; Darwiche, A.; Dontigny, M.; Clément, D.; Guerfi, A.; Trudeau, M.L.; Goodenough, J.B.; Zaghib, K. Behavior of Solid Electrolyte in Li-Polymer Battery with NMC Cathode via in-Situ Scanning Electron Microscopy. *Nano Lett.* **2020**, *20*, 1607–1613. [[CrossRef](#)]

98. Kobayashi, T.; Kobayashi, Y.; Tabuchi, M.; Shono, K.; Ohno, Y.; Mita, Y.; Miyashiro, H. Oxidation Reaction of Polyether-Based Material and Its Suppression in Lithium Rechargeable Battery Using 4 v Class Cathode,  $\text{LiNi}_{1/3}\text{Mn}_{1/3}\text{Co}_{1/3}\text{O}_2$ . *ACS Appl. Mater. Interfaces* **2013**, *5*, 12387–12393. [CrossRef] [PubMed]
99. Wu, N.; Chien, P.H.; Li, Y.; Dolocan, A.; Xu, H.; Xu, B.; Grundish, N.S.; Jin, H.; Hu, Y.Y.; Goodenough, J.B. Fast Li<sup>+</sup> Conduction Mechanism and Interfacial Chemistry of a NASICON/Polymer Composite Electrolyte. *J. Am. Chem. Soc.* **2020**, *142*, 2497–2505. [CrossRef] [PubMed]
100. Biensan, P.; Simon, B.; Péres, J.P.; De Guibert, A.; Broussely, M.; Bodet, J.M.; Perton, F. On Safety of Lithium-Ion Cells. *J. Power Sources* **1999**, *81–82*, 906–912. [CrossRef]
101. Li, J.; Daniel, C.; Wood, D. Materials Processing for Lithium-Ion Batteries. *J. Power Sources* **2011**, *196*, 2452–2460. [CrossRef]
102. Lux, S.F.; Schappacher, F.; Balducci, A.; Passerini, S.; Winter, M. Low Cost, Environmentally Benign Binders for Lithium-Ion Batteries. *J. Electrochem. Soc.* **2010**, *157*, A320. [CrossRef]
103. Kovalenko, I.; Zdyrko, B.; Magasinski, A.; Hertzberg, B.; Milicev, Z.; Burtovyy, R.; Luzinov, I.; Yushin, G. A Major Constituent of Brown Algae for Use in High-Capacity Li-Ion Batteries. *Science* **2011**, *334*, 75–79. [CrossRef] [PubMed]
104. Xu, J.; Chou, S.L.; Gu, Q.F.; Liu, H.K.; Dou, S.X. The Effect of Different Binders on Electrochemical Properties of  $\text{LiNi}_{1/3}\text{Mn}_{1/3}\text{Co}_{1/3}\text{O}_2$  Cathode Material in Lithium Ion Batteries. *J. Power Sources* **2013**, *225*, 172–178. [CrossRef]
105. Loeffler, N.; Von Zamory, J.; Laszczynski, N.; Doberdo, I.; Kim, G.T.; Passerini, S. Performance of  $\text{LiNi}_{1/3}\text{Mn}_{1/3}\text{Co}_{1/3}\text{O}_2$ /Graphite Batteries Based on Aqueous Binder. *J. Power Sources* **2014**, *248*, 915–922. [CrossRef]
106. Chen, Z.; Kim, G.; Chao, D.; Loe, N.; Copley, M.; Lin, J.; Shen, Z.; Passerini, S. Toward Greener Lithium-Ion Batteries: Aqueous Binder-Based Performance. *J. Power Sources* **2017**, *372*, 180–187. [CrossRef]
107. Zhong, H.; Sun, M.; Li, Y.; He, J.; Yang, J.; Zhang, L. The Polyacrylic Latex: An Efficient Water-Soluble Binder for  $\text{LiNi}_{1/3}\text{Co}_{1/3}\text{Mn}_{1/3}\text{O}_2$  Cathode in Li-Ion Batteries. *J. Solid State Electrochem.* **2016**, *20*, 1–8. [CrossRef]
108. Memm, M.; Hoffmann, A.; Wohlfahrt-Mehrens, M. Water-Based  $\text{LiNi}_{1/3}\text{Mn}_{1/3}\text{Co}_{1/3}\text{O}_2$ -Cathodes with Good Electrochemical Performance by Use of Additives. *Electrochim. Acta* **2018**, *260*, 664–673. [CrossRef]
109. Loeffler, N.; Kim, G.T.; Mueller, F.; Diemant, T.; Kim, J.K.; Behm, R.J.; Passerini, S. In Situ Coating of  $\text{Li}[\text{Ni}0.33\text{Mn}0.33\text{Co}0.33]\text{O}_2$  Particles to Enable Aqueous Electrode Processing. *ChemSusChem* **2016**, *9*, 1112–1117. [CrossRef]
110. Bichon, M.; Sotta, D.; De Vito, E.; Porcher, W.; Lestriez, B. Performance and Ageing Behavior of Water-Processed  $\text{LiNi}_{0.5}\text{Mn}_{0.3}\text{Co}_{0.2}\text{O}_2$ /Graphite Lithium-Ion Cells. *J. Power Sources* **2021**, *483*, 229097. [CrossRef]
111. Wood, M.; Li, J.; Ruther, R.E.; Du, Z.; Self, E.C.; Meyer, H.M.; Daniel, C.; Belharouak, I.; Wood, D.L. Chemical Stability and Long-Term Cell Performance of Low-Cobalt, Ni-Rich Cathodes Prepared by Aqueous Processing for High-Energy Li-Ion Batteries. *Energy Storage Mater.* **2020**, *24*, 188–197. [CrossRef]
112. Kuo, J.-H.; Li, C.-C. Water-Based Process to the Preparation of Nickel-Rich  $\text{Li}(\text{Ni}_{0.8}\text{Co}_{0.1}\text{Mn}_{0.1})\text{O}_2$  Cathode. *J. Electrochem. Soc.* **2020**, *167*, 100504. [CrossRef]
113. Brillon, A.; Poli, F.; Spina, G.E.; Samori, C.; Guidi, E.; Gualandi, C.; Maisuradze, M.; Giorgetti, M.; Soavi, F. Easy Recovery of Li-Ion Cathode Powders by the Use of Water-Processable Binders. *Electrochim. Acta* **2022**, *418*, 140376. [CrossRef]
114. Vauthier, S.; Alvarez-Tirado, M.; Guzmán-González, G.; Tomé, L.; Cotte, S.; Castro, L.; Guéguen, A.; Mecerreyres, D.; Casado, N. High-Performance Pyrrolidinium-Based Poly (Ionic Liquid) Binders for Li-Ion and Li-Air Batteries. *Mater. Today Chem.* **2023**, *27*, 101293. [CrossRef]
115. Zhang, H.; Yang, Y.; Ren, D.; Wang, L.; He, X. Graphite as Anode Materials: Fundamental Mechanism, Recent Progress and Advances. *Energy Storage Mater.* **2021**, *36*, 147–170. [CrossRef]
116. Xu, W.; Wang, J.; Ding, F.; Chen, X.; Nasybulin, E.; Zhang, Y.; Zhang, J.G. Lithium Metal Anodes for Rechargeable Batteries. *Energy Environ. Sci.* **2014**, *7*, 513–537. [CrossRef]
117. Zhang, H.; Yang, Y.; Xu, H.; Wang, L.; Lu, X.; He, X.  $\text{Li}_4\text{Ti}_5\text{O}_{12}$  Spinel Anode: Fundamentals and Advances in Rechargeable Batteries. *InfoMat* **2022**, *4*, e12228. [CrossRef]
118. Björklund, E.; Brandell, D.; Hahlin, M.; Edström, K.; Younesi, R. How the Negative Electrode Influences Interfacial and Electrochemical Properties of  $\text{LiNi}_{1/3}\text{Co}_{1/3}\text{Mn}_{1/3}\text{O}_2$  Cathodes in Li-Ion Batteries. *J. Electrochem. Soc.* **2017**, *164*, A3054–A3059. [CrossRef]
119. Fang, S.; Jackson, D.; Dreibelbis, M.L.; Kuech, T.F.; Hamers, R.J. Anode-Originated SEI Migration Contributes to Formation of Cathode-Electrolyte Interphase Layer. *J. Power Sources* **2018**, *373*, 184–192. [CrossRef]
120. Ohzuku, T.; Makimura, Y. Layered Lithium Insertion Material of  $\text{LiCo}_{1/3}\text{Ni}_{1/3}\text{Mn}_{1/3}\text{O}_2$  for Lithium-Ion Batteries. *Chem. Lett.* **2001**, *30*, 642–643. [CrossRef]
121. Wang, D.Y.; Dahn, J.R. A High Precision Study of Electrolyte Additive Combinations Containing Vinylene Carbonate, Ethylene Sulfate, Tris(Trimethylsilyl) Phosphate and Tris (Trimethylsilyl) Phosphite in  $\text{Li}[\text{Ni}_{1/3}\text{Mn}_{1/3}\text{Co}_{1/3}]\text{O}_2$  /Graphite Pouch Cells. *J. Electrochem. Soc.* **2014**, *161*, A1890–A1897. [CrossRef]
122. Wang, C.; Yu, L.; Fan, W.; Liu, J.; Ouyang, L.; Yang, L.; Zhu, M. 3,3'-(Ethylenedioxy)Dipropiononitrile as an Electrolyte Additive for 4.5 V  $\text{LiNi}_{1/3}\text{Co}_{1/3}\text{Mn}_{1/3}\text{O}_2$ /Graphite Cells. *ACS Appl. Mater. Interfaces* **2017**, *9*, 9630–9639. [CrossRef]
123. Zheng, X.; Huang, T.; Pan, Y.; Wang, W.; Fang, G.; Ding, K.; Wu, M. 3,3'-Sulfonyldipropiononitrile: A Novel Electrolyte Additive That Can Augment the High-Voltage Performance of  $\text{LiNi}_{1/3}\text{Co}_{1/3}\text{Mn}_{1/3}\text{O}_2$ /Graphite Batteries. *J. Power Sources* **2016**, *319*, 116–123. [CrossRef]

124. Zheng, X.; Huang, T.; Pan, Y.; Wang, W.; Fang, G.; Wu, M. High-Voltage Performance of  $\text{LiNi}_{1/3}\text{Co}_{1/3}\text{Mn}_{1/3}\text{O}_2$ /Graphite Batteries with Di(Methylsulfonyl) Methane as a New Sulfone-Based Electrolyte Additive. *J. Power Sources* **2015**, *293*, 196–202. [CrossRef]
125. Yu, Q.; Chen, Z.; Xing, L.; Chen, D.; Rong, H.; Liu, Q.; Li, W. Enhanced High Voltage Performances of Layered Lithium Nickel Cobalt Manganese Oxide Cathode by Using Trimethylboroxine as Electrolyte Additive. *Electrochim. Acta* **2015**, *176*, 919–925. [CrossRef]
126. Brox, S.; Röser, S.; Streipert, B.; Hildebrand, S.; Rodehorst, U.; Qi, X.; Wagner, R.; Winter, M.; Cekic-Laskovic, I. Innovative, Non-Corrosive LiTFSI Cyanoester-Based Electrolyte for Safer 4 V Lithium-Ion Batteries. *ChemElectroChem* **2017**, *4*, 304–309. [CrossRef]
127. Schmiegel, J.-P.; Qi, X.; Klein, S.; Winkler, V.; Evertz, M.; Nölle, R.; Henschel, J.; Reiter, J.; Terborg, L.; Fan, Q.; et al. Improving the Cycling Performance of High-Voltage NMC111 || Graphite Lithium Ion Cells by an Effective Urea-Based Electrolyte Additive. *J. Electrochem. Soc.* **2019**, *166*, A2910–A2920. [CrossRef]
128. Zheng, X.; Huang, T.; Pan, Y.; Wang, W.; Fang, G.; Ding, K.; Wu, M. Enhancing the High-Voltage Cycling Performance of  $\text{LiNi}_{1/3}\text{Co}_{1/3}\text{Mn}_{1/3}\text{O}_2$ /Graphite Batteries Using Alkyl 3,3,3-Trifluoropropionate as an Electrolyte Additive. *ACS Appl. Mater. Interfaces* **2017**, *9*, 18758–18765. [CrossRef]
129. Belharouak, I.; Sun, Y.; Liu, J.; Amine, K.  $\text{Li}(\text{Ni}_{1/3}\text{Mn}_{1/3}\text{Co}_{1/3})\text{O}_2$  as a Suitable Cathode for High Power Applications. *J. Power Sources* **2003**, *123*, 247–252. [CrossRef]
130. Qian, Y.; Niehoff, P.; Börner, M.; Grützke, M.; Mönnighoff, X.; Behrends, P.; Nowak, S.; Winter, M.; Schappacher, F.M. Influence of Electrolyte Additives on the Cathode Electrolyte Interphase (CEI) Formation on  $\text{LiNi}_{1/3}\text{Mn}_{1/3}\text{Co}_{1/3}\text{O}_2$  in Half Cells with Li Metal Counter Electrode. *J. Power Sources* **2016**, *329*, 31–40. [CrossRef]
131. Xu, C.; Renault, S.; Ebadi, M.; Wang, Z.; Björklund, E.; Guyomard, D.; Brandell, D.; Edström, K.; Gustafsson, T. LiTDI: A Highly Efficient Additive for Electrolyte Stabilization in Lithium-Ion Batteries. *Chem. Mater.* **2017**, *29*, 2254–2263. [CrossRef]
132. Zhang, L.; Ma, Y.; Cheng, X.; Zuo, P.; Cui, Y.; Guan, T.; Du, C.; Gao, Y.; Yin, G. Enhancement of High Voltage Cycling Performance and Thermal Stability of  $\text{LiNi}_{1/3}\text{Co}_{1/3}\text{Mn}_{1/3}\text{O}_2$  Cathode by Use of Boron-Based Additives. *Solid State Ion.* **2014**, *263*, 146–151. [CrossRef]
133. Qian, Y.; Schultz, C.; Niehoff, P.; Schwieters, T.; Nowak, S.; Schappacher, F.M.; Winter, M. Investigations on the Electrochemical Decomposition of the Electrolyte Additive Vinylene Carbonate in Li Metal Half Cells and Lithium Ion Full Cells. *J. Power Sources* **2016**, *332*, 60–71. [CrossRef]
134. Aiken, C.P.; Self, J.; Petibon, R.; Xia, X.; Paulsen, J.M.; Dahn, J.R. A Survey of In Situ Gas Evolution during High Voltage Formation in Li-Ion Pouch Cells. *J. Electrochem. Soc.* **2015**, *162*, A760–A767. [CrossRef]
135. Self, J.; Aiken, C.P.; Petibon, R.; Dahn, J.R. Survey of Gas Expansion in Li-Ion NMC Pouch Cells. *J. Electrochem. Soc.* **2015**, *162*, A796–A802. [CrossRef]
136. Nelson, K.J.; d'Eon, G.L.; Wright, A.T.B.; Ma, L.; Xia, J.; Dahn, J.R. Studies of the Effect of High Voltage on the Impedance and Cycling Performance of  $\text{Li}[\text{Ni}_{0.4}\text{Mn}_{0.4}\text{Co}_{0.2}]\text{O}_2$ /Graphite Lithium-Ion Pouch Cells. *J. Electrochem. Soc.* **2015**, *162*, A1046–A1054. [CrossRef]
137. Ma, L.; Xia, J.; Dahn, J.R. Improving the High Voltage Cycling of  $\text{Li}[\text{Ni}_{0.42}\text{Mn}_{0.42}\text{Co}_{0.16}]\text{O}_2$  (NMC442)/Graphite Pouch Cells Using Electrolyte Additives. *J. Electrochem. Soc.* **2014**, *161*, A2250–A2254. [CrossRef]
138. Petibon, R.; Xia, J.; Ma, L.; Bauer, M.K.G.; Nelson, K.J.; Dahn, J.R. Electrolyte System for High Voltage Li-Ion Cells. *J. Electrochem. Soc.* **2016**, *163*, A2571–A2578. [CrossRef]
139. Xia, J.; Nie, M.; Burns, J.C.; Xiao, A.; Lamanna, W.M.; Dahn, J.R. Fluorinated Electrolyte for 4.5 v  $\text{Li}(\text{Ni}_{0.4}\text{Mn}_{0.4}\text{Co}_{0.2})\text{O}_2$ /Graphite Li-Ion Cells. *J. Power Sources* **2016**, *307*, 340–350. [CrossRef]
140. Xia, J.; Dahn, J.R. Improving Sulfolane-Based Electrolyte for High Voltage Li-Ion Cells with Electrolyte Additives. *J. Power Sources* **2016**, *324*, 704–711. [CrossRef]
141. Rong, H.; Xu, M.; Xie, B.; Huang, W.; Liao, X.; Xing, L.; Li, W. Performance Improvement of Graphite/ $\text{LiNi}_{0.4}\text{Co}_{0.2}\text{Mn}_{0.4}\text{O}_2$  Battery at High Voltage with Added Tris (Trimethylsilyl) Phosphate. *J. Power Sources* **2015**, *274*, 1155–1161. [CrossRef]
142. Lei, Q.; Yang, T.; Zhao, X.; Fan, W.; Wang, W.; Yu, L.; Guo, S.; Zuo, X.; Zeng, R.; Nan, J. Lithium Difluorophosphate as a Multi-Functional Electrolyte Additive for 4.4 V  $\text{LiNi}_{0.5}\text{Co}_{0.2}\text{Mn}_{0.3}\text{O}_2$ /Graphite Lithium Ion Batteries. *J. Electroanal. Chem.* **2019**, *846*, 113141. [CrossRef]
143. Zuo, X.; Fan, C.; Liu, J.; Xiao, X.; Wu, J.; Nan, J. Lithium Tetrafluoroborate as an Electrolyte Additive to Improve the High Voltage Performance of Lithium-Ion Battery. *J. Electrochem. Soc.* **2013**, *160*, A1199–A1204. [CrossRef]
144. Hu, Z.; Wang, K.; Che, Y.; Liu, M.; Zhang, W.; Xing, L.; Wang, H.; Li, S.; Liu, X.; Li, W. A Novel Electrolyte Additive Enables High-Voltage Operation of Nickel-Rich Oxide/Graphite Cells. *J. Phys. Chem. Lett.* **2021**, *12*, 4327–4338. [CrossRef]
145. Guo, R.; Che, Y.; Lan, G.; Lan, J.; Li, J.; Xing, L.; Xu, K.; Fan, W.; Yu, L.; Li, W. Tailoring Low-Temperature Performance of a Lithium-Ion Battery via Rational Designing Interphase on an Anode. *ACS Appl. Mater. Interfaces* **2019**, *11*, 38285–38293. [CrossRef] [PubMed]
146. Zuo, X.; Fan, C.; Liu, J.; Xiao, X.; Wu, J.; Nan, J. Effect of Tris(Trimethylsilyl)Borate on the High Voltage Capacity Retention of  $\text{LiNi}_{0.5}\text{Co}_{0.2}\text{Mn}_{0.3}\text{O}_2$ /Graphite Cells. *J. Power Sources* **2013**, *229*, 308–312. [CrossRef]
147. Rong, H.; Xu, M.; Zhu, Y.; Xie, B.; Lin, H.; Liao, Y.; Xing, L.; Li, W. A Novel Imidazole-Based Electrolyte Additive for Improved Electrochemical Performance of High Voltage Nickel-Rich Cathode Coupled with Graphite Anode Lithium Ion Battery. *J. Power Sources* **2016**, *332*, 312–321. [CrossRef]

148. Lee, S.H.; Yoon, S.; Hwang, E.H.; Kwon, Y.G.; Lee, Y.G.; Cho, K.Y. [4,4"-Bi(1,3,2-Dioxathiolane)] 2,2"-Dioxide: A Novel Cathode Additive for High-Voltage Performance in Lithium Ion Batteries. *J. Power Sources* **2018**, *378*, 112–118. [[CrossRef](#)]
149. Shi, X.; Zheng, T.; Xiong, J.; Zhu, B.; Cheng, Y.J.; Xia, Y. Stable Electrode/Electrolyte Interface for High-Voltage NCM 523 Cathode Constructed by Synergistic Positive and Passive Approaches. *ACS Appl. Mater. Interfaces* **2021**, *13*, 57107–57117. [[CrossRef](#)]
150. Jung, S.K.; Gwon, H.; Hong, J.; Park, K.Y.; Seo, D.H.; Kim, H.; Hyun, J.; Yang, W.; Kang, K. Understanding the Degradation Mechanisms of LiNi<sub>0.5</sub>Co<sub>0.2</sub>Mn<sub>0.3</sub>O<sub>2</sub> Cathode Material in Lithium Ion Batteries. *Adv. Energy Mater.* **2014**, *4*, 1300787. [[CrossRef](#)]
151. Zhang, L.; Zhang, C.; Li, N.; Tong, W. Influence of Charge Cutoff Voltage on the Cycling Behavior of LiNi<sub>0.5</sub>Mn<sub>0.3</sub>Co<sub>0.2</sub>O<sub>2</sub> Cathode. *J. Electrochem. Soc.* **2020**, *167*, 120509. [[CrossRef](#)]
152. Hong, P.; Xu, M.; Liao, B.; Wu, Y.; Lin, N.; Huang, Q.; Li, W. Enhancing the Cycling Performance of High Voltage (4.5 V) Li/LiNi<sub>0.5</sub>Mn<sub>0.3</sub>Co<sub>0.2</sub>O<sub>2</sub> Cell by Tailoring Sulfur-Derivative Cathode Passivation Film. *J. Electrochem. Soc.* **2017**, *164*, A2914–A2921. [[CrossRef](#)]
153. Zhang, Q.; Liu, K.; Ding, F.; Li, W.; Liu, X.; Zhang, J. Enhancing the High Voltage Interface Compatibility of LiNi<sub>0.5</sub>Co<sub>0.2</sub>Mn<sub>0.3</sub>O<sub>2</sub> in the Succinonitrile-Based Electrolyte. *Electrochim. Acta* **2019**, *298*, 818–826. [[CrossRef](#)]
154. Jung, R.; Strobl, P.; Maglia, F.; Stinner, C.; Gasteiger, H.A. Temperature Dependence of Oxygen Release from LiNi<sub>0.6</sub>Mn<sub>0.2</sub>Co<sub>0.2</sub>O<sub>2</sub> (NMC622) Cathode Materials for Li-Ion Batteries. *J. Electrochem. Soc.* **2018**, *165*, A2869–A2879. [[CrossRef](#)]
155. Wang, W.; Yang, T.; Li, S.; Lu, J.; Zhao, X.; Fan, W.; Fan, C.; Zuo, X.; Tie, S.; Nan, J. 1,4-Phenylene Diisocyanate (PPDI)-Containing Low H<sub>2</sub>O/HF and Multi-Functional Electrolyte for LiNi<sub>0.6</sub>Co<sub>0.2</sub>Mn<sub>0.2</sub>O<sub>2</sub> /Graphite Batteries with Enhanced Performances. *J. Power Sources* **2021**, *483*, 229172. [[CrossRef](#)]
156. Liao, B.; Hu, X.; Xu, M.; Li, H.; Yu, L.; Fan, W.; Xing, L.; Liao, Y.; Li, W. Constructing Unique Cathode Interface by Manipulating Functional Groups of Electrolyte Additive for Graphite/LiNi<sub>0.6</sub>Co<sub>0.2</sub>Mn<sub>0.2</sub>O<sub>2</sub> Cells at High Voltage. *J. Phys. Chem. Lett.* **2018**, *9*, 3434–3445. [[CrossRef](#)]
157. Lu, J.; Wang, W.; Yang, T.; Li, S.; Zhao, X.; Fan, W.; Fan, C.; Zuo, X.; Nan, J. Hexamethylene Diisocyanate (HDI)-Functionalized Electrolyte Matching LiNi<sub>0.6</sub>Co<sub>0.2</sub>Mn<sub>0.2</sub>O<sub>2</sub>/Graphite Batteries with Enhanced Performances. *Electrochim. Acta* **2020**, *352*, 136456. [[CrossRef](#)]
158. Lin, Y.; Xu, M.; Wu, S.; Tian, Y.; Cao, Z.; Xing, L.; Li, W. Insight into the Mechanism of Improved Interfacial Properties between Electrodes and Electrolyte in the Graphite/LiNi<sub>0.6</sub>Mn<sub>0.2</sub>Co<sub>0.2</sub>O<sub>2</sub> Cell via Incorporation of 4-Propyl-[1,3,2]Dioxathiolane-2,2-Dioxide (PDTD). *ACS Appl. Mater. Interfaces* **2018**, *10*, 16400–16409. [[CrossRef](#)]
159. Yan, X.; Chen, C.; Zhu, X.; Pan, L.; Zhao, X.; Zhang, L. Aminoalkyldisiloxane as Effective Electrolyte Additive for Improving High Temperature Cycle Life of Nickel-Rich LiNi<sub>0.6</sub>Co<sub>0.2</sub>Mn<sub>0.2</sub>O<sub>2</sub>/Graphite Batteries. *J. Power Sources* **2020**, *461*, 228099. [[CrossRef](#)]
160. Che, Y.; Lin, X.; Xing, L.; Guan, X.; Guo, R.; Lan, G.; Zheng, Q.; Zhang, W.; Li, W. Protective Electrode/Electrolyte Interphases for High Energy Lithium-Ion Batteries with p-Toluenesulfonyl Fluoride Electrolyte Additive. *J. Energy Chem.* **2020**, *52*, 361–371. [[CrossRef](#)]
161. Qin, Z.; Hong, S.; Hong, B.; Duan, B.; Lai, Y.; Feng, J. Triisopropyl Borate as an Electrolyte Additive for Improving the High Voltage. *J. Electroanal. Chem.* **2019**, *854*, 113506. [[CrossRef](#)]
162. Deng, B.; Wang, H.; Ge, W.; Li, X.; Yan, X.; Chen, T.; Qu, M.; Peng, G. Investigating the Influence of High Temperatures on the Cycling Stability of a LiNi<sub>0.6</sub>Co<sub>0.2</sub>Mn<sub>0.2</sub>O<sub>2</sub> Cathode Using an Innovative Electrolyte Additive. *Electrochim. Acta* **2017**, *236*, 61–71. [[CrossRef](#)]
163. Wang, H.; Sun, D.; Li, X.; Ge, W.; Deng, B.; Qu, M.; Peng, G. Alternative Multifunctional Cyclic Organosilicon as an Efficient Electrolyte Additive for High Performance Lithium-Ion Batteries. *Electrochim. Acta* **2017**, *254*, 112–122. [[CrossRef](#)]
164. Gao, H.; Maglia, F.; Lamp, P.; Amine, K.; Chen, Z. Mechanistic Study of Electrolyte Additives to Stabilize High-Voltage Cathode-Electrolyte Interface in Lithium-Ion Batteries. *ACS Appl. Mater. Interfaces* **2017**, *9*, 44542–44549. [[CrossRef](#)] [[PubMed](#)]
165. Sun, H.; Liu, J.; He, J.; Wang, H.; Jiang, G.; Qi, S.; Ma, J. Stabilizing the Cycling Stability of Rechargeable Lithium Metal Batteries with Tris(Hexafluoroisopropyl)Phosphate Additive. *Sci. Bull.* **2022**, *67*, 725–732. [[CrossRef](#)] [[PubMed](#)]
166. Liang, H.; Zuo, X.; Zhang, L.; Huang, W.; Chen, Q.; Zhu, T.; Liu, J.; Nan, J. Nonflammable LiTFSI-Ethylene Carbonate/1,2-Dimethoxyethane Electrolyte for High-Safety Li-Ion Batteries Electrolyte for High-Safety Li-Ion Batteries. *J. Electrochem. Soc.* **2020**, *167*, 090520. [[CrossRef](#)]
167. Su, C.; He, M.; Amine, R.; Chen, Z.; Sahore, R.; Dietz, N.; Amine, K. Cyclic Carbonate for Highly Stable Cycling of High Voltage Lithium Metal Batteries. *Energy Storage Mater.* **2019**, *17*, 284–292. [[CrossRef](#)]
168. Lee, W.J.; Prasanna, K.; Jo, Y.N.; Kim, K.J.; Kim, H.S.; Lee, C.W. Depth Profile Studies on Nickel Rich Cathode Material Surfaces after Cycling with an Electrolyte Containing Vinylene Carbonate at Elevated Temperature. *Phys. Chem. Chem. Phys.* **2014**, *16*, 17062–17071. [[CrossRef](#)]
169. Liu, L.; Wang, S.; Zhang, Z.; Fan, J.; Qi, W.; Chen, S. Fluoroethylene Carbonate as an Electrolyte Additive for Improving Interfacial Stability of High-Voltage LiNi<sub>0.6</sub>Co<sub>0.2</sub>Mn<sub>0.2</sub>O<sub>2</sub> Cathode. *Ionics* **2019**, *25*, 1035–1043. [[CrossRef](#)]
170. Beltrop, K.; Klein, S.; No, R.; Wilken, A.; Lee, J.J.; Ko, T.K.; Reiter, J.; Tao, L.; Liang, C.; Winter, M.; et al. Triphenylphosphine Oxide as Highly Effective Electrolyte Additive for Graphite/NMC811 Lithium Ion Cells. *Chem. Mater.* **2018**, *30*, 2726–2741. [[CrossRef](#)]
171. Lan, G.; Xing, L.; Bedrov, D.; Chen, J.; Guo, R.; Che, Y.; Li, Z.; Zhou, H.; Li, W. Enhanced Cyclic Stability of Ni-Rich Lithium Ion Battery with Electrolyte Film-Forming Additive. *J. Alloys Compd.* **2020**, *821*, 153236. [[CrossRef](#)]

172. Lu, J.; Xu, X.; Fan, W.; Xin, Y.; Wang, W.; Fan, C.; Cheng, P.; Zhao, J.; Liu, J.; Huo, Y. Phenyl 4-Fluorobenzene Sulfonate as a Versatile Film-Forming Electrolyte Additive for Wide-Temperature-Range NCM811//Graphite Batteries. *ACS Appl. Energy Mater.* **2022**, *5*, 6324–6334. [CrossRef]
173. Qiu, Y.; Lu, D.; Gai, Y.; Cai, Y. Adiponitrile (ADN): A Stabilizer for the LiNi<sub>0.8</sub>Co<sub>0.1</sub>Mn<sub>0.1</sub>O<sub>2</sub> (NCM811) Electrode/Electrolyte Interface of a Graphite/NCM811 Li-Ion Cell. *ACS Appl. Mater. Interfaces* **2022**, *14*, 11398–11407. [CrossRef]
174. Li, S.; Li, C.; Yang, T.; Wang, W.; Lu, J.; Fan, W.; Zhao, X.; Zuo, X.; Tie, S.; Nan, J. 3,3-Diethylene Di-Sulfite (DES) as a High-Voltage Electrolyte Additive for 4.5 V LiNi<sub>0.8</sub>Co<sub>0.1</sub>Mn<sub>0.1</sub>O<sub>2</sub>/Graphite Batteries with Enhanced Performances. *ChemElectroChem* **2021**, *8*, 745–754. [CrossRef]
175. Cheng, F.; Zhang, X.; Wei, P.; Sun, S.; Xu, Y.; Li, Q.; Fang, C.; Han, J. Tailoring Electrolyte Enables High-Voltage Ni-Rich NCM Cathode against Aggressive Cathode Chemistries for Li-Ion Batteries. *Sci. Bull.* **2022**, *67*, 2225–2234. [CrossRef] [PubMed]
176. Wang, J.; Dong, H.; Wang, P.; Fu, X.L.; Zhang, N.S.; Zhao, D.N.; Li, S.Y.; Cui, X.L. Adjusting the Solvation Structure with Tris(Trimethylsilyl)Borate Additive to Improve the Performance of LNCM Half Cells. *J. Energy Chem.* **2022**, *67*, 55–64. [CrossRef]
177. Jung, K.; Oh, S.H.; Yim, T. Triphenyl Phosphate as an Efficient Electrolyte Additive for Ni-Rich Ncm Cathode Materials. *J. Electrochem. Sci. Technol.* **2021**, *12*, 67–73. [CrossRef]
178. Zhang, X.; Zhang, J.; Jia, M.; Peng, L.; Zhang, N.; Qi, S.; Zhang, L. Bifunctional Additive Phenyl Vinyl Sulfone for Boosting Cyclability of Lithium Metal Batteries. *Green Chem. Eng.* **2022**, *4*, 49–56. [CrossRef]
179. Li, G.; Liao, Y.; Li, Z.; Xu, N.; Lu, Y.; Lan, G.; Sun, G.; Li, W. Constructing a Low-Impedance Interface on a High-Voltage LiNi<sub>0.8</sub>Co<sub>0.1</sub>Mn<sub>0.1</sub>O<sub>2</sub> Cathode with 2,4,6-Triphenyl Boroxine as a Film-Forming Electrolyte Additive for Li-Ion Batteries. *ACS Appl. Mater. Interfaces* **2020**, *12*, 37013–37026. [CrossRef]
180. Zhang, L.; Min, F.; Luo, Y.; Dang, G.; Gu, H.; Dong, Q.; Zhang, M.; Sheng, L.; Shen, Y.; Chen, L.; et al. Practical 4.4 V Li || NCM811 Batteries Enabled by a Thermal Stable and HF Free Carbonate-Based Electrolyte. *Nano Energy* **2022**, *96*, 107122. [CrossRef]
181. Jiang, S.; Xu, X.; Yin, J.; Wu, H.; Zhu, X.; Gao, Y. Multifunctional Electrolyte Additive for Bi-Electrode Interphase Regulation and Electrolyte Stabilization in Li/LiNi<sub>0.8</sub>Co<sub>0.1</sub>Mn<sub>0.1</sub>O<sub>2</sub> Batteries. *ACS Appl. Mater. Interfaces* **2022**, *14*, 38758–38768. [CrossRef]
182. Hu, H.; Wang, W.; Zeng, X.; Fan, W.; Fan, C.; Nan, J. Interfacial Film Regulation and Electrochemical Performance Using Cyclopropane Sulphonic Amide Functionalized Electrolyte to Stabilize Lithium Metal Batteries with a LiNi<sub>0.8</sub>Mn<sub>0.1</sub>Co<sub>0.1</sub>O<sub>2</sub> Cathode. *ACS Appl. Energy Mater.* **2022**, *5*, 5053–5063. [CrossRef]
183. You, B.; Wang, Z.; Shen, F.; Chang, Y.; Peng, W.; Li, X.; Guo, H.; Hu, Q.; Deng, C.; Yang, S.; et al. Research Progress of Single-Crystal Nickel-Rich Cathode Materials for Lithium Ion Batteries. *Small Methods* **2021**, *5*, 2100234. [CrossRef] [PubMed]
184. Langdon, J.; Manthiram, A. A Perspective on Single-Crystal Layered Oxide Cathodes for Lithium-Ion Batteries. *Energy Storage Mater.* **2021**, *37*, 143–160. [CrossRef]
185. Zhang, X.; Zhang, Y.; Liu, J.; Yan, Z.; Chen, J. Syntheses, Challenges and Modifications of Single-Crystal Cathodes for Lithium-Ion Battery. *J. Energy Chem.* **2021**, *63*, 217–229. [CrossRef]
186. Klein, S.; Bärmann, P.; Fromm, O.; Borzutzki, K.; Reiter, J.; Fan, Q.; Winter, M.; Placke, T.; Kasnatscheew, J. Prospects and Limitations of Single-Crystal Cathode Materials to Overcome Cross-Talk Phenomena in High-Voltage Lithium Ion Cells. *J. Mater. Chem. A* **2021**, *9*, 7546–7555. [CrossRef]
187. Hall, D.S.; Soc, J.E.; Cells, L.; Hall, D.S. Dioxazolone and Nitrile Sulfite Electrolyte Additives for Lithium-Ion Cells Dioxazolone and Nitrile Sulfite Electrolyte Additives For. *J. Electrochem. Soc.* **2018**, *165*, A2961–A2967. [CrossRef]
188. Harlow, J.E.; Ma, X.; Li, J.; Logan, E.; Liu, Y.; Zhang, N.; Ma, L.; Glazier, S.L.; Cormier, M.M.E.; Genovese, M.; et al. A Wide Range of Testing Results on an Excellent Lithium-Ion Cell Chemistry to Be Used as Benchmarks for New Battery Technologies. *J. Electrochem. Soc.* **2019**, *166*, A3031–A3044. [CrossRef]
189. Li, H.; Li, J.; Ma, X.; Dahn, J.R. Synthesis of Single Crystal LiNi<sub>0.6</sub>Mn<sub>0.2</sub>Co<sub>0.2</sub>O<sub>2</sub> with Enhanced Electrochemical Performance for Lithium Ion Batteries. *J. Electrochem. Soc.* **2018**, *165*, A1038–A1045. [CrossRef]
190. Logan, E.R.; Hebecker, H.; Ma, X.; Quinn, J.; HyeJeong, Y.; Kumakura, S.; Paulsen, J.; Dahn, J.R. A Comparison of the Performance of Different Morphologies of LiNi<sub>0.8</sub>Mn<sub>0.1</sub>Co<sub>0.1</sub>O<sub>2</sub> Using Isothermal Microcalorimetry, Ultra-High Precision Coulometry, and Long-Term Cycling. *J. Electrochem. Soc.* **2020**, *167*, 060530. [CrossRef]
191. Song, W.; Harlow, J.; Logan, E.; Hebecker, H.; Coon, M.; Molino, L.; Johnson, M.; Dahn, J.; Metzger, M. A Systematic Study of Electrolyte Additives in Single Crystal and Bimodal LiNi<sub>0.8</sub>Mn<sub>0.1</sub>Co<sub>0.1</sub>O<sub>2</sub>/Graphite Pouch Cells. *J. Electrochem. Soc.* **2021**, *168*, 090503. [CrossRef]
192. Zhang, N.; Li, J.; Li, H.; Liu, A.; Huang, Q.; Ma, L.; Li, Y.; Dahn, J.R. Structural, Electrochemical, and Thermal Properties of Nickel-Rich LiNi<sub>x</sub>Mn<sub>y</sub>Co<sub>z</sub>O<sub>2</sub> Materials. *Chem. Mater.* **2018**, *30*, 8852–8860. [CrossRef]
193. Ge, M.; Wi, S.; Liu, X.; Bai, J.; Ehrlich, S.; Lu, D.; Lee, W.K.; Chen, Z.; Wang, F. Kinetic Limitations in Single-Crystal High-Nickel Cathodes. *Angew. Chem. Int. Ed.* **2021**, *60*, 17350–17355. [CrossRef]
194. Lee, S.; Jin, W.; Kim, S.H.; Joo, S.H.; Nam, G.; Oh, P.; Kim, Y.; Kwak, S.K.; Cho, J. Oxygen Vacancy Diffusion and Condensation in Lithium-Ion Battery Cathode Materials. *Angew. Chem.* **2019**, *131*, 10588–10595. [CrossRef]
195. Han, Y.; Heng, S.; Wang, Y.; Qu, Q.; Zheng, H. Anchoring Interfacial Nickel Cations on Single-Crystal LiNi<sub>0.8</sub>Co<sub>0.1</sub>Mn<sub>0.1</sub>O<sub>2</sub> Cathode Surface via Controllable Electron Transfer. *ACS Energy Lett.* **2020**, *5*, 2421–2433. [CrossRef]
196. Ryu, H.H.; Namkoong, B.; Kim, J.H.; Belharouak, I.; Yoon, C.S.; Sun, Y.K. Capacity Fading Mechanisms in Ni-Rich Single-Crystal NCM Cathodes. *ACS Energy Lett.* **2021**, *6*, 2726–2734. [CrossRef]

197. Han, G.M.; Kim, Y.S.; Ryu, H.H.; Sun, Y.K.; Yoon, C.S. Structural Stability of Single-Crystalline Ni-Rich Layered Cathode upon Delithiation. *ACS Energy Lett.* **2022**, *7*, 2919–2926. [[CrossRef](#)]
198. Li, X.; Peng, W.; Tian, R.; Song, D.; Wang, Z.; Zhang, H.; Zhu, L.; Zhang, L. Excellent Performance Single-Crystal NCM Cathode under High Mass Loading for All-Solid-State Lithium Batteries. *Electrochim. Acta* **2020**, *363*, 137185. [[CrossRef](#)]
199. Wang, C.; Hwang, S.; Jiang, M.; Liang, J.; Sun, Y.; Adair, K.; Zheng, M.; Mukherjee, S.; Li, X.; Li, R.; et al. Deciphering Interfacial Chemical and Electrochemical Reactions of Sulfide-Based All-Solid-State Batteries. *Adv. Energy Mater.* **2021**, *11*, 2100210. [[CrossRef](#)]
200. Liu, X.; Zheng, B.; Zhao, J.; Zhao, W.; Liang, Z.; Su, Y.; Xie, C.; Zhou, K.; Xiang, Y.; Zhu, J.; et al. Electrochemo-Mechanical Effects on Structural Integrity of Ni-Rich Cathodes with Different Microstructures in All Solid-State Batteries. *Adv. Energy Mater.* **2021**, *11*, 2003583. [[CrossRef](#)]
201. Doerrer, C.; Capone, I.; Narayanan, S.; Liu, J.; Grovenor, C.R.M.; Pasta, M.; Grant, P.S. High Energy Density Single-Crystal NMC/Li<sub>6</sub>PS<sub>5</sub>Cl Cathodes for All-Solid-State Lithium-Metal Batteries. *ACS Appl. Mater. Interfaces* **2021**, *13*, 37809–37815. [[CrossRef](#)]
202. Conforto, G.; Ruess, R.; Schröder, D.; Trevisanello, E.; Fantin, R.; Richter, F.H.; Janek, J. Editors' Choice—Quantification of the Impact of Chemo-Mechanical Degradation on the Performance and Cycling Stability of NCM-Based Cathodes in Solid-State Li-Ion Batteries. *J. Electrochem. Soc.* **2021**, *168*, 070546. [[CrossRef](#)]
203. Guo, X.; Hao, L.; Yang, Y.; Wang, Y.; Lu, Y.; Yu, H. High Cathode Utilization Efficiency through Interface Engineering in All-Solid-State Lithium-Metal Batteries. *J. Mater. Chem. A* **2019**, *7*, 25915–25924. [[CrossRef](#)]
204. Wang, C.; Yu, R.; Hwang, S.; Liang, J.; Li, X.; Zhao, C.; Sun, Y.; Wang, J.; Holmes, N.; Li, R.; et al. Single Crystal Cathodes Enabling High-Performance All-Solid-State Lithium-Ion Batteries. *Energy Storage Mater.* **2020**, *30*, 98–103. [[CrossRef](#)]
205. Jeon, H.; Kwon, D.H.; Kim, H.; Lee, J.H.; Jun, Y.; Son, J.W.; Park, S. Tailoring Shape and Exposed Crystal Facet of Single-Crystal Layered-Oxide Cathode Particles for All-Solid-State Batteries. *Chem. Eng. J.* **2022**, *445*, 136828. [[CrossRef](#)]
206. Yi, M.; Li, J.; Fan, X.; Bai, M.; Zhang, Z.; Hong, B.; Zhang, Z.; Hu, G.; Jiang, H.; Lai, Y. Single Crystal Ni-Rich Layered Cathodes Enabling Superior Performance in All-Solid-State Batteries with PEO-Based Solid Electrolytes. *J. Mater. Chem. A* **2021**, *9*, 16787–16797. [[CrossRef](#)]
207. Yi, M.; Li, J.; Wang, M.; Fan, X.; Hong, B.; Zhang, Z.; Zhang, Z.; Jiang, H.; Wang, A.; Lai, Y. Suppressing Structural Degradation of Single Crystal Nickel-Rich Cathodes in PEO-Based All-Solid-State Batteries: Mechanistic Insight and Performance. *Energy Storage Mater.* **2023**, *54*, 579–588. [[CrossRef](#)]
208. Ma, X.; Vanaphutti, P.; Fu, J.; Hou, J.; Liu, Y.; Zhang, R.; Bong, S.; Yao, Z.; Yang, Z.; Wang, Y. A Universal Etching Method for Synthesizing High-Performance Single Crystal Cathode Materials. *Nano Energy* **2021**, *87*, 106194. [[CrossRef](#)]
209. Kimijima, T.; Zetsu, N.; Teshima, K. Growth Manner of Octahedral-Shaped Li(Ni<sub>1/3</sub>Co<sub>1/3</sub>Mn<sub>1/3</sub>)O<sub>2</sub> Single Crystals in Molten Na<sub>2</sub>SO<sub>4</sub>. *Cryst. Growth Des.* **2016**, *16*, 2618–2623. [[CrossRef](#)]
210. Li, F.; Kong, L.; Sun, Y.; Jin, Y.; Hou, P. Micron-Sized Monocrystalline LiNi<sub>1/3</sub>Co<sub>1/3</sub>Mn<sub>1/3</sub>O<sub>2</sub> as High-Volumetric-Energy-Density Cathode for Lithium-Ion Batteries. *J. Mater. Chem. A* **2018**, *6*, 12344–12352. [[CrossRef](#)]
211. Huang, Z.D.; Liu, X.M.; Oh, S.W.; Zhang, B.; Ma, P.C.; Kim, J.K. Microscopically Porous, Interconnected Single Crystal LiNi<sub>1/3</sub>Co<sub>1/3</sub>Mn<sub>1/3</sub>O<sub>2</sub> Cathode Material for Lithium Ion Batteries. *J. Mater. Chem.* **2011**, *21*, 10777–10784. [[CrossRef](#)]
212. Zhao, W.; Zheng, G.; Lin, M.; Zhao, W.; Li, D.; Guan, X.; Ji, Y.; Ortiz, G.F.; Yang, Y. Toward a Stable Solid-Electrolyte-Interfaces on Nickel-Rich Cathodes: LiPO<sub>2</sub>F<sub>2</sub> Salt-Type Additive and Its Working Mechanism for LiNi<sub>0.5</sub>Mn<sub>0.25</sub>Co<sub>0.25</sub>O<sub>2</sub> Cathodes. *J. Power Sources* **2018**, *380*, 149–157. [[CrossRef](#)]
213. Fan, X.; Liu, Y.; Ou, X.; Zhang, J.; Zhang, B.; Wang, D.; Hu, G. Unravelling the Influence of Quasi Single-Crystalline Architecture on High-Voltage and Thermal Stability of LiNi<sub>0.5</sub>Co<sub>0.2</sub>Mn<sub>0.3</sub>O<sub>2</sub> Cathode for Lithium-Ion Batteries. *Chem. Eng. J.* **2020**, *393*, 124709. [[CrossRef](#)]
214. Zhong, Z.; Chen, L.; Huang, S.; Shang, W.; Kong, L.; Sun, M.; Chen, L.; Ren, W. Single-Crystal LiNi<sub>0.5</sub>Co<sub>0.2</sub>Mn<sub>0.3</sub>O<sub>2</sub>: A High Thermal and Cycling Stable Cathodes for Lithium-Ion Batteries. *J. Mater. Sci.* **2020**, *55*, 2913–2922. [[CrossRef](#)]
215. Zhu, X.; Cheng, L.; Yu, H.; Xu, F.; Wei, W.; Fan, L. Critical Rate Capability Barrier by the (001) Microtexture of a Single-Crystal Cathode for Long Lifetime Lithium-Ion Batteries. *J. Mater.* **2022**, *8*, 649–655. [[CrossRef](#)]
216. Li, J.; Cameron, A.R.; Li, H.; Glazier, S.; Xiong, D.; Chatzidakis, M.; Allen, J.; Botton, G.A.; Dahn, J.R. Comparison of Single Crystal and Polycrystalline LiNi<sub>0.5</sub>Mn<sub>0.3</sub>Co<sub>0.2</sub>O<sub>2</sub> Positive Electrode Materials for High Voltage Li-Ion Cells. *J. Electrochem. Soc.* **2017**, *164*, A1534–A1544. [[CrossRef](#)]
217. Li, J.; Li, H.; Stone, W.; Glazier, S.; Dahn, J.R. Development of Electrolytes for Single Crystal NMC532/Artificial Graphite Cells with Long Lifetime. *J. Electrochem. Soc.* **2018**, *165*, A626–A635. [[CrossRef](#)]
218. Wang, L.; Wu, B.; Mu, D.; Liu, X.; Peng, Y.; Xu, H.; Liu, Q.; Gai, L.; Wu, F. Single-Crystal LiNi<sub>0.6</sub>Co<sub>0.2</sub>Mn<sub>0.2</sub>O<sub>2</sub> as High Performance Cathode Materials for Li-Ion Batteries. *J. Alloys Compd.* **2016**, *674*, 360–367. [[CrossRef](#)]
219. Liu, L.; Zhang, Y.; Zhao, Y.; Jiang, G.; Gong, R.; Li, Y.; Meng, Q.; Dong, P. Surface Growth and Intergranular Separation of Polycrystalline Particles for Regeneration of Stable Single-Crystal Cathode Materials. *ACS Appl. Mater. Interfaces* **2022**, *14*, 29886–29895. [[CrossRef](#)]
220. Huang, B.; Wang, M.; Zuo, Y.; Zhao, Z.; Zhang, X.; Gu, Y. The Effects of Reheating Process on the Electrochemical Properties of Single Crystal LiNi<sub>0.6</sub>Mn<sub>0.2</sub>Co<sub>0.2</sub>. *Solid State Ion.* **2020**, *345*, 115200. [[CrossRef](#)]

221. Chen, Z.; Guo, F.; Zhang, Y. Micron-Sized Monodisperse Particle  $\text{LiNi}_{0.6}\text{Co}_{0.2}\text{Mn}_{0.2}\text{O}_2$  Derived by Oxalate Solvothermal Process Combined with Calcination as Cathode Material for Lithium-Ion Batteries. *Materials* **2021**, *14*, 2576. [CrossRef]
222. Huang, B.; Wang, M.; Zhang, X.; Xu, G.; Gu, Y. Optimized Preparation of  $\text{LiNi}_{0.6}\text{Mn}_{0.2}\text{Co}_{0.2}\text{O}_2$  with Single Crystal Morphology Cathode Material for Lithium-Ion Batteries. *Ionics* **2020**, *26*, 2689–2698. [CrossRef]
223. Qian, G.; Zhang, Y.; Li, L.; Zhang, R.; Xu, J.; Cheng, Z.; Xie, S.; Wang, H.; Rao, Q.; He, Y.; et al. Single-Crystal Nickel-Rich Layered-Oxide Battery Cathode Materials: Synthesis, Electrochemistry, and Intra-Granular Fracture. *Energy Storage Mater.* **2020**, *27*, 140–149. [CrossRef]
224. Zhang, H.; Cen, T.; Tian, Y.; Zhang, X. Synthesis of High-Performance Single-Crystal  $\text{LiNi}_{0.8}\text{Co}_{0.1}\text{Mn}_{0.1}\text{O}_2$  Cathode Materials by Controlling Solution Super-Saturation. *J. Power Sources* **2022**, *532*, 231037. [CrossRef]
225. Xu, X.; Huo, H.; Jian, J.; Wang, L.; Zhu, H.; Xu, S.; He, X.; Yin, G.; Du, C.; Sun, X. Radially Oriented Single-Crystal Primary Nanosheets Enable Ultrahigh Rate and Cycling Properties of  $\text{LiNi}_{0.8}\text{Co}_{0.1}\text{Mn}_{0.1}\text{O}_2$  Cathode Material for Lithium-Ion Batteries. *Adv. Energy Mater.* **2019**, *9*, 1803963. [CrossRef]
226. Guo, F.; Xie, Y.; Zhang, Y. Low-Temperature Strategy to Synthesize Single-Crystal  $\text{LiNi}_{0.8}\text{Co}_{0.1}\text{Mn}_{0.1}\text{O}_2$  with Enhanced Cycling Performances as Cathode Material for Lithium-Ion Batteries. *Nano Res.* **2022**, *15*, 2052–2059. [CrossRef]
227. Azhari, L.; Meng, Z.; Yang, Z.; Gao, G.; Han, Y.; Wang, Y. Underlying Limitations behind Impedance Rise and Capacity Fade of Single Crystalline Ni-Rich Cathodes Synthesized via a Molten-Salt Route. *J. Power Sources* **2022**, *545*, 231963. [CrossRef]
228. Zheng, L.; Bennett, J.C.; Obrovac, M.N. All-Dry Synthesis of Single Crystal NMC Cathode Materials for Li-Ion Batteries. *J. Electrochem. Soc.* **2020**, *167*, 130536. [CrossRef]
229. Huang, B.; Wang, M.; Zhang, X.; Zhao, Z.; Chen, L.; Gu, Y. Synergistic Coupling Effect of Single Crystal Morphology and Precursor Treatment of Ni-Rich Cathode Materials. *J. Alloys Compd.* **2020**, *830*, 154619. [CrossRef]
230. Zou, Y.G.; Meng, F.; Xiao, D.; Sheng, H.; Chen, W.P.; Meng, X.H.; Du, Y.H.; Gu, L.; Shi, J.L.; Guo, Y.G. Constructing a Stable Interfacial Phase on Single-Crystalline Ni-Rich Cathode via Chemical Reaction with Phosphomolybdic Acid. *Nano Energy* **2021**, *87*, 106172. [CrossRef]
231. Zhang, X.; Hu, G.; Peng, Z.; Cao, Y.; Li, L.; Tan, C.; Wang, Y.; Wang, W.; Du, K. Synthesis and Characterization of Mono-Dispersion  $\text{LiNi}_{0.8}\text{Co}_{0.1}\text{Mn}_{0.1}\text{O}_2$  Micrometer Particles for Lithium-Ion Batteries. *Ceram. Int.* **2021**, *47*, 25680–25688. [CrossRef]
232. Zhu, J.; Zheng, J.; Cao, G.; Li, Y.; Zhou, Y.; Deng, S.; Hai, C. Flux-Free Synthesis of Single-Crystal  $\text{LiNi}_{0.8}\text{Co}_{0.1}\text{Mn}_{0.1}\text{O}_2$  Boosts Its Electrochemical Performance in Lithium Batteries. *J. Power Sources* **2020**, *464*, 228207. [CrossRef]
233. Yang, C.; Zhu, Z.; Wei, W.; Zhou, L. Superior Cycle Stability of Single Crystal Nickel-Rich Layered Oxides with Micron-Scale Grain Size as Cathode Material for Lithium Ion Batteries. *Int. J. Electrochem. Sci.* **2020**, *15*, 5031–5041. [CrossRef]
234. Kim, Y. Lithium Nickel Cobalt Manganese Oxide Synthesized Using Alkali Chloride Flux: Morphology and Performance as a Cathode Material for Lithium Ion Batteries. *ACS Appl. Mater. Interfaces* **2012**, *4*, 2329–2333. [CrossRef] [PubMed]
235. Pang, P.; Tan, X.; Wang, Z.; Cai, Z.; Nan, J.; Xing, Z.; Li, H. Crack-Free Single-Crystal  $\text{LiNi}_{0.83}\text{Co}_{0.10}\text{Mn}_{0.07}\text{O}_2$  as Cycling/Thermal Stable Cathode Materials for High-Voltage Lithium-Ion Batteries. *Electrochim. Acta* **2021**, *365*, 137380. [CrossRef]
236. Guo, Q.; Huang, J.; Liang, Z.; Potapenko, H.; Zhou, M.; Tang, X.; Zhong, S. The Use of a Single-Crystal Nickel-Rich Layered NCM Cathode for Excellent Cycle Performance of Lithium-Ion Batteries. *New J. Chem.* **2021**, *45*, 3652–3659. [CrossRef]
237. Zhu, H.; Tang, Y.; Wiaderek, K.M.; Borkiewicz, O.J.; Ren, Y.; Zhang, J.; Ren, J.; Fan, L.; Li, C.C.; Li, D.; et al. Spontaneous Strain Buffer Enables Superior Cycling Stability in Single-Crystal Nickel-Rich NCM Cathode. *Nano Lett.* **2021**, *21*, 9997–10005. [CrossRef]
238. Wang, J.; Lu, X.; Zhang, Y.; Zhou, J.; Wang, J.; Xu, S. Grain Size Regulation for Balancing Cycle Performance and Rate Capability of  $\text{LiNi}_{0.9}\text{Co}_{0.055}\text{Mn}_{0.045}\text{O}_2$  Single Crystal Nickel-Rich Cathode Materials. *J. Energy Chem.* **2022**, *65*, 681–687. [CrossRef]
239. Lee, S.H.; Sim, S.J.; Jin, B.S.; Kim, H.S. High Performance Well-Developed Single Crystal  $\text{LiNi}_{0.91}\text{Co}_{0.06}\text{Mn}_{0.03}\text{O}_2$  Cathode via  $\text{LiCl-NaCl}$  Flux Method. *Mater. Lett.* **2020**, *270*, 127615. [CrossRef]
240. Placke, T.; Kloepsch, R.; Dühnen, S.; Winter, M. Lithium Ion, Lithium Metal, and Alternative Rechargeable Battery Technologies: The Odyssey for High Energy Density. *J. Solid State Electrochem.* **2017**, *21*, 1939–1964. [CrossRef]
241. Wentker, M.; Greenwood, M.; Leker, J. A Bottom-up Approach to Lithium-Ion Battery Cost Modeling with a Focus on Cathode Active Materials. *Energies* **2019**, *12*, 504. [CrossRef]
242. Tyagi, A.; Nagmani; Puravankara, S. Opportunities in Na/K [Hexacyanoferrate] Frameworks for Sustainable Non-Aqueous  $\text{Na}^+/\text{K}^+$ -batteries. *Sustain. Energy Fuels* **2022**, *6*, 550–595. [CrossRef]
243. Nagmani, D.P.; Tyagi, A.; Puravankara, S. Lithium-Ion Battery Technologies for Electric Mobility—State-of-the-Art Scenario. *ARAI J. Mobil. Technol.* **2022**, *2*, 233–248. [CrossRef]
244. Schmuck, R.; Wagner, R.; Hörpel, G.; Placke, T.; Winter, M. Performance and Cost of Materials for Lithium-Based Rechargeable Automotive Batteries. *Nat. Energy* **2018**, *3*, 267–278. [CrossRef]
245. Houache, M.S.E.; Yim, C.H.; Karkar, Z.; Abu-Lebdeh, Y. On the Current and Future Outlook of Battery Chemistries for Electric Vehicles—Mini Review. *Batteries* **2022**, *8*, 70. [CrossRef]

**Disclaimer/Publisher's Note:** The statements, opinions and data contained in all publications are solely those of the individual author(s) and contributor(s) and not of MDPI and/or the editor(s). MDPI and/or the editor(s) disclaim responsibility for any injury to people or property resulting from any ideas, methods, instructions or products referred to in the content.